AMINE PROMOTION OF HYDROGEN EVOLUTION REACTION SUPPRESSION AND CO2 CONVERSION FOR ARTIFICIAL PHOTOSYNTHESIS

BY
WEI ZHU

DISSERTATION
Submitted in partial fulfillment of the requirements
for the degree of Doctor of Philosophy in Chemical Engineering
in the Graduate College of the
University of Illinois at Urbana-Champaign, 2011

Urbana, Illinois

Doctoral Committee

Professor Richard I. Masel
Professor Paul Kenis
Professor Andrew Gewirth
Professor Hyun Joon Kong

Abstract

Recycling CO_2 back into fuels or other useful products is critically important to the global efforts to reduce greenhouse gases and global warming [1-3]. The electrochemical method is regarded as a promising means to do this because it has the advantage that water can be used as the proton source [4, 5]. However, the overpotential for electrolysis of water is low, whereas the overpotential of electrochemical conversion of CO_2 is too high. Increasing the overpotential of water decomposition and lowering the overpotential of CO_2 reduction is considered one of the grand challenges for catalysis.

Choline based products are chosen as ideal electrolytes to achieve both hydrogen evolution reaction suppression and lowering of CO_2 reduction overpotential of. Experiments combining both electrochemical methods and surface enhanced Raman spectroscopy (SERS) techniques obtain a fairly complete picture of hydrogen evolution reaction and CO_2 reduction in choline products.

Based on the experimental data, we have discovered that if we conduct CO_2 reduction in choline based quaternary ammonium salts, the overpotential decreases and the starting potential of hydrogen evolution increases. This can be contributed to the fact that amine from choline based electrolyte initiates the suppression of the hydrogen evolution reaction and also acts like a co-catalyst to stabilize intermediates of CO_2 reduction.

In particular, we discovered that:

1. Choline based quaternary ammonium salts achieve hydrogen evolution reaction suppression because a thin layer of choline ions forms on the catalyst surface and blocks the protons from getting close to the surface.
2. Different reaction products are forming during CO_2 reduction in choline based electrolytes: CO mainly on gold, platinum and platinum/ruthenium; formic acid on palladium.
3. CO_2 reduction happens in a variety of catalysts with much lower overpotential because the thin layer of choline ions on the catalyst surface will form lower energy intermediates with CO_2, which will make the carbon dioxide reduction process easier.
4. Different anions in choline based electrolytes have little effect on CO_2 reduction as well as hydrogen evolution reaction.

Dedication

To mum and dad

Acknowledgement:

I want to thank Dr. Richard I. Masel, my advisor. He introduced me to electrochemistry, surface chemistry and kinetics and catalysis, and got me thinking about energy. I also want to thank my Dissertation committee members, for their time and effort reviewing my Dissertation and Defense.

I want to thank all my lab mates in Dr. Masel's research group. I want to thank to Dr. Zach Dunbar, who taught me all about fuel cells during my first year in graduate school. I also want to thank Dr. John Haan and Brian Rosen, who shared their knowledge of electrochemistry with me. I also want to thank Dr. Amin Salehi-khojin who gave me a lot of suggestions on my research. Thank you to everyone in the front office, Rob Morgan, Kevin Lin, Maryam Sayyah for such a helpful and enjoyable work environment. I also want to thank Nick Ndiege, Priya Desai, Hae-Kwon Jeong, Il-Whan Oh, Matt Luebbers, Chelsea Monty, Nick Londono, Tianjiao Wu, Linjuan Shen, Cody Jenson and Bogdan Gurau. I want to thank Mike Thorson and Devin Whipple from Professor Kenis' group for the useful discussion during our regular meetings. I want to thank Nicole Honesty, who is in Professor Gewirth's group, to help me to do the SERS experiments. Her patience and technical expertise was invaluable. I want to thank Dr. Leilei Yin from Beckman Institute, who is extremely kind and helpful in Micro-CT experiments for my master research.

I would also like to acknowledge the excellent work by the SCS Machine Shop and SCS Glass Shop, without whom this project would have been impossible.

In addition, I need to thank all my friends, many of whom have been mentioned above. Finally, I want to thank my family, for supporting me in basically every decision I've ever made.

This work was supported by the US Department of Energy under grant DE-SC0004453. I would like to thank them for their generosity. The views expressed in this paper are those of the authors and do not necessarily represent the views of the US Department of Energy.

Table of Contents

Chapter 1 Introduction

Global warming, diminishing fossil fuel sources and geopolitical uncertainty have led to an increasing interest in the search for alternative energy sources as well as reducing greenhouse gases. For reducing greenhouse gases, natural photosynthesis, which involves the photo- generation of carbon compounds and oxygen from abundant raw materials (carbon dioxide and water), cannot meet the need to mass-reduce the carbon dioxide in the atmosphere. Among all alternative energies, solar, hydroelectric, geothermal, wind, biomass, and nuclear energy sources have become the dominant alternative energy sources.

The use of biomass to produce energy is based on natural photosynthesis that generates energy directly using sunlight and CO_2 in the atmosphere. However, it is still unlikely that the natural production of biomass will be able to meet all our needs for fuels and chemicals in the foreseeable future. Therefore, although biomass will keep playing an important role in alternative fuels in the future, it would be unwise to rely exclusively on it for future renewable supplies of fuels and chemicals. As the world's population increases, there will be increased demand for biological resources for food and shelter, too. As a result, the transfer of biomass into energy source still remains controversial.

Artificial photosynthetic systems offer the possibility of producing fuels and chemicals from CO_2 and sunlight in fewer steps and with higher efficiencies than is possible in natural photosynthesis. There are several ways to reduce carbon dioxide: (1)

homogeneous photochemical reduction of CO_2, (2) heterogeneous photochemical reduction of CO_2, (3) photoelectrochemical CO_2 fixation, and (4) electrochemical reduction of CO_2 using solar electric power.

Homogeneous photochemical reduction is utilized because in the photochemical reduction of CO_2, the one-electron reduction to CO_2- requires extremely strong reducing agents that are generally difficult to produce by photochemical methods [6]. Catalysts such as transition-metal complexes or organic dyes are used because they can accept multiple electrons during the catalytic cycle of CO_2 reduction. Homogeneous photochemical reduction has several advantages such as the lack of side reactions that deactivate the photosensitizer or catalyst/mediator; the ability to undergo multi-electron transfer; long-lived intermediates, and so forth. Nevertheless, it failed to achieve the condition of not using sacrificial reagents.

For heterogeneous photochemical reduction of CO_2, photo-generated carriers were considered to promote multi-electron reduction of CO_2 and multi-hole oxidation of water [7]. Semiconductors such as $SiTiO_3$, $CaFe_2O_4$ and Nd_2O_3 have been used. Meanwhile, in efforts to enhance the yield of CO_2 reduction, surface treatment with a metal oxide and loading metal on semiconductors were tried. After quantum size effects in light absorption and chemical reactivity were discovered, a remarkable improvement in photocatalytic reduction of CO_2 was achieved using quantized or colloidal semiconductors [8].

In photoelectrochemical processes, the molecular sensitizer is replaced with a p-type semiconductor electrode such as Si, In, GaP, or InP [9]. With irradiation of light of higher energy than the band gap of the semiconductor electrode, electrochemical CO_2 reduction can be achieved at much lower potentials. The electric field gradient, which exists at the interface between the semiconductor and the solution, produces a charge separation with the electrons moving to the electrode surface for CO_2 reduction [10]. In a typical photoelectrochemical cell, the anode and cathode compartments are separated. The separation of the oxidized and reduced products occurs naturally. Bare semiconductors are used for photoelectrochemical CO_2 reduction with and without metal catalysts or organic solvents. The major reduction products are HCOOH and CO, but methanol formation is also reported in some cases [11].

The long term goal of our research is to develop better electrochemical systems for CO_2 reduction in room-temperature electrolyte that could lead to efficient processes for the large-scale conversion of CO_2 into formic acid or other products. Plants have the natural mechanism to produce carbohydrates, namely photosynthesis from CO_2 and H_2O by the catalytic action of the chloroplast with the solar light, but the electrochemical way of artificial photosynthesis has not yet reached realization [12] . If CO_2 could be recycled in large scale back into fuels or chemicals using solar generated electricity, global warming could be greatly slowed or reversed. At present the limiting factor in these processes is the ability to convert CO_2. So far one can only obtain reasonable efficiencies by using catalysts like mercury, silver or copper at high overportentials, and

even then the efficiency is low. Moreover, there is no commercially viable process for large scale CO_2 recycling into synfuels or other products because CO_2 is difficult to activate. The free energy change of the reaction to compose an original organic compound from CO_2 and H_2O is positive and does not proceed spontaneously.

The objective of our work is to learn how to use artificial electrochemical synthesis to create materials for renewable fuels. Specifically, we will be examining the mechanism of CO_2 conversion on different catalysts in one choline based quaternary ammonium salt. We project using electricity generated from solar power plant to convert CO_2 and water into CO, H_2 and formic acid, one useful product of CO_2 reduction. Over the globe, the demand of formic acid is growing. Significant amounts of formic acid are produced as a byproduct in the manufacturing of other chemicals, especially acetic acid. When methanol and carbon monoxide are combined with the presence of a strong base, the formic acid is produced. However, these processes are neither straightforward nor environmentally friendly [13, 14].

We have been exploring the use of amines to suppress water electrolysis and enhance CO_2 electrolysis. We find that the presence of choline ion raises the onset of hydrogen evolution, and lowers the overpotential for CO_2 conversion. The result shows that there is a region of potential where CO_2 electrolysis is more rapid than hydrogen evolution. The products vary with the catalysts.

Based on SERS data, we suggest that hydrogen evolution reaction is suppressed because choline ions formed a layer on the catalyst surface and blocked the adsorption of

the protons. Moreover, CO_2 reduction happens at such a modest potential because choline cations in the electrolyte are forming a complex with key anionic intermediates of the CO_2 reduction reaction such as $(CO_2)–$. The stabilization of the anionic intermediates leads to the substantial reduction in the required potential for CO_2 reduction.

In this work, experiments combining both electrochemical conversion methods and surface enhanced Raman spectroscopy (SERS) obtained a fairly complete picture of CO_2 reduction in choline products. Particularly, we discovered that:

1. Choline based quaternary ammonium salts achieve hydrogen evolution reaction suppression because a thin layer of choline ions forms on the catalyst surface and blocks the protons from coming close to the surface.
2. Different reaction products form during CO_2 reduction in choline electrolyte: CO mainly on gold, platinum and platinum/ruthenium; formic acid on palladium.
3. CO_2 reduction happens in various catalysts with much lower overpotential because the thin layer of choline ions on the catalyst surface will form lower energy intermediates with CO_2, which will make the CO_2 reduction process easier.
4. Different anions in choline based electrolytes have little effect on CO_2 reduction as well as hydrogen evolution reaction.

Chapter 2: Literature Review and Background Theory

2.1 Electrochemistry Background

Electrochemical reactions can be considered as two kinds of reactions: a chemical reaction driven by an external electric power supply, or a voltage generated by a chemical reaction. During this process, oxidation/reduction reactions happen when electrons are transferred between different molecules and ions. Generally, the topics in electrochemistry research are divided into two parts: chemical reactions which take place in a conducting solution at the interface of an ion conductor and an electron conductor, and electron transfer process between the electrodes and the species in electrolyte.

2.1.1 Electrochemical System and Related

The electrochemical cell is regarded as one of the most important parts of an electrochemical system. It is a device where the electrochemical reaction takes place and produces an output electrical current. Specifically, simple electrochemical cells are composed of two conductive electrodes and the electrolyte. The electrodes are the anode and the cathode: oxidation reactions happen at the anode and reduction reactions occurs at the cathode. The materials of electrodes can be chosen from any sufficiently

conductive materials, such as metals, semiconductors, graphite, and conductive polymers. In between these electrodes is the electrolyte, which contains ions that can freely move.

2.1.1.1 Nernst Equation

The Nernst equation is named after the German physical chemist Walther Nernst [15]. It is very important to explain the Nernst Equation here because it is an equation that can be used to determine the equilibrium reduction potential of a half-cell in an electrochemical cell. Typically, the Nernst equation is written as follow[16]:

$$E_{cell} = E^{0}_{cell} - \frac{RT}{zF}\ln Q$$

where E_{cell} is the cell potential which we need to calculate; E^{0}_{cell} is the standard cell potential at the temperature of interest; R is the universal gas constant: R = 8.314 472(15) J K−1 mol−1; T is the absolute temperature (K); F is the Faraday constant, F = 9.648 533 99(24)×104 C mol−1; z is the number of moles of electrons transferred in the half-reaction; Q is the reaction quotient.

To simplify the equation, RT/F is firstly treated as a constant of 25.693 mV for cells at room temperature (25 ℃), later the Nernst equation is expressed in logarithmic terms:

$$E_{cell} = E^{0}_{cell} - \frac{0.05916}{z}\log_{10}\frac{a_{Red}}{a_{Ox}}$$

It is important to note here that later in our chapters, we will use another version [17] of Nernst equation to calibrate the reversible hydrogen electrode vs. the standard hydrogen electrode:

$$E_{RHE} = E^{0}_{SHE} - 0.059 * pH$$

Where E_{RHE} is the reversible hydrogen electrode potential, E_{SHE}^{0} is the standard hydrogen electrode at a desired temperature.

2.1.1.2 Three-electrode system

People use a two-electrode system (Figure 2.1) because most electrochemical measurements need to measure the potential of an electrode while measuring the generated current. In a two-electrode system, a working electrode contacts the electrolyte and provides charges to or receives charges from the reactions happening in the electrolyte, which will generate the current. Other than the working electrode, the reference electrode has a known potential which can provide a basis for measuring the potential of the working electrode. However, as soon as a current passes, the reference electrode will be polarized, and its potential varies with the current.

In order to maintain a stable potential, no current should be allowed to pass through the reference electrode. Under this circumstance, the three-electrode cell (Figure 2.2) was

introduced to solve this problem[18]. Particularly, the three electrodes include a working electrode (WE), a counter electrode (CE) and a reference electrode (RE). In this system, the reference electrode is only functioning to reference the potential with the working electrode and there is no charge passing through. Instead, the counter electrode is used to conduct all the charges needed and balance the current with working electrode.

2.1.1.3 Potentiostat

The potentiostat was created to control the three-electrode cell [19]. It simultaneously measures the potential between the working electrode and the reference electrode, and the current flow between the counter electrode and the working electrode.

A potentiostat can be simplified into the circuit diagram demonstrated below (Figure 2.3). In operation, the voltage intended to be applied between the reference electrode and the sample is provided as the input voltage for the potentiostat. The actual WE-RE voltage is measured by a voltmeter and compared to the input voltage by a control amplifier. A matching current is fed to the counter electrode CE. The control circuit is closed by the cell, where the current passes the electrolyte from the counter electrode to the working electrode. In case there is a difference between the input voltage and the WE-RE voltage, the control amplifier will increase/decrease the voltage to the cell until the actual equals the input voltages. The I/U converter measures the cell current by

forcing it through the resistor R_k, whose voltage drop across is proportional to the cell current.

2.1.2 Cyclic Voltammetry

Cyclic voltammetry is a type of electrochemical measurement where potential is ramped linearly versus time. It is widely used in electrochemistry to analyze the properties of the electrode surface or the electrolyte. Unlike typical linear sweep voltammetry, which ends when it reaches a set potential, cyclic voltammetry takes the experiment a step further. The potential scan is reversed at the end of the first scan [20]. Therefore, cyclic voltammetry is an extended version of linear sweep voltammetry.

Cyclic voltammogram is plotted based on the potential change and the current at the working electrode. In cyclic voltammetry, the electrode potential ramping speed is known as the experiment's scan rate (V/s). In a three electrode system, as being mentioned before, the potential is applied between the working electrode and the reference electrode, and the current is measured between the working electrode and the counter electrode. A typical picture of potential sweep of cyclic voltammetry is demonstrated below.

As Figure 2.4 shows, the potential changes linearly with time as the linear sweep voltammetry. After the potential reaches the maximum set value, it goes back to the

original value with the same scan rate. This kind of potential sweep will create a typical cyclic votammogram (Figure 2.5).

During the forward scan from t0 to t1 in Figure 2.4, a current peak demonstrates the reduction or oxidation process through the range of the potential scanned. If it is a reversible reaction and the potential is reversed, it will repeat the potential and reoxidize the product formed from the previous reaction. In this process, a shifted current peak with reversed polarity will form.

Cyclic voltammogram can provide information about the redox potential and electrochemical reaction rates of the compounds. Basically, the current increases as the potential reaches the reduction potential of the electrolyte, and then falls off because the concentration of the electrolyte is depleted close to the electrode surface [21].

Cyclic voltammetry has several properties: first, based on the Cottrell equation [22], if the electron transfer at the surface is fast and the current is limited by the diffusion of species to the electrode surface, then the current peak will be proportional to the square root of the scan rate. Second, cyclic voltammetry is highly dependent on the target electrolyte. The ideal electrolyte should be redox active within the experimental potential window and is desirable to display a reversible cyclic voltammetry wave.

There are some concepts we will need to know before proceeding to later chapters. First, overpotential refers to the potential (voltage) difference between a half-reaction's thermodynamically determined reduction potential and the potential at which the redox event is experimentally observed [23]. This overpotential appears because of a

combination of electrolyte diffusion rate limitation and the intrinsic activation barrier of transferring electrons from an electrode to the electrolyte. Second, the half-cell potential $E^0_{1/2}$ can be determined from a ratio of the peak currents passed at reduction (i_{pc}) and oxidation (i_{pa}). This ratio can be perturbed for reversible couples in the presence of a following chemical reaction, stripping wave, or even nucleation event. When waves are semi-reversible such as when i_{pa}/i_{pc} is less than or greater than 1, it is possible to determine even more information, especially kinetic processes like following chemical reaction. If waves are non-reversible, $E^0_{1/2}$ can be determined with equal quantities of the analyte in both oxidation states.

2.1.3 Chronoamperometry

Chronoamperometry is a potential step method and a very useful electrochemical technique for electrocatalyst [24]. In a single step experiment, the potential of the working electrode is stepped and the resulting current from faradic processes is monitored as a function of time. In a double step experiment, the potential is applied symmetrically around the formal potential of the redox center in small increments [25].

There are several significant aspects we should take into consideration: First, the potential limits of the electrolyte and electrode must be analyzed before setting the potential limits. It is important for the initial potential to make all redox centers in the

same oxidation state. Second, the length of time between potential steps is also critical because it should allow the decay of the current to complete. Moreover, the time should be long enough for the faradaic current, which is due to electron transfer events and is most often the current component of interest, to be separated from the charging current for an accurate measurement. Usually, the appropriate time is determined experimentally by observing the time it takes for the current to return to the baseline level.

During chronoamperometry, limited information about the identity of the electrolyzed specie can be obtained from the ratio of the peak oxidation current versus the peak reduction current. The Faradaic current decays as described in the Cottrell equation. Since the current is integrated over relatively long time intervals, chronoamperometry gives a better signal to noise ratio in comparison to other amperometric techniques.

For example, in the case of irreversible formic acid oxidation with semi-infinite linear diffusion, one can fit the current-time curve, coupled with the diffusivity D_{FA} found from equation below, to find the reaction rate of formic acid.

$$i(t) = F\ A\ k\ C_{FA,\ bulk}\ \exp(k^2\ t / D_{FA})\ \mathrm{erfc}(k\ t^{1/2} / D_{FA}^{1/2})$$

where i(t) = chronoamperometric current as a function of time

F= Faraday's constant, 96,485 C / mol

k = reaction rate constant for formic acid electro-oxidation, cm/s

t = time, s

A more complete discussion of chronoamperometry for different reactions can be found in Bard and Faulkner [24]. In actual practice, because of other effects besides

mass transfer and elementary reactions, it is more complicated. Nevertheless, there is still much information to be gained from chronoamperometry.

Figure 2.6 shows a typical chronoamperometric scan for Pt in formic acid at 0.2 V vs. the Reversible Hydrogen Electrode (RHE). The electro-oxidation activity (current density) starts out very high on the active Pt surface. Then formic acid is depleted near the electrode surface and then CO is strongly adsorbed on the Pt surface. The current density rapidly drops, and eventually a steady concentration profile develops and the Pt has reached its equilibrium of poisoning by CO, and the steady activity of the catalyst can be determined. At 0.2 V vs. RHE the activity of the Pt catalyst is quite low due to the CO poisoning. Usually, Pt is a better catalyst at higher potentials where CO can be removed from the surface more easily.

2.2 Electrochemical Reactions of Carbon Dioxide Conversion

There are always other reactions happening when carbon dioxide is electrochemically reduced. In an aqueous system, the hydrogen evolution reaction is considered as the one of the most important or undesired 'by-reactions'. Here, we will first review the research area of the hydrogen evolution reaction and its effect on carbon dioxide conversion, and then discuss more about the mechanism involved in carbon dioxide reduction.

2.2.1 Hydrogen Evolution Reaction

The hydrogen evolution reaction (HER) is one of the most studied reactions in electrochemistry [26]. Typically, the hydrogen evolution reaction demonstrates the Volmer–Heyrovsky–Tafel mechanism [27-29]: a proton first adsorbs on the catalyst surface and then goes through reduction process to release hydrogen.

Here is a little discussion about the kinetics of the hydrogen evolution reaction (HER) in alkaline (or acid) solution [30]. The basic equation for the hydrogen evolution reaction is:

$H_{2(g)} \leftrightarrow 2H^+ + 2e^-$

It contains three elementary steps:

Tafle process: $H_{2(g)} + 2S \leftrightarrow H_{(a)} + H_{(a)}$

Heyrovsky process: $H_{2(g)} + S \leftrightarrow H_{(a)} + H^+ + e^-$

Volmer process: $H_{(a)} + S \leftrightarrow H^+ + e^-$

where S is an adsorption site.

As there are three elementary steps and only one intermediate species, the whole reaction can be verified through two independent routes, which in this case are the Tafel-Volmer and Heyrovsky-Volmer routes.

Although our research does not focus on kinetic models of the hydrogen evolution reaction and we will not discuss in detail about kinetics simulations of HER, it is still

necessary to have the basic conceptions about conditions of HER in mind. In previous research[31], in order to carry out the description of the kinetics of the HER in the whole domain of operative potentials, three critical factors should be taken into account simultaneously: first, the diffusion process of the molecular hydrogen to the electrode cannot be ignored, which is obvious for the HOR but sometime ignored in the case of the HER; second, during the HER process, the surface coverage of adsorbed hydrogen strongly depends on overpotential, therefore, the usual Langmuir equation [32] is not enough to describe the adsorption process; finally, both forward and backward chemical reactions should be considered in order to describe the kinetics of each elementary reaction step.

The study of the hydrogen evolution reaction has many applications. For instance, in battery manufacturing, the HER is desired to be reduced because it occasionally takes place on the cathode with very negative potentials and reduces the amount of water and may lead to battery failure [33]. For lead-acid batteries, bismuth's existence is detrimental because on this metal, the hydrogen evolution reaction has a lower overpotential than on lead which will compete with the desired reactions on the catalyst surface. Therefore, much work has been performed to understand the effect of bismuth on battery performance [34, 35]. Another example is the hydrogen storage issue [36]. Titanium and its alloys exhibit very strong interaction with hydrogen and it is used as one of the hydrogen storage elements. Research shows that after hydrogenation, titanium samples formed the γ-hydride, which desorbed more than half of the hydrogen [37]

In many cases [38-41], the hydrogen evolution reaction is promoted on purpose because hydrogen is an attractive energy source. Molecular hydrogen is consumed in fuel cells to generate electricity with relatively high conversion efficiency [42]. As in the production of hydrogen, the electrolysis of water is a costly alternative than steam methane reforming [43]. In addition, rare metals, such as platinum, rhodium, or ruthenium are used as catalysts because of their low overpotentials among the metallic electrocatalysts [44]. In order to reduce the overpotential as well as the cost of using rare metals, organic compounds have been added to work with some cheaper catalysts. For example, 4,4′-bipyridine monolayer adsorbed on an Ag electrode catalytically enhances hydrogen evolution reactions in basic and neutral solutions [45]. Moreover, thiourea was discovered to facilitate the hydrogen evolution process in neutral solution [46].

In some other electrolysis reactions, hydrogen is not an ideal product and we desire to suppress the production as much as possible. For example, in the CO_2 conversion process, the hydrogen evolution reaction competes with carbon dioxide reduction in aqueous electrolyte [47-49]. This happens since hydrogen production takes less electrical energy than the formation of a carbon complex. As a consequence, protons will adsorb to the catalyst surface before carbon dioxide does, therefore blocking the active catalyst surface area for further carbon dioxide reduction. Details will be discussed later in chapters related to carbon dioxide reduction.

Some studies have demonstrated the ability of quaternary ammonium salts to suppress the hydrogen evolution reaction [50-52]. Tetraalkylammonium hydroxide

hydrates attract attention as the electrolytes because of their relatively large conductivity at low temperature [53-55], however, such low temperatures are not achievable in liquid aqueous electrolytes. Other quaternary ammonium salts, such as stearylbenzyldimethylammonium chloride and cetyltrimethylammonium bromide [56, 57], are regarded as ideal inhibitors added in electrolytes for reduction of hydrogen ions during the process of metal electrodeposition. In addition, monomeric and polymeric organic quaternary ammonium salts are tested in acid electrolyte as the corrosion inhibitors for metal catalysts [58, 59]. Moreover, tetrabutylammonium hydrogen sulfate and dibutyl ammonium hydrogen sulfate [50, 60] are used as minor addictives to other electrolytes to achieve hydrogen evolution reaction suppression. No data is available of these quaternary ammonium salts as electrolytes alone. Moreover, almost all the quaternary ammonium salts studied before are either toxic or expensive, or both. As a consequence, they are not practical electrolytes to achieve suppression of hydrogen evolution in large scale production.

2.2.2 General Discussion of Carbon Dioxide Conversion

Carbon dioxide is a potential carbon resource abundant on earth. There are a lot of ways to release carbon dioxide. It forms partially because of stoichiometric combustion of carbon, and its release is proportional to energy consumption. Moreover, living

animals' respiration process, volcanoes, hot springs, burning of plants and so forth can provide the large amount of carbon dioxide. During natural photosynthesis, as part of the carbon cycle, carbon dioxide can be absorbed by green plants, algae, and cyanobacteria. With the energy provided by sunlight and water as a proton donation compound, carbon dioxide is converted to carbohydrate energy for plants and oxygen is released as a waste product.

Due to the Industrial Evolution, the consumption of fossil fuels has led to the increase of carbon dioxide in the atmosphere from 280ppm to 390ppm [21] over the past century. Carbon dioxide contributed to almost one quarter of greenhouses gases, which is the main reason of global warming. Therefore, carbon dioxide utilization was one of the grand challenges identified in the Bell report [61].

Chemical fixation of CO_2 is an attractive technique for recycling carbon resources, as well as for reducing the atmospheric concentration of CO_2. However, under normal conditions, CO_2 is regarded as the most stable compound among carbon based substances. Therefore, for a long time, it has not been considered as a major industrial material.

As noted in the introduction, there are several ways to reduce carbon dioxide. Here, only electrochemistry methods will be discussed in detail. As early as the 19th century, researchers have studied the fundamentals of the electrochemical reduction of CO_2, and this topic has continued and attracted more attention in recent years.

In this section, we will first focus on the basic concepts related to electrochemical reduction of carbon dioxide and later discuss carbon dioxide reduction on different catalysts.

2.2.2.1 Equilibrium Potential of Carbon Dioxide Conversion

We would like to know the equilibrium potential for carbon dioxide reduction because this value can be compared with the experiment potential to determine the overpotential. Basically, the difference between the equilibrium potential of a reaction and the actual potential of the same reaction is called the overpotential, and it represents the lost energy in a conversion process. Not surprisingly, the overpotential should be reduced to minimum to make any electrochemical reaction economically sound. Therefore, we want to minimize the overpotential as much as possible.

During the electrochemistry reduction in aqueous solution, although the chemical activity of carbon dioxide is low, the equilibrium potentials of CO_2 reduction are not very negative as compared with that of the hydrogen evolution reaction (HER). From Nernst equation (discussed in a previous chapter), we notice that the change of pH value will shift the potential (Figure 2.7). Therefore, the standard potentials for CO_2 reduction and HER, estimated from thermodynamic data, decrease similarly with pH as is apparent in aqueous media at 25 ℃ with respect to SHE. The standard potentials are conveniently

given at pH 7.0, where most of the actual CO_2 reductions are measured. At PH 7.0, the value of the equilibrium redox potentials E_0 vs. the normal hydrogen electrode for the multielectron transfer reactions of carbon dioxide are demonstrated as follows:

Table 2.1 Equilibrium Potential for Carbon Dioxide Reduction to Different Products

Product	Reactions	Equilibrium redox potential (V)
Formic acid	$CO_2 + 2H^+ + 2e^- \rightarrow HCOOH$	-0.61
Carbon monoxide	$CO_2 + 2H^+ + 2e^- \rightarrow CO + H_2O$	-0.52
Formaldehyde	$CO_2 + 4H^+ + 4e^- \rightarrow HCHO + H_2O$	-0.48
Methanol	$CO_2 + 6H^+ + 6e^- \rightarrow CH_3OH + H_2O$	-0.38
Methane	$CO_2 + 8H^+ + 8e^- \rightarrow CH_4 + 2H_2O$	-0.24

2.2.2.2 Active Species during Carbon Dioxide Conversion

When carbon dioxide dissolves in aqueous solutions, it releases the carbonate ion and bicarbonate ion, and the reaction equations are as follows:

$$CO_2 + H_2O = HCO_3^- + H^+$$

$$HCO_3^- = CO_3^{2-} + H^+$$

Since the solubility of CO_2 is as low as 30 mM in water below 1 atm at the ambient temperature, the rate of electrochemical reduction of CO_2 in aqueous media is limited by the transport process. It is thus important to know whether HCO_3^- or CO_3^{2-}

can be electrochemically reduced. Or, in the aqueous solution, carbon dioxide molecules, carbonate ions and bicarbonate ions are all possible active species. However, Teeter and Rysselberghe reported that CO_2 is reduced to HCOOH at the Hg cathode [62] and showed that the polarographic wave height depends on the CO_2 concentration in the electrolyte solution. Their result reveals that the electroactive species of CO_2 reduction is the CO_2 molecule, neither HCO_3^- nor CO_3^{2-}. Although later articles argue that HCO_3^- can be reduced at different metal electrodes [63, 64], the results demonstrated partial current density of CO_2 reduction was below 0.1 mA cm^{-2} [65] and the data was not confirmed by quantitative chemical analysis [66]. Therefore, researchers conclude that in aqueous solution, HCO_3^- is decomposed to CO_2 first and the active species near the electrode is the CO_2 molecule [67, 68].

This conclusion still has its own suspicions. If the active species is the CO_2 molecule, based on thermodynamic calculations, the CO_2 reduction potential should be not very negative. However, the reduction potential of CO_2 is actually more negative than the values estimated from the thermodynamic data. Therefore, another form of carbon compound, $CO_2^{\cdot -}$ anion radical is presumed to be an intermediate species because it requires highly negative potential for formation.

Based on a polargraphis study, Jordan and Smith [69] first proposed that formation of $CO_2^{\cdot -}$ anion radical occurs by one electron transfer to CO_2 molecule as an initial step in CO_2 reduction process, as follows:

$$CO_2 + e^- = CO_2^{\cdot -}$$

Later Eyring and his coworkers [70] proposed the theory that CO_2 reduces to $HCOO^-$ at an Hg electrode in aqueous electrolytes containing HCO_3^{2-}, and discussed the reaction mechanism with $CO_2^{\cdot -}$ anion radical as the initial intermediate. The following equations demonstrate each step of $HCOO^-$ formation:

$$CO_2^{\cdot -} + H_2O = HCOO^{\cdot} + OH^-$$

$$HCOO^{\cdot} + e^- = HCOO^-$$

Hori et al. [71] further verified that the rate determining step is the first electron transfer to form $CO_2^{\cdot -}$ anion radical. Pacansky et al. [72] also suggested that $CO_2^{\cdot -}$ is ready to react as a nucleophilic reactant at the carbon atom. Aylmer-Kelly et al. experimentally verified that the $CO_2^{\cdot -}$ anion radical [73] with a Pb electrode in CO_2 saturated aqueous, acetonitrile and propylene carbonate electrolytes by ultraviolet (UV) spectroscopy, which confirmed that $CO_2^{\cdot -}$ anion radical is mostly present freely in both aqueous and nonaqueous electrolyte solutions. Schiffrin [74] and Hori [71] showed that the potential of the reduction does not depend on pH and H_2O is the proton donor in the formate formation from $CO_2^{\cdot -}$. Figure 2.8 illustrates the elementary steps of CO_2 reduction on different catalysts, and $CO_2^{\cdot -}$ was regarded as the intermediate in all the reactions.

Table 2.1 shows that CO formed with relatively lower overpotentials than $HCOO^-$ formation. It is suggested that CO is produced by a mechanism different from $HCOO^-$ formation which may proceed with free $CO_2^{\cdot -}$ intervening. Usually, adsorbed and stabilized $CO_2^{\cdot -}$ on an electrode will have the extra negative charge on O atoms [75],

which facilitates protonation leading to CO formation. During this process, adsorbed $CO_2^{\cdot -}$ would be nucleophilic at O atoms, and H_2O in aqueous solution will react with the O atom of adsorbed $CO_2^{\cdot -}$, forming $CO_{(ad)}$ and OH^- (figure 3).

In non-aqueous electrolytes, a reaction scheme is that one electron transfer to CO_2 molecule initiates the process, forming CO_2·-. However, $CO_2^{\cdot -}$ is not adsorbed on the catalyst surface, and is freely present in nonaqueous electrolyte solutions. As discussed, in aqueous solution, if H_2O is present in the electrolyte, a $CO_2^{\cdot -}$ will react with a H_2O molecule at the nucleophilic carbon atom and further reduce to formate. Here, the H_2O molecule reacts as a Lewis acid [76]. If an H_2O molecule is not available as in a non-aqueous solution, and plenty of CO_2 is present, a CO_2 molecule will play the role of a Lewis acid with the nucleophilic C of $CO_2^{\cdot -}$. The coupling of $CO_2^{\cdot -}$ and CO_2 will lead to formation of an adduct $(CO_2)_2^{\cdot -}$ [75, 77], which will lead to other products. Further discussion and more examples will be given in the following sections.

2.2.2.3 Carbon Dioxide Conversion with Different Metal Catalyst

Gold electrodes yield CO in CO_2 reduction in aqueous media [78, 79]. Some papers reported that kinetic aspects of the CO formation begin at −1.1 V vs. SHE [79]. This low overpotential indicates that the CO forms with intermediate intervention of $CO_2^{\cdot -}$ stabilized by adsorption on the electrode. This research also suggests that the CO_2

reduction proceeds in the 1st order with respect to CO_2, and the rate-determining step of the reaction is the first electron transfer to CO_2. For kinetics research, Ikeda et al. [80]demonstrated that CO formation at the Au electrode does not depend on the pH of the electrolyte, and that the proton donor is H_2O instead of the H^+.

Platinum electrodes also result in CO as the main product, which is strongly adsorbed on the Pt electrode [81, 82]. CO forming on the Pt surface has different structures. In addition to linearly bonded CO as the major adsorbed species, small amounts of bridged and multibonded CO are also detected[83, 84]. CO appears on the Pt surface as demonstrated in the following equation, and its appearance will decrease the catalytic active sites and inhibit further reduction of CO_2 in aqueous media.

$$CO_2 + 2H_{(ads)} = CO_{(ads)} + H_2O$$

Besides CO, some other products are discovered on the Pt catalyst. Brisard et al. [85] demonstrated that methanol and formaldehyde produced during CO_2 reduction process in 0.1 M $HClO_4$ was very low. In connection with this finding, Sakata et al.[86] showed that CH_4 is produced from CO_2 in 0.5 M $KHCO_3$ aqueous solution with a Pt electrode.

The major products at the Pd electrode are CO and formate in aqueous media [87]. Iwakura et al. [88] reduced CO_2 to formic acid at a palladized Pd/CO_2 interface in a gas compartment without any protic solvent. Methanol formation at the Pd electrode is also reported by some researchers, and these reports showed that methanol is produced with

very low overpotential or even a potential close to the equilibrium one. Moreover, adsorbed CO forms at the potential more positively than in continuous electrolysis [89].

2.2.3 Electrochemical Conversion of Carbon Dioxide in Aqueous System

Electrochemical reduction of CO_2 in aqueous solutions has many benefits: 1) it is possible to use water as the proton source; 2) it is much more economical than in organic solvents; 3) it is able to achieve higher densities.

However, because of water's presence, the hydrogen evolution reaction (HER) easily takes place by cathodic polarization, usually competing with CO_2 reduction. The HER rate is proportional to the proton activity in the electrolyte at a constant potential [90]. Most of the CO_2 reduction studies were done with neutral electrolyte solutions because HER is prevalent, particularly in acidic solutions, and CO_2 molecules do not exist in a basic solution.

In order to suppress the HER during the CO_2 reduction process, many previous studies were carried out in aqueous solutions with metal electrodes of high hydrogen overvoltage such as mercury and lead. For example, Eyring et al. [78] studied CO_2 reduction with an Hg electrode and showed that $HCOO^-$ was produced with high faradaic efficiency in neutral aqueous electrolytes. Suzuki et al. [71]discovered that the partial

current of $HCOO^-$ formation at an Hg electrode is not pH-dependable, but the HER is proportional to proton activity.

Ito et al. studied CO_2 reduction at Zn, Sn, In, Cd and Pb electrodes in hydrogen carbonate solutions with various alkali metal cations. They analyzed the products by infrared spectroscopy, and reported that formic acid is the only product from these metal electrodes. Here, carbon dioxide reduction on an In electrode to yield HCOOH at very negative value at –1.4 V vs. SHE [78].

After formic acid was discovered as the only major product in electrochemical CO_2 reduction in aqueous solutions, detections of methanol and methane with extremely low current density were reported. Hori and his coworkers [91] revealed that CO_2 reduction in aqueous solutions yields a measurable amount of CO, CH_4 and other hydrocarbons as well as formic acid. The product selectivity is greatly affected by the purity of the electrode metals and that of the electrolyte solution.

Metal electrodes are still divided into 4 groups based on different products formed in aqueous solutions (Table 3). Pb, Hg, In, Sn, Cd, Tl, and Bi give formate ion as the major product. Au, Ag, Zn, Pd, and Ga, the 2nd group metals, form CO as the major product. Cu electrode produces CH_4, C_2H_4 and alcohols in quantitatively reproducible amounts. The 4th metals, Ni, Fe, Pt, and Ti, do not practically give product from CO_2 reduction continuously. The classification of metals is not related with that in the periodic table. Sakata and his coworkers applied 32 metals to CO_2 reduction at –2.2 V vs. SCE in

0.05 M $KHCO_3$. They showed that Ni and Pt electrodes can reduce CO_2 to CO or formic acid under elevated pressure (60 atm) [92, 93].

In addition to the major products mentioned above, formation of higher carboxylic acids in aqueous solution has been disputed for many years. Bewick and Greener reported that electrochemical reduction of CO_2 produces malate from an Hg cathode, and glycolate from a Pb cathode in aqueous tetraalkyl ammonium electrolytes [94]. Although Wolf and Rollin confirmed Bewick and Greener's results [95], Kaizer and Heitz later examined the reaction, and concluded that Bewick and Greeners' results cannot be reproduced [96]. They showed that oxalic acid is reduced to glycolic, glyoxylic and maleic acids at Ni, Al, Pb and Hg electrodes in aqueous electrolytes in the presence of quarternary ammonium salts. But no oxalic acid was produced from these electrodes in aqueous electrolytes. Ito et al. [97]detected slight amounts of oxalic and propionic acids in tetraethylammonium aqueous electrolytes using Pb, Sn and In electrodes. Eggins et al. also supported Bewick and Greeners' results; they employed carbon and Hg electrodes in aqueous solutions of tetramethylammonium chloride and tetramethylammonium hydroxide. They obtained oxalic and glyoxylic acids in addition to formic acid, as confirmed by high performance liquid chromatography [67].

In addition, many papers reported that CH_4 or CH_3OH is formed from the CO_2 reduction at various metal and semiconductor electrodes near the equilibrium potential. However, the amount of CH_4 or CH_3OH appearing in these reports is extremely low, and any increase to reasonable value at higher overpotential is not shown. Reproducibility of

the findings has not been confirmed by other work. Thus, Table 4 does not contain the results with the partial current of the CO_2 reduction estimated below 0.1 mA cm^{-2}.

At PH 7.0, the value of the equilibrium redox potentials E_0 vs. the normal hydrogen electrode for the multielectron transfer reactions of carbon dioxide are demonstrated in Table 2.1. More experimental values related to carbon dioxide conversion to different products are shown in Table 2.2.

Table 2.2 CO_2 Reduction in Aqueous Systems

Product	Mechanism	Electrodes	Electrolyte	Potential
$HCOO^-$	$CO_{2(ads)} + e^- = CO_2^-{}_{(ads)}$ $CO_2^-{}_{(ads)} + BH + e^- \rightarrow HCOO^- + B^-$	Bi, Sb, Cd, Zn, Cu, Pb, Ga, Ag, Au, Ni, Fe, W, Mo, glassy carbon[98-101]Cu-Sn, Cu-Pb [102, 103]	$NaHCO_3$	
	$H^+ \rightarrow H^+_{(ad)}$ $H^+_{(ad)} + e \rightarrow H_{(ad)}$ $H_{(ad)} + CO_2 \rightarrow HCOO_{(ad)} \rightarrow HCOO^-_{(ad)}$	Sn [104, 105]	Na_2SO_4	-0.85 vs SHE -1.2 vs SHE

Table 2.2 (Cont.)

Product	Mechanism	Electrode	Electrolyte	Potential
CO	$CO_2 + H^+ + 2e^+ \rightarrow CO + H_2O$	Pt (100), Pt (110) [106]	$HClO_4$	-0.55 vs SHE
	$CO_2 + 2H_{ad} \rightarrow CO_{ad} + H_2O$	Pt (111) [107-109]	H_2SO_4	
	$CO_{2\ (ads)} + e^- \rightarrow CO_2^-{}_{(ads)}$	Au [110]	Phosphate buffer	
	$CO_2^-{}_{(ads)} + H_2O + e^- \rightarrow CO + 2OH^-$	Zn [97]	$KHCO_3$	Faradaic efficiency = 70% at - 1.4 V vs. Ag-AgCl
	$X + CO_2 \rightarrow XO + CO$ $X + 2CO_2 \rightarrow XO + 2CO$	Sn[104, 105]	Na_2SO_4	Tin metal is oxidized by CO_2 at less cathodic potentials (>-0.5 V vs. SCE).

Table 2.2 (Cont.)

Product	Mechanism	Electrode	Electrolyte	Potential
Hydro-carbons	CO_2 → CO → Surface-bound formyl → Surface carbene→ hydrocarbons	Cu [111], Cu-Ag [112]		-2.00V vs SHE
	$CO_2 + 6H^+ + 6e^-$ → 1/2 $C_2H_4 + 2H_2O$	Gas diffusion electrodes		
Methanol	$2CO_2 + 3Me + 4H_2O = 2CH_3OH + 3MeO_2$ $3MeO_2 + 12e^- + 12H^+ = 3 Me + 6H_2O$	Mo/MoO_2, Ru/RuO_2 [113-115] Prussian blue coated platinum[66, 116] Cu - Ni[103]	$KHCO_3$	-0.7V vs SHE for Mo; -0.5V vs SHE for Ru;-0.35V vs SCE for Pt;
	$MeO_2 + H^+ + e^-$ → MeOOH	$RuO_2 + TiO_2$ [117]	H_2SO_4	-0.1V vs SHE
Ethanol	Stepwise hydrogeneration by H_{ad}, and ethanol	Co+Fe[118]	KCl	

2.2.4 Electrochemical Conversion of Carbon Dioxide in Non-aqueous Solution

Non-aqueous solutions are utilized for electrochemical reduction of CO_2 because there are a lot of advantages [119]. First, the hydrogen evolution reaction, which always competes with carbon dioxide reduction process, can be suppressed because no water or just a small amount of water is present in the electrolyte. Second, even if water is needed in the reaction, its concentration can be accurately regulated. With diverse concentrations of water, the reaction mechanism that includes proton transfer could be more easily studied. Third, the solubility of CO_2 in organic solvents is much higher than in water. As a result, it is possible that the efficiency of carbon dioxide reduction will increase.

Different non-aqueous solutions are studied for CO_2 reduction, such as propylene carbonate (PC), acetonitrile (AN), DMF, and dimethyl sulfoxide (DMSO), and Methanol. Here we will give some examples about carbon dioxide reduction based on different electrolytes types and electrodes.

Tyssee et al. [120] showed that oxalic acid formed from CO_2 reduction at an Hg electrode in DMF. With Pb and Hg, Savéant and his coworkers [121] discovered that the electrochemical reduction of CO_2 in H_2O-DMF solutions give CO, HCOOH and $(COOH)_2$. The reaction schemes are assumed that a presumed intermediate $CO_2^{\cdot -}$ is not adsorbed on Pb or Hg and no specific interaction exists between intermediates or

products and the electrodes [122]. With tetraalkyl ammonium salt as the electrolyte, Kaizer and Heitz employed Cr-Mo-Ni steel as a cathode in AN and PC. They discovered that oxalic acid was the main product [96]. DMSO was used as the electrolyte with Au and Hg electrode in Haynes and Sawyer's chronopotentiometric study of CO_2 reduction [63]. They demonstrated that the reduction products at both electrodes are carbon monoxide and carbonate ion. If water is added to the solvent, some formate and bicarbonate ions were formed.

Ito et al. [87] tested tetraethylammonium perchlorate (TEAP) as the electrolyte with small water content. They employed various electrode metals for constant potential electrolysis of CO_2 reduction at –2.8 V vs. Ag/AgCl in PC. Based on this study, they classified these electrode metals into three groups: (1) Cu,Ag, Au, Zn, In, Sn, Ni, and Pt mainly yield CO; (2) Pb, Hg, and Tl give $C_2O_4^{2-}$ as the main product with small amounts of glycolic acid and glyoxylic acid if water is added in the electrolyte solution; and (3) Fe, Cr, Mo, Pd, and Cd form both $C_2O_4^{2-}$ and CO [76]. However, for the Pt catalyst, Tomita et al. [123] noticed that Ag+ ions in Ag/AgCl reference electrodes easily leaked. This situation will affect the products formation on the electrode and CO is consequently the major product from the contaminated Pt electrode. Nevertheless, a Pt electrode without Ag contamination gives $(COOH)_2$ as the major product.

Oxalic acid is also formed as a major product in non-aqueous electrolytes, and is further reduced to higher carboxylic acids (glyoxylic acid, glycolic acid etc.) at Cr-Ni-Mo steel electrodes [96], Pb and Hg electrodes [87]. The mechanism proposed is as follows:

$$2CO_2 + 2e_- \rightarrow (COO)_2^{2-}$$

$$(COO)_2^{2-} + 2H_2O + 2e^- \rightarrow HCO{-}COO^- + 3OH^-$$

$$HCO{-}COO^- + 2\,H_2O + 2e^- \rightarrow H_2C(OH){-}COO^- + 2OH^-$$

Methanol is an attractive solvent for non-aqueous electrolyte solutions. It has advantages that other non-aqueous solutions have: high CO_2 solubility, hydrogen evolution reaction suppression and a relatively easy-to-study mechanism. It also has advantages that other non-aqueous solutions do not have: it is inexpensive, has low toxicity, and can be produced at a large industrial scale. Although methanol is a non-aqueous solvent, it is normally classified as a protic solvent with many similarities with water. The product selectivity of CO_2 reduction depends on the electrode metal in methanol based electrolytes as well. Formate is favorably produced instead of oxalate in methanol based electrolytes. However, if some other additives are added into methanol electrolyte, there will be formation of other products.

Thus, many studied CO_2 reduction at metal electrodes in methanol-based electrolytes. Ohta and his coworkers[119] reduced CO_2 at a Cu electrode to produce CH_4, C_2H_4 as well as CO in high faradaic efficiencies. However, with PC or AN, hydrocarbon formation at a Cu electrode was not observed with small amounts of H_2O [87]. Based on this result, the hydrogen molecules in products are assumed from hydrogen of the hydroxyl group attached to a methanol molecule. Later, Ohta et al. [119] argued that the proton in the products is derived from residual water contained in methanol, but relevant

experimental data has not been showed.

Quaternary ammonium salts were utilized as an additive in methanol electrolyte in order to facilitate the carbon dioxide reduction process. Fujishima et al. [124, 125] employed tetraalkyl ammonium salts in methanol-CO_2 mixture and $HCOCH_3$ and CO are the major products. It was assumed that CO_2 first reduced to HCOOH and later transferred to $HCOCH_3$. They also showed that CH_4 and C_2H_4 were mainly produced in TEAP solution, instead of CO and $HCOCH_3$ [126]. In addition to metal electrodes, polyaniline and polypyrole were also investigated as electrode materials.

The following tables (Table 2.3 –Table 2.6) show the products of different electrode & electrolyte combinations [76]. (BC: Benzalconium chloride, HA: Hydroxylamin, TBATF: Tetrabutyl ammonium tetrafluoroborate, TEAB: Tetraethylammonium bromide, TEAH: Tetraethyl ammonium hydroxide, TEAP: Tetraethylammonium perchlorate. Ppy: Polypyrrole, PAn: Polyaniline. PC: polypropylene carbonate)

Table 2.3 Oxalate formation during CO_2 Reduction

Electrode	Electrolyte	Major products	References
Pb	PC, AN, DMF, TEABr	$(COOH)_2$, CO, glyoxylate, glycolate	[122, 127, 128]
	MeOH/TEAP, HA		[129]
	MeOH/TEAP, KOH	HCOOH, CO	[125, 130]
Hg	DMSO/TEAP, DMF, PC/TEAP	$(COOH)_2$, CO, HCOOH	[127, 128, 131-134]
Tl	PC/0.1 M TEAP	$(COOH)_2$	[128]
Pt	PC/TEAP, PC/TEAH, AN/0.1 M TEAP	$(COOH)_2$, CO, HCOOH	[123, 125, 128]
	MeOH/TBABF4	HCOOH, CO	[125]
Ni	PC/0.1 M TEAP	$(COOH)_2$, CO	[128]
	MeOH/TBAP	HCOOH, CO, CH_4, C_2H_4	[125]

Table 2.4 CO Formation during CO_2 Reduction

Electrode	Electrolyte	Major products	References
Cu	PC/0.1 M TEAP	CO	[128]
	MeOH/BC	CO, CH_4, C_2H_4	[124]
	MeOH/TEAP, TBABF4	CO, HCOOH, CH_4, C_2H_4	[125, 126, 135, 136]
	MeOH/LiCl, LiBr, etc.	CH_4, C_2H_4, CO	[137]
	MeOH/TBABF4	CO	[138]
	EtOH	CH_3OH	[139]
Sn	PC/0.1-M TEAP, MeOH/BC, TBABF4	CO	[119, 125, 128]
Ag	PC/TEAP, MeOH/KOH, BC, TBABF4	CO, HCOOH	[119, 125, 128, 140]
Zn	PC/0.1-M TEAP, MeOH/BC, MeOH/KOH, TBABF4	CO	[119, 125, 128, 141]
In	PC/0.1-M TEAP	CO	[128]
	MeOH/KOH	CO, HCOOH	[142]
Au	DMSO/TEAP, PC/0.1-M TEAP, MeOH/KOH, BC	CO, HCOOH	[119, 128, 131, 143]

Table 2.5 Oxalate and CO formation during CO_2 Reduction

Electrode	Electrolyte	Major products	References
Fe	PC/0.1 M TEAP	$(COOH_{)2}$, CO	[128]
Cr	PC/0.1 M TEAP	$(COOH)_2$	[128]
Mo	PC/ TEAP	$(COOH)_2$, CO	[128]
Pd	PC/0.1 M TEAP, TBAP	CO, $(COOH)_2$	[125, 128]
Cd	PC/0.1 M TEAP	CO, $(COOH)_2$	[128]
Ti	PC/0.1 M TEAP, MeOH/KOH	CO, $(COOH)_2$, HCOOH	[128, 144]
Nb	PC/0.1 M TEAP	CO, $(COOH)_2$, HCOOH	[128]
Cr-Ni-Mo Steel	AN/TEAH, PC/TEAH	HCOOH, $(COOH)_2$, glyoxylate, glycolate	

Table 2.6 Other Product formation during CO_2 Reduction

Electrode	Electrolyte	Major products	References
Re/Au	MeOH/LiClO4	CO, CH_4	[145]
Ppy-Re/Aua	MeOH/LiClO4	CO, CH_4	[146]
Ppy-Re, Cu/Aub	MeOH/LiClO4	CO, CH_4	[146]
Ppy/Pt	MeOH/LiClO4	HCHO, HCOOH, HOAc	[147]
Pan	MeOH/LiClO4, H2SO4	HCHO, HCOOH, HOAc	[148, 149]

2.3 Surface Enhanced Raman Spectroscopy (SERS)

More than thirty years ago, Fleischmann et al.[150] observed intense Raman scattering from pyridine adsorbed onto a roughened silver electrode surface. Their purpose was to develop a specific spectroscopic method to study electrochemical processes. This was the first discovery that a rough surface will enhance the Ramen scattering. In the early 1980s, SERS research accelerated dramatically. Its experimental facts were recognized as valid evidence for the essential features of the reaction mechanisms. Here, the physical principles and applications of SERS will be discussed in detail.

2.3.1 Physical Principle of SERS

After Fleischmann's observation, Jeanmaire et al. [151] recognized that the large intensities observed could not simply result from the increase in the number of scatterers present. They proposed that an enhancement of the Raman intensity occurred in the adsorbed state and tentatively proposed an electric field enhancement mechanism. With the same discovery, Albrecht et al. [152] argued that the increase of resonance Raman

scattering was because of molecular electronic states as well as their interaction with the metal surface.

Although SERS can be applied to examine a very large number of molecules adsorbed on the surfaces, relatively few metals can be used as the target surface. These metals include gold, silver and copper. There are different kinds of rough surfaces: electrode surfaces roughened by one or more cyclic voltammetry cycles, island films deposited on glass surfaces at elevated temperatures, films deposited by evaporation or sputtering onto cold substrates, colloids, nanoparticles and arrays of such particles prepared by lithographic techniques. Usually, the largest enhancements of SERS occur on the roughened surface at the nanoscale of 10–100 nm.

Many mechanisms were proposed in the early days of SERS to account for the experimental facts mentioned above. There are two primary theories. The former is called electromagnetic enhancement, focusing on the enhanced electromagnetic fields generated from the roughened surface structure. These electromagnetic fields are supported on metal surfaces with appropriate morphologies as well as on changes in the electronic structure of adsorbed molecules leading to resonance Raman scattering. The latter is a chemical theory, which only applies for species forming a chemical bond with the surface. Therefore, chemical theory cannot explain the observed signal enhancement in all cases. Nevertheless, the electromagnetic theory can apply even in those cases where the specimen is only physisorbed to the surface. Here we will discuss both of the theories in detail.

2.3.1.1 Electromagnetic Enhancement

To illustrate the theory of electromagnetic enhancement, it is important for us to know what plasmon is. The collective excitation of the electron "gas" of a conductor is called plasmon. If the excitation is confined to the near surface region it is called surface plasmon. Surface plasmon can either be propagating on the surface (e.g., of a grating), or localized on the surface (e.g., of a spherical particle).

In order for scattering to occur, the plasmon oscillations must be perpendicular to the surface. If they are in-plane with the surface, no scattering will occur. A rough surface can provide an area on which these localized collective oscillations can occur. Therefore, roughened surfaces or special arrangements of nanoparticles are typically employed in SERS experiments. Surface roughness or curvature is required for the excitation of surface plasmon by light. The electromagnetic field of light at the surface can be greatly enhanced with surface plasmon excitation. Through the interaction with the surface, the amplification of both the incident laser field and the scattered Raman field constitutes the electromagnetic SERS mechanism.

There have been many types of electromagnetic theory developed over the years which treat physical situations at different levels of completeness. Model systems which have been treated include isolated spheres, isolated ellipsoids, interacting spheres,

interacting ellipsoids, randomly rough surfaces treated as collections of hemispherical bumps and so forth.

The simplest treatments generate the electrostatic approximation using sharp boundaries and local, bulk dielectric functions for the substrate. Taking it one step further, full electrodynamic calculations have been carried out and the effects of a nonlocal dielectric response have been discussed [153]. The textbook example of a metal sphere in an external electric field illustrates the essential physics underlies the electromagnetic mechanism. If a spherical particle's radius is much smaller than the wavelength of light, the electric field is uniform across the particle. Under this condition, the electrostatic (Rayleigh) can be well approximated. The electromagnetic field generated at the surface of the sphere is related to the external laser field. Excitation of the surface plasmon greatly increases the local field experienced by a molecule adsorbed on the surface of the particle. For example, if a particle is localized under plane wave of light with a dipole field centered in the sphere, it does not only enhance the incident laser field but also the Raman scattered field.

The choice of surface metal is also dictated by the plasmon resonance frequency. Silver and gold are typical metals for SERS experiments because their plasmon resonance frequencies fall within these wavelength ranges, providing maximum enhancement for visible and near-infrared radiation (NIR) light. Copper's absorption spectrum also falls within the acceptable range for SERS experiments.[154] Although some research showed that platinum and palladium nanostructures also display plasmon resonance within visible

and NIR frequencies [155], they are still not considered as ideal metal surface for SERS experiment.

2.3.1.2 Chemical Bond Theory

While the electromagnetic theory of enhancement can be applied regardless of the molecule being studied, it does not fully explain the magnitude of the enhancement observed in many systems. For many molecules which can bond to the surface, a different enhancement mechanism has been described[156]. Therefore, a second enhancement mechanism, which does not involve surface plasmon, operates independently of the electromagnetic mechanism. Sometimes, systems are simultaneously operative with both mechanisms and the effects are multiplicative. However, because it has been very difficult to separate these two types of effects and electromagnetic enhancement always demonstrates the strongest influence, the early evidence for the existence of chemical enhancement was mostly inferential.

With electromagnetic enhancement, all molecules should be the nonselective amplifier for Raman scattering by all molecules adsorbed on a particular surface. However, the molecules CO and N_2 differ by a factor of 200 in their SERS intensities under the same experimental conditions. This is the first evidence of supporting chemical mechanism theory. The second line of evidence of a chemical mechanism comes from

potential-dependent electrochemical experiments. If the potential is scanned at a fixed laser frequency, or the laser frequency is scanned at a fixed potential, broad resonances are observed. There are two explanations of these observations: first, the electronic states of the adsorbate are shifted and broadened by their interaction with the surface; second, chemisorptions result in new electronic states which serve as resonant intermediate states in Raman scattering.

Evidence supports the latter assumption. Sometimes, the highest occupied molecular orbital (HOMO) and lowest unoccupied molecular orbital (LUMO) of the adsorbate are symmetrically disposed in energy with respect to the Fermi level of the metal [157]. Under this circumstance, charge transfer excitations can occur at about half the energy needed by the intrinsic intramolecular excitations of the adsorbate. In the near ultraviolet region, molecules commonly studied by SERS typically have their lowest-lying electronic excitations. These excitations would put the charge transfer excitations of this simple model in the visible region of the spectrum.

There are a lot of reprints of original articles related to this field[156, 158]. Chalmers et al. [159] studied Raman spectra of the α-, β-, ϒ- and smectic polymorphs of isotactic polypropylene. At 298 K the spectra of the polymorphs were very similar except in the antisymmetric C-H stretching region. However, at 16 K the Raman spectra of the polymorphs show different features in several wavenumber shift regions. Vo-Dinh et al. [160] discussed recent advances in chemical sensors and biosensors based on surface-enhanced Raman scattering (SERS) detection. They illustrated the different uses of the

SERS method for the identification and quantification of important environmental and biological compounds. In this article, the SERS-active probes involve silver-coated microstructured substrates designed to amplify the Raman signals of adsorbed molecules. More specific examples of application of SERS technique will be given in a later chapter.

2.3.2 SERS Research Application

As mentioned before, although surface-enhanced Raman scattering (SERS) is a useful technique with strongly increased Raman signals for wide range of molecules attached to nanometer sized metallic structures [161], it had not developed into a powerful surface diagnostic technique that can be widely used because of some obstacles. First, only three metals Au, Ag, and Cu could provide large enhancement, limiting the applications of other metallic materials of both fundamental and practical importance [162-164]. Second, the maximum enhancement with SERS active metals is achieved with a roughness scale of 10-100nm. These submicroscopic dimensions fabricated by various surface-roughening procedures inevitably consist of various microscopic dimensions. These non-ideal structures such as ad-atoms, ad-clusters, kinks, and vacancies as well as surface complexes should be avoided in SERS experiments.

In this section, we will first discuss the SERS research related to different metal electrodes, and then give more examples about SERS research for the hydrogen evolution reaction and the carbon dioxide reduction process.

For detecting single molecules, silver is used to make single molecule Raman spectroscopy a reality. Kneipp et al.[161] revealed that the detection of a single molecule of cresyl violet adsorbed on aggregated clusters of colloidal silver. Spectra observed in a time sequence exhibited the expected Poisson distribution for actually measuring 0 to 3 molecules. Nie and Emory [165] combined surface and resonance enhancement (SERRS) to detect a dye molecule adsorbed on the surface of a single silver particle. Constantino et al. [166] used the Langmuir-Blodgett (LB) monolayer technique to fabricate a single molecule LB monolayer containing bis(phenethylimido)perylene (PhPTCD), transferred it onto Ag island films to obtain spatially resolved surface-enhanced resonance Raman scattering (SERRS) spectra.

Klar et al. [167] measured the homogeneous line shape of the surface-plasmon resonance in single gold nanoparticles using a near-field optical antenna effect. They interpret the deviations of individual particles as being due to variations in the local nano-environment. Lee et al. [168] demonstrated microfluidic chips using novel thin micro gold shells modified with Raman tags using in situ surface-enhanced Raman scattering (SERS) decoding. SERS spectra from a variety of combinations of Raman tags were successfully acquired from the gold microshells moving in channels on a glass microfluidic chip. Eliasson et al. [169] showed the possibility of determining individual

organic compounds introduced into single living cell with SERS. Gold colloids were allowed to diffuse into lymphocytes and provided enhancement under Raman scattering.

Chant et al. [170] examined the adsorption of benaotriazole (BTAH) on copper in aqueous electrolytes by means of SERS. Spectral figures suggested surface attachment of the molecular structure and demonstrated transformation from adsorbed benzotriazole to a CuIBTA film at higher potentials. Sugimasa et al. [171] investigated the adlayer structures of benzotriazole (BTA) on different copper structures in aqueous $HClO_4$ solution. The BTA molecules were adsorbed in parallel to the surfaces of Cu(110) and Cu(100), whereas they stacked vertically on Cu(111) to form molecular rows. Moreover, the molecular orientation of BTA was found to affect electrochemical reactions, such as the hydrogen evolution reaction on the Cu electrodes.

Besides SERS active metals, SERS on net transition metals is also generated by applying various roughening procedures or optimizing the performance of the confocal Raman microscope. Meanwhile, ordered nano-structures of transition metals were introduced as a promising class of highly SERS-active substrates. In addition, researchers have extended SERS to the study of other non-metallic surfaces too.

Yamada et al. [172] revealed that surface enhanced Raman spectra of adsorbed pyridine were clearly observed on Ni and Pt as well as on Ag and Au. Results showed a remarkable intensity dependence on the excitation wavelength. Meanwhile, by using confocal microprobe Raman spectroscopy and a unique electrochemical pretreatment procedure for the Pt surface, Tian et al. [173] investigated the adsorbates such as SCN^-

and CO on bare Pt electrodes in a wide potential region. The SERS data yielded detailed information that surface coverage, coadsorbate, electrolyte ions, and electrode potential are affected by surface bonding. Not the same as the roughened Ag, Cu, and Au electrodes, the dispersed Pt surface has shown better stability and reproducibility for the Raman measurements. In another study, Ren et al. [174] reports pyridine at Pt and Ni electrode surfaces utilizing a highly sensitive confocal Raman microscope. They discovered that the study can be extended further to the commonly interesting hydrogen adsorption process at roughened Pt electrodes. Guo et al. [175] showed a remarkable SERS activity on iron nanoparticles. Electrocatalysis of H_2O_2 with high efficiency in the presence of oxygen over the iron nanoparticles is demonstrated. Rubim et al. [176] discovered that Raman scattering from silver covered glassy carbon is affected. This is tentatively assigned to the scattering of intermediate electrons by the phenons. Aramaki et al. [176] investigated ofpyridine and pyridinium chloride adsorbed on iron using a SERS-active silver electrode covered with an iron layer. They discovered that apyridine molecule is chemisorbed on the iron surface.

To understand fundamental aspects of the CO_2 electroreduction on different catalyst surface, SERS is utilized to provide useful information about the possible adsorbed reaction intermediates, and then delineate the mechanisms involved. Batista et al. [177] studied carbon dioxide electroreduction on a copper electrode in K_2SO_4 aqueous solutions with different pH values. The spectral features indicate the presence of a structure containing a double C=C bond, a carboxyl group, and C-H bonds on the

electrode's surface. Zheng et al. [178] conducted research on the photoelectrocatalytic effect for the reduction of CO_2 mediated with methylviologen at mercury, polished silver and roughened silver electrodes using electrochemical and SERS techniques. They discovered a larger photoelectrocatalytic effect for the reduction of CO_2 at the roughened silver electrode than on mercury and polished silver electrodes. Ichinohe et al. [179] investigated the electrochemical reduction of CO_2 at a polycrystalline Ag electrode in $KHCO_3$ aqueous solution. Raman scattering from the oxidation-reduction cycled Ag electrode suggests the formation of CO and HCOOH by CO_2 reduction. Smith et al. [180] also studied the electrochemical reduction of CO_2 on the copper electrode surface with SERS. Their focus is the effect of different oxidation reduction cycles on the observed SERS. The time-dependent decay of the SERS bands and the increase of a new band was attributed to the formation of a poisoning species on copper catalyst.

2.4 Figure

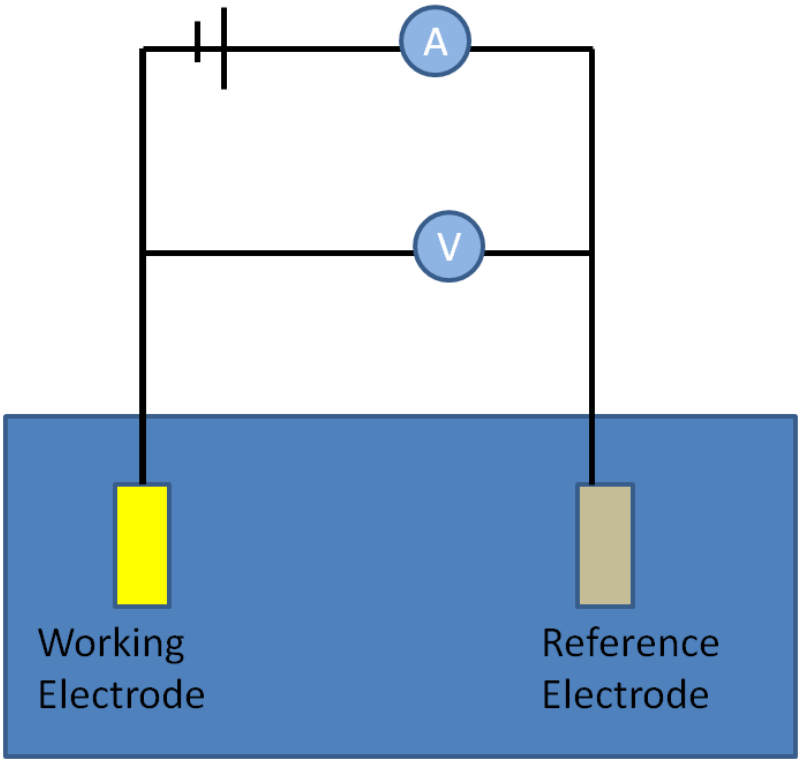

Figure 2.1 Two-electrode system

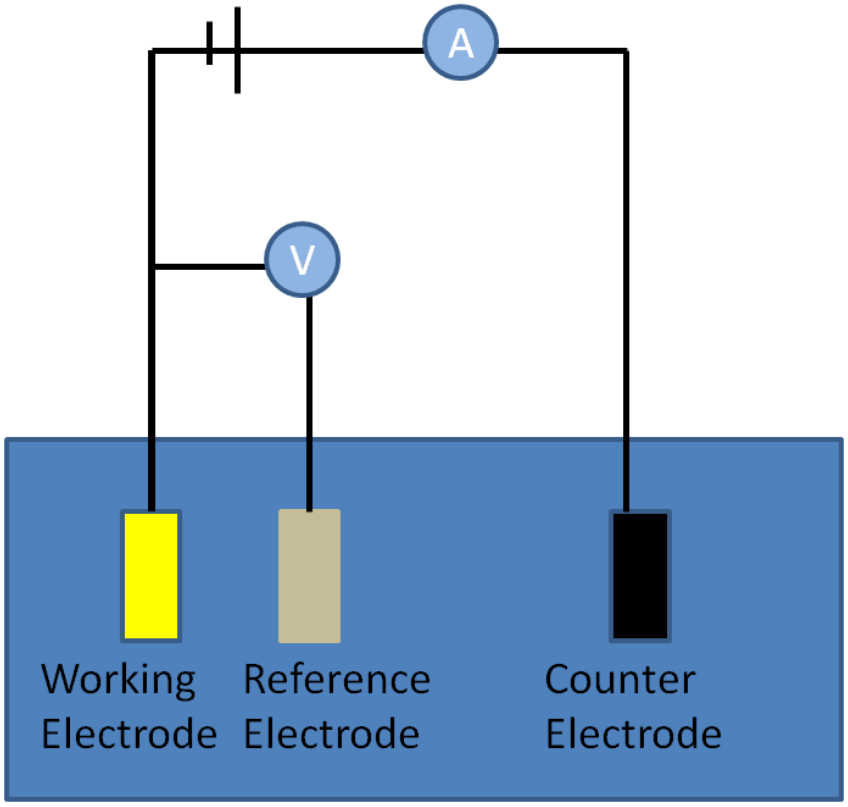

Figure 2.2 Three-electrode System

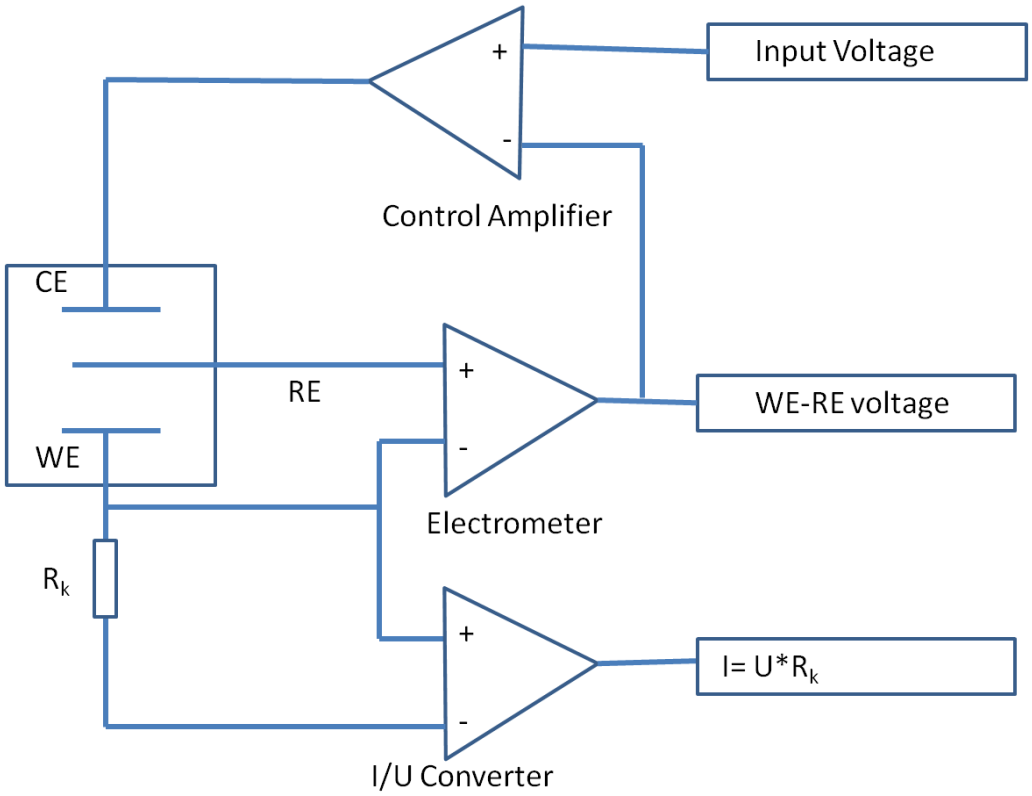

Figure 2.3 Circuit diagram of potentiostat

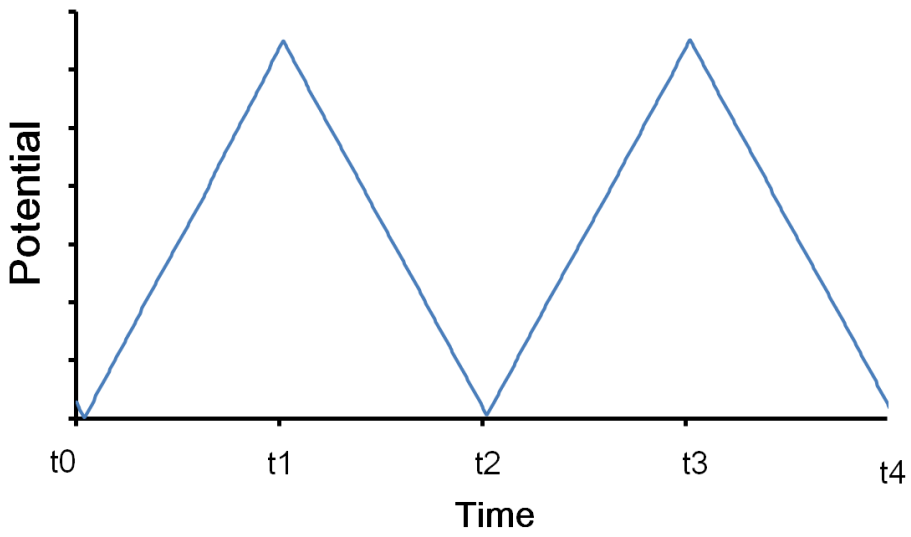

Figure 2.4 Typical potential sweep

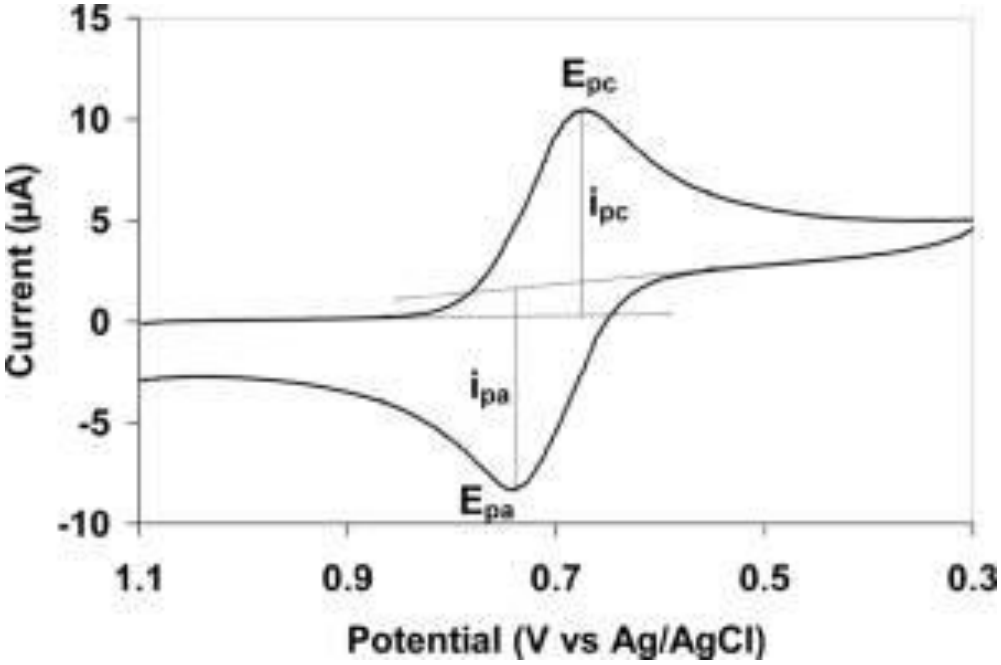

Figure 2.5 Typical cyclic voltammogram[22]

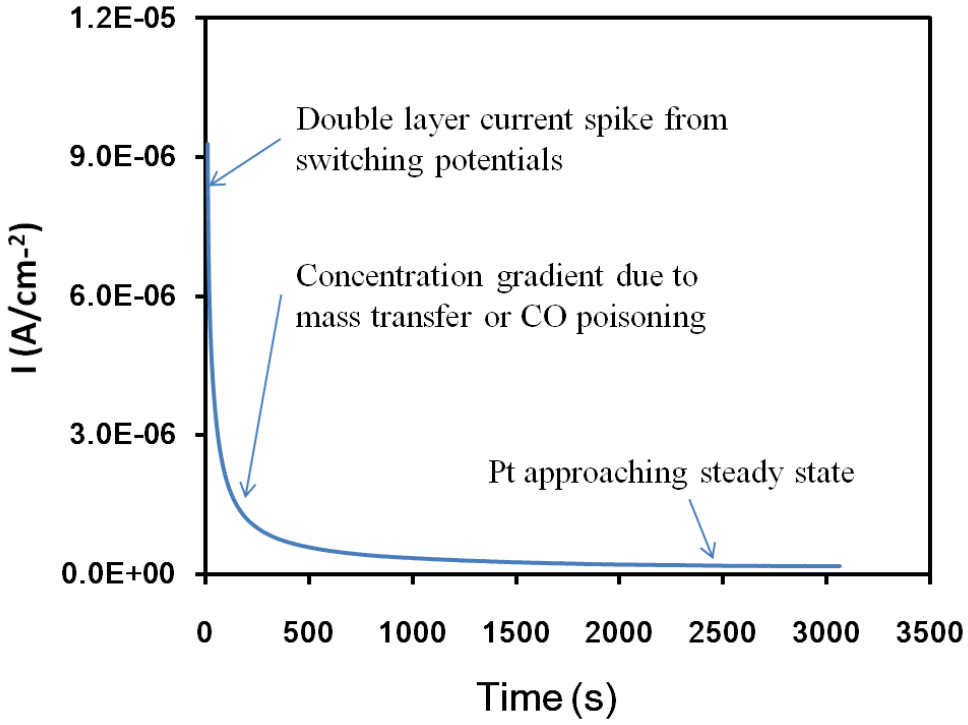

Figure 2.6 Chronoamperometric data for Pt black on gold electrode (HiSpec 1000®, Alfa Aesar) electro-oxidation of formic acid at 0.2 V vs. RHE in 0.01M HCOOH with argon degassed atmosphere.

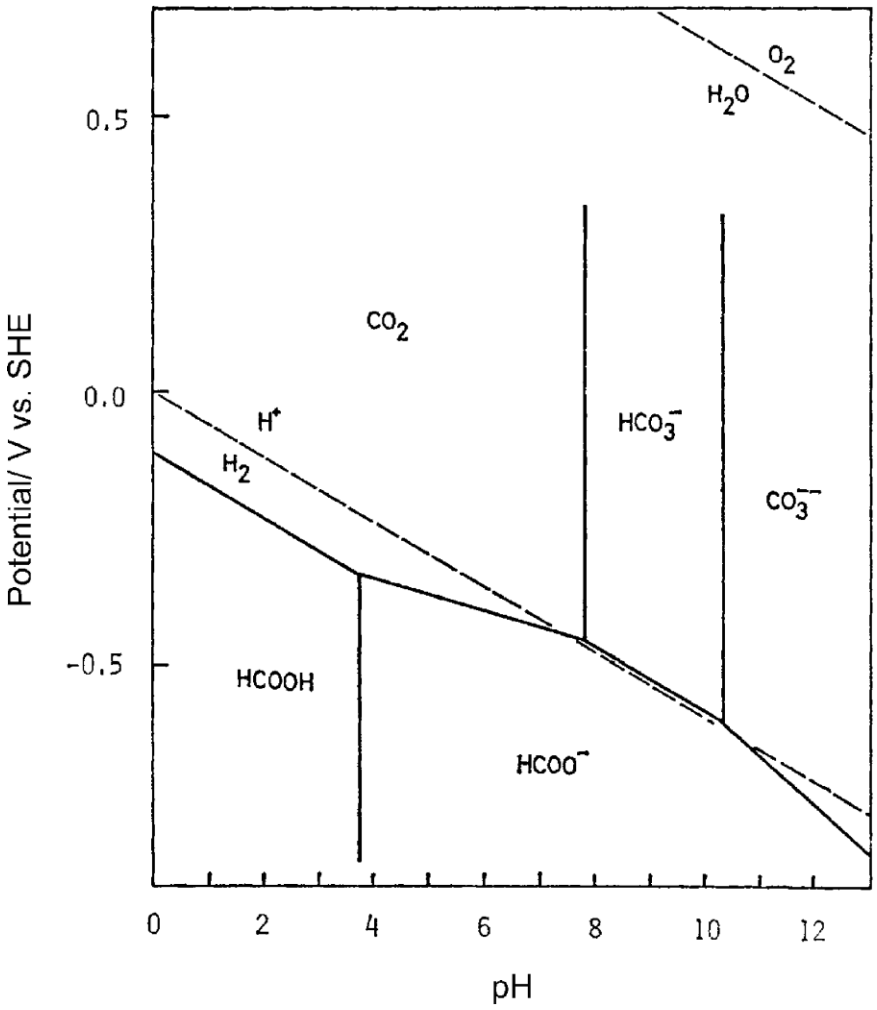

Figure 2.7 pH potential diagram of CO and its related substances. pH potion tential relations for water are shown in broken lines [181].

(1) $CO_2^{\cdot -}$ not adsorbed on metal electrode

Aqueous media (Cd, Sn, In, Pb, Tl, Hg)

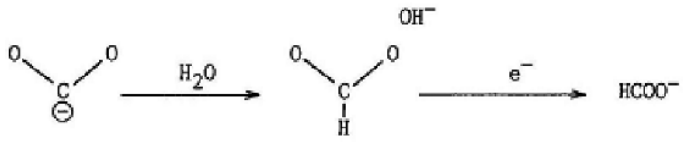

Nonaqueous media (Pb, Tl, Hg)

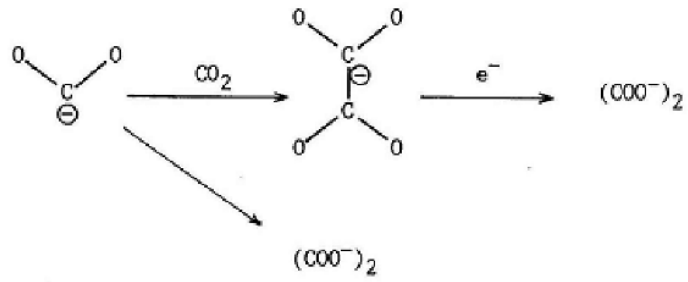

(2) $CO_2^{\cdot -}$ adsorbed on metal electrode

Aqueous media (Au, Ag, Cu, Zn)

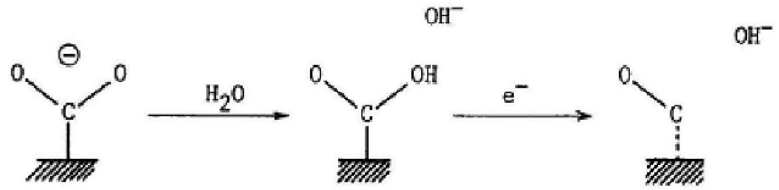

Nonaqueous media (Au, Ag, Cu, Zn, Cd, Sn, In)

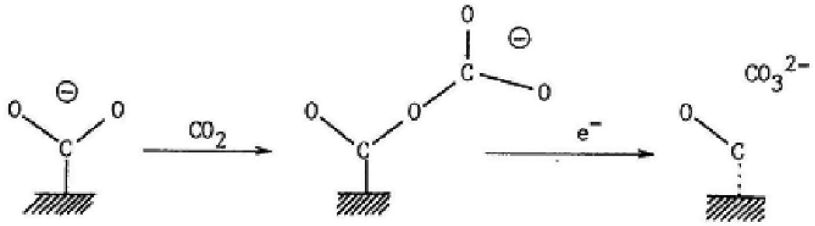

Figure 2.8 Reaction scheme of the electrochemical reduction of CO_2 [181].

Chapter 3: Statement of Purpose

The key long-term question that we are to consider in our work is: What does the choline based electrolyte contribute to the conversion of CO_2 that allows the reaction to proceed at such modest potentials? In particular, we wish to test the hypothesis that imidazolium cation of the choline ion is the factor that interacts with the catalyst surface. Because of the interaction, the hydrogen evolution reaction is suppressed and CO_2 reduction occurs at a much less negative potential than before.

In order to test that hypothesis, we need to answer several questions:

1. Whether and how will choline based electrolyte achieve hydrogen evolution reaction suppression?

In our research, we pursue the suppression of hydrogen evolution reaction in water solutions. Choline based electrolytes are employed in this research as an electrolyte suppressing the hydrogen evolution reaction. We propose to show the choline based electrolytes suppresses the hydrogen evolution by shifting the reacting potential to lower values. When dissolved in water, choline based electrolytes release amine cation: choline ion. By interfering with the hydrogen adsorption process, the amine cations influence the evolution of hydrogen. In this process, a single layer of choline cations is formed on the

surface of the catalyst, which blocks the hydrogen adsorption on the catalyst surface, and therefore blocks the reaction of hydrogen evolution.

2. Whether and why CO_2 reduction will happen in various catalysts with much lower overpotentials?

We would like to demonstrate the ability of choline based electrolytes to reduce the overpotential in carbon dioxide reduction process. In choline based electrolytes, the hydrogen evolution reaction was suppressed because choline based electrolytes reduce the hydrogen adsorption. Here, we would like to show it does not only suppress hydrogen evolution reaction but also lowers the overpotential for CO_2 conversion. As a result, the overpotential for carbon dioxide reduction was reduced to much lower values in different catalysts, which is very beneficial to efficient large-scale production.

3. What are the main reaction products formed during the experiment?

We will study which species are formed during the reaction of CO_2 reduction through electrochemical and spectroscopic study.

4. Whether different ions will affect the electrochemical reaction process in choline based electrolyte?

Another key question is whether other types of anions will affect the HER and CO_2 reduction process. By using different kinds of choline salts, we can make valuable comparison.

Chapter 4: Experimental Apparatus and Procedure

4.1 Electrochemical Cell

The electrochemical cell used for this study consists of a custom-designed glass three-electrode cell including a working electrode, a counter electrode, and a reference electrode. Supporting equipment includes valves, flow lines, and a potentiostat (Solartron SI 1287 attached to a PC using the CorrWare software). The design details are described below.

4.1.1 Three-electrode Glass Cell

The electrochemical cell is constructed from glass by the chemistry department glass shop and is cleaned in a sulfuric acid bath. It is designed to give a nearly contamination-free environment with a controlled atmosphere. It is a 150 mL flask with three 14/20 joints at the top and on the sides. These joints allow insertion of the rotating disk electrode, the counter electrode, and solution additions as necessary. In addition to the glass cell body, it consists of the working electrode, the counter electrode, the reference electrode, the lure joint for inlet gas, a glass tube to the reference electrode

reservoir and a glass fitting. Figure 4.1 depicts the design of the three-electrode cell shown with the working electrode, counter electrode, and reference electrode installed.

4.1.2 Working Electrode

The working electrode consisted of a Teflon tube with cylindrical gold slug, which was inserted into the tube. The rotating disk electrode was screwed onto a RDE controller which can adjust the rotating speed during the experiment. The controller was attached to the potentiostat during experimentation.

4.1.3 Counter Electrode

Two kinds of counter electrodes were used in this experiment. For platinum and palladium catalysts, the counter electrode is made by a 25x25mm platinum mesh (size 52) attached to a 5-inch platinum wire (99.9%, 0.004 inch diameter). For the gold electrode, the counter electrode is made by a 25x25mm gold mesh (size 52) attached to a 5-inch gold wire (99.9%, 0.002 inch diameter). The mesh was cleaned carefully before each experiment.

4.1.4 Reference Electrode

The reference electrode is a silver-silver chloride electrode with a Flexible Connector. It was stored in concentrated potassium chloride to maintain a constant chloride concentration, which can maintain a constant reference potential (±2 mV) over several months. However, because all results are reported versus the reversible hydrogen electrode (RHE) and the standard hydrogen electrode, the reference electrode was calibrated versus RHE and SHE frequently. The calibration method is described in later chapters.

4.2 Electrochemical Cell Setup

4.2.1 Preparation of Catalysts on the Working Electrode

The working electrode is prepared by using catalysts in the powder form. Although materials such as metal foil can also be simply used with an alligator clip attaching the foil, power-form catalysts have their own advantages, such as more reaction surface area and easier surface area calculation.

To prepare the powder based working electrode, a catalyst ink was mixed and dried onto an electrode surface. The ink was a combination of 5.6 mg metal power and 1 g water. Some researchers use Nafion® as a binding agent because it makes the catalyst stick better on the metal surface. Here, however, we avoid using such kinds of binding agents because it is not inert in some electrolytes. There are two kinds of rotating disk electrodes which we can choose from: gold and glassy carbon. Gold electrode was chosen over glass carbon because without a binding agent because the catalyst ink typically sticks better to the gold electrode. Please note that the electrode was polished with 300-grain or finer sandpaper before adding catalyst powder to make sure no debris could be observed coming off the electrode on the Kimwipes®. For the case of adding catalyst powder onto gold electrode, the catalyst was fixed to the working electrode in the following manner:

1. Prepare the solution with 5.6 mg of catalyst powder and 1g of Millipore® water,
2. The solution was then sonicated for another 10 minutes,
3. 12.5 μL of solution was then placed onto a gold working electrode using a micropipette,
4. The solution was allowed to dry under air for at least one hour,
5. The catalyst layer was then rinsed with Millipore water and used.
6. Check to make sure no catalyst particles detach during experimentation.

When the experiment was finished, the catalyst was removed from the electrode by wiping it off with a Kimwipe® and rinsing with Millipore® water. The electrode was again polished with sandpaper as before and wiped with Kimwipes® and rinsed with Millipore® water.

4.2.2 Platinization of the Counter Electrode

In order to create high surface area of the counter electrode, the counter electrode surface area was increased by platinization before experiments were carried out. In general, this only needs to be done once for the counter electrode, and we do not apply it to the gold counter electrode because gold is not inert in some environments with strong acid. The typical platinization procedure follows steps described in the references [182, 183].

4.2.3 Calibration of the Reference Electrode

To report results in terms of the RHE, the Ag/AgCl reference electrode had to be calibrated versus the RHE. Typically, a RHE is set up by bubbling hydrogen over the platinum counter electrode and the potential of this electrode is compared to the reference

electrode. All potentials can then be converted to RHE potentials by subtracting this difference. The following steps were taken to calibrate the reference electrode [184]:

1. Prepare the targeted electrolyte solution and fill the cell and reference electrode reservoir with this solution,
2. Place the reference electrode in the reference electrode reservoir and attach the reference electrode lead from the potentiostat to the reference electrode,
3. Attach both the working electrode lead and the counter electrode lead from the potentiostat to the wire attached to the platinum mesh counter electrode of the electrochemical cell,
4. Bubble hydrogen under the counter electrode in the cell,
5. Measure the open cell potential difference between the reference electrode and the counter electrode until it stabilizes. It usually takes 10 minutes.
6. This value can then be used to convert all potentials to the absolute scale of the RHE.

To convert the Ag/AgCl reference electrode with SHE, we just need to add 0.197V on the experimental value. No pH effect needs to be considered.

4.2.4 Electrolytes Used in the Electrochemical Cell

Several kinds of electrolytes were used in this research. For investigating the hydrogen evolution reaction, four kinds of electrolyte are used: 0.5M choline chloride, 0.5M sodium bicarbonate, 0.5M sulfuric acid and buffer solution. Meanwhile, formic acid solution was prepared with or without 0.5M choline chloride, with concentrations of 0.001M, 0.01M and 0.03M. For carbon dioxide reduction research, only 0.5M choline chloride was used. For examining the effect of different cations in choline based electrolytes, two other choline products were utilized: 0.05M choline BF_4 and 0.05M choline acetate.

In all cases, solutions were prepared using Millipore® water. After each use, the solution was drained from the electrochemical cell. The cell was then triple rinsed thoroughly with Millipore® water and put into the acid base.

4.3 Typical Electrochemical Experiment Procedure

4.3.1 Cyclic Voltammetry

In order to gain a close examination of reactions on the catalyst surface, the cyclic voltammetry (CV) technique is used. CV has many applications such as discovering the surface reaction, surface area calculation and products identification. For discovering the surface reaction, every time when there is a surface reaction, it creates a Faraday peak at a certain potential value. Based on the control experiment or literature data, we could determine the specific surface reaction. The figure below demonstrates the typical CV curve of Pt in sulfuric acid solution from our experiment. From this figure, we can observe the clear hydrogen or proton reaction peaks. In the hydrogen region, protons interact with the catalyst surface, adsorbing to the surface in the cathodic scan and desorbing in the anodic scan. The multiple peaks reveal that the hydrogen adsorbs or desorbs on different facet of the Pt catalyst. In the oxygen region, hydroxide ions oxidize the surface in the anodic scan and are reduced from the surface in the cathodic scan. Between these regions is the double layer region, in which only double layer charging occurs. The increased surface area from nanoparticles (as compared with smooth polycrystalline electrodes or single crystals) results in a higher current magnitude in this region.

Usually, the supporting electrolyte consisting of diluted sulfuric acid was used to determine the cleanliness of an electrode surface and the electrochemical surface area (ECSA). From the Figure, we can also determine the ECSA of a high surface area catalyst. Integration of the hydrogen desorption peaks can be used to calculate the charge passed for the one or two electron process, respectively. It is widely accepted that both

platinum and palladium can be characterized in this manner, where the surface area from the hydrogen peaks is determined from the relationship of 210 C cm^{-2}. [185, 186]

4.3.2 Chronoamperometry

Chronoamperometry experiments were also performed when the potential was held constant for a period of time. It is used to study the stability of the catalyst. The typical experiment of this nature was carried out at 0.2 V vs. RHE for formic acid oxidation. The experiment duration was as long as 8 hours to construct plots using pure 0.1 M formic acid and formic acid with 0.5M choline chloride. Sometimes, a rotating disk electrode was used for these experiments for two reasons: to probe kinetics without contributions from mass transport and to remove carbon dioxide bubbles formed at the catalyst surface during formic acid oxidation. The rotation speed was chosen at 2000 rpm. It was previously shown that there was very little variation in current at different rotation speeds since the reaction is sluggish enough to be kinetically limited [184]. Therefore, the rotation speed was chosen primarily to permit adequate removal of carbon dioxide bubbles from the electrode surface.

4.3.3 Stripping Experiment

Every reaction on the catalyst surface will create a Faraday peak, and every product has its own Faraday peak on a certain catalyst surface. Therefore, we can identify the adsorbed products based on the location of these Faraday peaks. This method is called a stripping experiment. Basically, in order to produce the ideal products, potential was held constant at a certain value for enough time, usually around 20 minutes. The value of the potential can be decided based on the CV curve. Later, three cycles of CV were conducted from very positive values to negative values. Please note, however, the positive value we choose should be higher than the target products stripping value we find in control experiment or literature. If there are adsorbed products on the catalyst surface, they will be stripped off in the first cycle, creating a typical Faraday peak. In the second and third cycles, because there is no or very little adsorbed species on the surface, the Faraday peak will disappear or decay. From the CV data, we could identify the products.

Specifically, the potential is held at the value where carbon dioxide reduction dominated and no hydrogen evolution reaction is seen for 20 minutes. Cyclic voltammetry is once again conducted at a sweep rate of 10mV/s in the range from 1V to carbon dioxide reduction dominate potential for three cycles. In order to have a control experiment which demonstrates the CO stripping peak or formic acid stripping peak, CO stripping voltammetry and fomic acid stripping voltammetry are also conducted during the experiment. For CO stripping, the electrolyte is saturated with carbon monoxide by bubbling the CO for 20 minutes. During these 20 minutes, the working electrode is held

at -0.5V vs SHE. Then argon is blown into and over the electrolyte solution for 30 minutes to remove the remaining CO in the electrolyte. Then two voltammograms are monitored. For formic acid stripping, electrolytes with different concentration of formic acid (0.001M, 0.01M and 0.03M) are tested. After the blank cyclic voltammetry taken by bubbling argon into the 0.5M choline based electrolytes, different amounts of formic acid are added into the electrolyte. Cyclic voltammetry is taken again and different cyclic voltammetry figures are compared to acquire the formic acid reaction peak in the electrolyte. Ideally, the faraday peak demonstrates the formic acid should be increased with the increase of its concentration.

4.4 Typical SERS Experiment Procedure

4.4.1 SERS Experiment Preparation and Setup

4.4.1.1 Electrode surface polishing

The working electrode for SERS experiments was a 1 cm diameter Au or Ag disk. The surface of the electrode was first mechanically polished on 800, and 1200 grit

Carbimet paper (Buehler) and using 9, 3, 1, 0.25 micron aqueous diamond suspension on a Microcloth pad (Buehler).

Following the procedure described previously [187], the crystal was roughened electrochemically in 0.1M potassium chloride. For Au crystals the potential was first held at -1.16V for 10 min and stepped to -0.06V for 2 min. The potential was then swept from -0.06V to 1.44V and back for 20 oxidation reduction cycles at 750mV/s. During each cycle, the potential was held at -0.06V for 30 s and then at 1.44 V for 2 s. Finally, the potential was held at -0.36V for 2 mins to desorb adsorbed Cl. For Ag crystals the anodic limit was 0.2 and the cathodic limit was -0.3 versus Ag/AgCl with a scan rate of 500 mV/s for the same amount of cycles as with Au. After potential cycling, the roughened disk was rinsed with coupious amounts of 18.2 MΩ water (Milli-pore).

4.4.1.2 SERS Electrochemical cell setup

A flat quartz window was used, and the working electrode was pulled slightly back from the window. Room temperature SERS were obtained using an in-situ cell that was described previously (Cite: M. E. Biggin, Ph.D. Thesis, University of Illinois at Urbana-Champaign, Champaign, IL (2001)). An He–Ne laser (λ=632.8 nm,Meridith Instruments) or a diode pumped laser (λ=532 nm, CrystaLaser) was projected onto the Au

or Ag surface at ~45 °incidence. Scattered radiation was collected with F/4 focusing lens (Canon) and focused at the entrance slit of a monochromator (Acton Spectrapro). A 1200 grooves/mm grating dispersed radiation onto a cooled charge-coupled device (Andor). The typical acquisition time was 30 s.

4.4.2Electrochemical Surface Enhanced Ramen Spectroscopy

The solution cell, optical layout and procedure used here were a modification of those used in earlier work[188]. The glass and Kel-F cell was equipped with a solution delivery port, a purge gas delivery port, an outgas bubbler, a counter electrode inserted through a Teflon fitting, solution port leading to a capillary bridged reference electrode, and an adjustable plunger for the electrochemically roughened surface (the working electrode) behind a quartz window sealed with an o-ring. The working electrode was positioned such that it was pulled end of the plunger by Teflon tape, and contact was made to the back side of the working electrode by using a loop of Au wire placed between the electrode and the o-ring. The counter electrode was a Pt wire and the reference was Ag/AgCl.

Potential control was achieved using a CV-27 potentiostat (Bioanalytical Systems). Before introduction into the cell, solution was purged with Ar (g). Solution was

then delivered to the cell and subsequently to the bubbler and reference electrode compartment via Ar pressure through Teflon tubing. Furthermore, Ar was bubbled through the cell throughout the experiment.

4.5 Figures

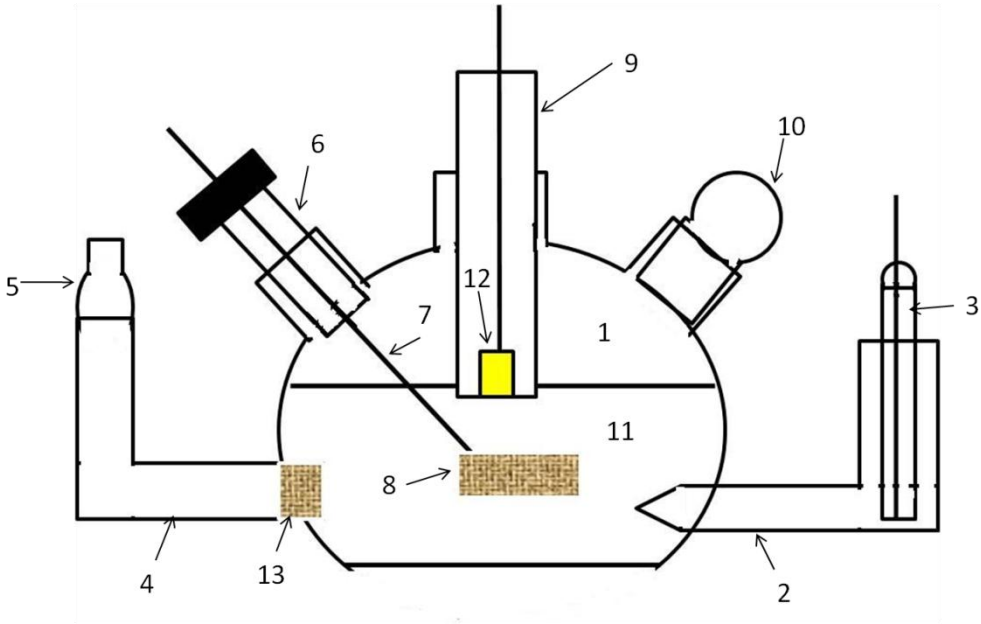

Figure 4.1 A schematic of the electrochemical cell, 1-Three neck flask, 2- Luggin Capillary, 3- Ag/AgCl reference electrode, 4- Sparging tube, 5-Lure joint for sparging gas, 6-Counter electrode, 7-Platinum or gold wire (counter), 8-Platinum or gold mesh (counter), 9-working electrode, 10-Glass frit, 11-Electrolyte, 12- Working electrode disk, 13-Glass cap

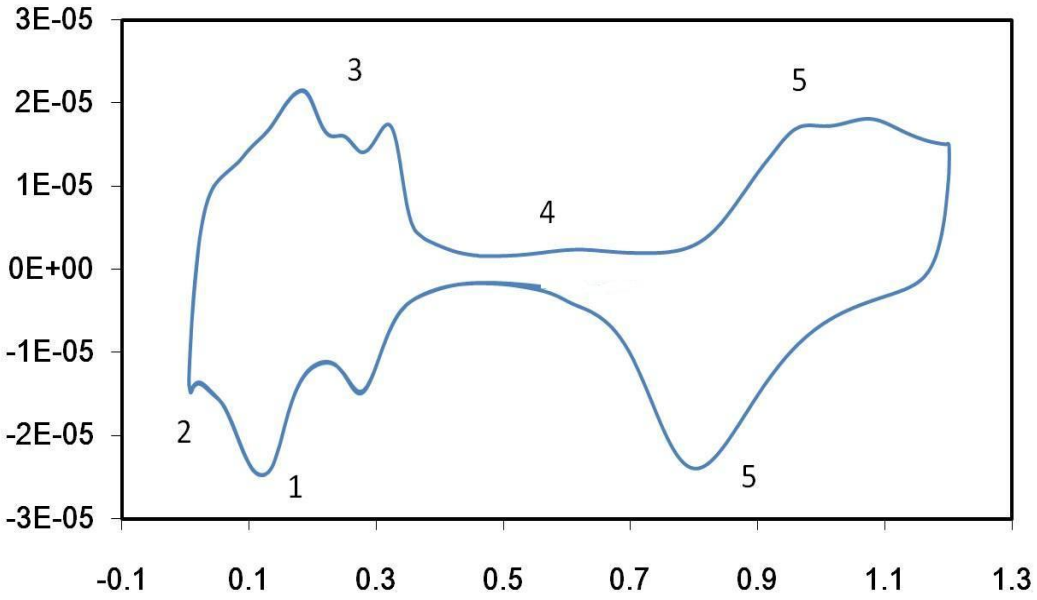

Figure 4.2 (1) Hydrogen adsorption (2) Hydrogen evolution reaction (3) Hydrogen oxidation reaction and desorption (4) Double layer and (5) Palladium oxides formation–dissolution.

Chapter 5 Monolayer of Choline Ion Can Suppress the Hydrogen Evolution Reaction and Enhance the Desired Reactions

5.1 Introduction

The content in this chapter is a continuation of our efforts to determine whether monolayers of organic molecules could be used as "helper catalysts" to speed desired electrocatalytic reactions and inhibit undesirable reactions. The idea of a "helper catalyst" is described in Masel [189]. When a monolayer of an organic compound adsorbs on a metal surface, the presence of the organic compound can change the binding energy of key intermediates. That can lead to changes in rate. For example the adsorption of a cationic species such as a quaternary amine tends stabilize anionic intermediates and destabilize cationic intermediates. If the amine binds too strongly, it will simply poison the surface, but if the binding strength is modest, rate enhancement is possible.

At this point there is very little experimental evidence outside of our laboratory that adsorbed molecules can act as helper catalysts although we have started to publish results [189, 190]. Still, previous workers had found tetrabutylammonium hydrogen sulfate and dibutyl ammonium hydrogen sulfate[50, 60], can suppress the hydrogen evolution in batteries, so there is the possibility of real effects.

The objective of this paper was to determine whether, a simple quaternary amine, choline chloride, could be used as a helper catalyst. Choline chloride is a common food additive for livestock that is also sold as a dietary supplement for humans. It is inexpensive and edible so it is an attractive as a "helper catalyst". Importantly, the structure of choline chloride is such that it should not bind strongly on transition metals. Therefore there was the possibility that choline chloride could be an effective helper catalyst.

In this work we examine the effect of choline chloride on two different reactions: The hydrogen evolution reaction (HER) and formic acid electrooxidation. The HER can occur via cationic intermediates so if the arguments in Masel[189] and Rosen et al[190] are correct Formic acid electrooxidation which can occur by two pathways: a direct pathway which has been theorized to occur via a formate intermediate or related species[191-196], and an indirect pathway leading to an adsorbed CO. If the arguments in Masel[189] and Rosen et al[190] are correct and the amine does not bind too strongly, there is the possibility that formic acid electrooxidation to be enhanced.

Importantly, both are desirable results. The HER is undesirable during CO_2 conversion in aqueous media, because HER competes with the main reaction, CO_2 conversion[181, 197-199]. It is also a side reaction in formic acid fuel cells. Therefore inhibition of the HER would be desirable. On the other hand formic acid electrooxideation is the main reaction in formic acid fuel cells[200-206]. Enhancements would be helpful.

The objective of the work here was to determine whether choline chloride changes the rate of the hydrogen evolution reaction and formic acid electrooxidation. In detail we examined the effect of choline chloride on the rate of both reactions on platinum, palladium and gold using mainly cyclic voltametry (CV). We also compared to three standard solutions 0.5M sodium bicarbonate, 0.5M sulfuric acid and a borax buffer solution. Sulfuric acid was an internal standard. Sodium bicarbonate and the borax buffer have a similar pH to our choline chloride solutions, so they were good comparison cases. Our results clearly show a significant suppression of the HER and enhancement of formic acid electrooxidation in the presence of the choline chloride.

5.2 Experimental Section

5.2.1 Materials

The catalyst metal black ink is prepared by mixing 5.6mg of metal black (Alfa Aesar 99.9% metal basis) with 1ml deoxygenated Millipore water. There are two kinds of counter electrodes used in this experiment. For platinum and palladium catalyst, the counter electrode is made by attaching a 25x25mm platinum mesh (size 52) to a 5 inch platinum wire (99.9%, 0.004 inch diameter). For gold electrode, the counter electrode is

made by attaching a 25x25mm gold mesh (size 52) to a 5 inch gold wire (99.9%, 0.002 inch diameter). The reference electrode is a silver-silver chloride electrode with Flexible Connector (Table 1). Four kinds of electrolyte are used: 0.5M choline chloride, 0.5M sodium bicarbonate, 0.5M sulfuric acid and buffer solution. The solutions are prepared with triple distilled water. Measurements are taken at 25 ℃ under argon gas (99.999% purity) bubbling at 1 atm.

5.2.2 Instruments

The measurements were made with a Solartron SI 1287 potentiostat in a standard three-electrode electrochemical cell with a Ag/AgCl reference electrode. The working electrode is prepared by applying the metal black ink onto the gold surface of a rotating electrode. The catalyst is applied on the surface of the rotating electrode by adding 12.5μL of the ink to the surface and allowing the water to evaporate under ambient temperature for 60 minutes.

5.2.3 Cyclic voltammetry

The electrolytes are first loaded into the glass cell and then purged with dry argon (99.99%) for two hours in order to remove oxygen from the electrolytes. Prior to all experiments, a 20-40 linear sweep cyclic voltammograms at 75mV.s^{-1} is taken between -1.5V and +1V vs. Ag/AgCl reference electrode in order to conditioning the electrodes and removing oxides from the surfaces. Then several cycles are performed at 10mV.s-1 before taking the final cycle to insure that the CV had stabilized (i.e., any "dirt" or other material is removed from the surfaces). Finally, cleaning and stabilizing CV cycles are performed at 10mV.s-1. Later, formic acid is added in the electrolyte and the final concentrations are 0.001M, 0.01M and 0.03M. CV is obtained again to investigate the reaction between formic acid and catalyst surface. In order to ensure the quality of the measurements, special attention is paid to the material cleaning and solution purity [207, 208].

5.2.4 Calibration of the reference electrode

We initially used a Ag/AgCl reference electrode connected to the cell through a lugging cappillary and were hoping that the reference electrode would be stable. However, we found that the reference electrode would drift when it was exposed to a choline chloride mixture. Therefore we were careful to calibrate the reference electrode against a reversible hydrogen electrode (RHE) during each experiment. Essentially, a

RHE is set up by bubbling hydrogen over the counter electrode and the potential of this electrode is compared to the reference electrode. To measure RHE potential, we short the working and the counter electrode lead, then, after bubbling the hydrogen under counter electrode for 20 minutes, we measure the open cell potential until it stabilizes. The open cell potential is the RHE vs. Ag/AgCl electrode. This let us determine a reference potential for each run. In the work that follows we plotted the data against the measured potential of the reversible hydrogen electrode, to avoid issues with the drift of the reference electrode.

Table 5.1: Calculated and measured values of the potential of the Ag/AgCl electrode

	pH	Equilibrium potential of the Ag/AgCL electrode after exposure to the solution, V vs SHE
Choline Chloride	8.6	0.08
1 M sulphuric acid	1.2	0.27
Sodium Bicarbonate	8.5	0.27
Buffer	8.6	0.28

5.2.5 Chronoamperometry

Chronoamperometry is generally performed by stepping from open cell potential to the potential of interest, unless noted otherwise. The potential mentioned for chronoamperometric data is the potential that is stepped to from open cell potential. We prepare two kinds of electrolyte for measurement: 0.01M formic acid solution and 0.01M formic acid in 0.5M choline chloride. The potential is hold at 0.2V vs RHE and the current-time (I-t) curve is recorded with potentiostat.

Theoretically, formic acid first adsorbs on the catalyst surface and then goes into two reaction routes[209]: direct formation of carbon dioxide and water; or firstly transferring to adsorbed carbon monoxide and then becoming carbon dioxide. Here, we contribute the elevated current density in choline electrolyte to choline ion's ability to prefer the reaction through the first route instead of forming adsorbed CO on the surface.

5.2.6 SERS Spectra

In-situ SERS spectral measurements are carried out with a laser source(HeNe 632.8nm, power-IDK) to excite the samples, a spectrometer (acton spectrapro mocel sp2300i ccd Andor idus 420A-bV 26 micron by 26 micron pixels) to detect the Raman

signal, a computer for the system control and data acquisition, a potentiostat to control the potential of the working electrode and an EC-SERS cell to accommodate the reaction.

In detail, working electrode is a 10 mm diameter Au disk polished to 1 um with a diamond suspension (Buehler) and flamed for 10 minutes with a hydrogen torch. The crystal is then electrochemically roughened as shown previously [210] except in a solution of 0.5 M choline with an anodic limit of 1.5 V vs Ag/AgCl. The counter electrode is a gold wire flamed with hydrogen torch for 2 min and the reference is Ag/AgCl.

Raman experiments are performed using an in-situ electrochemical cell. The He–Ne laser (λ=632.8 nm) is projected onto the sample at ~45 °incidence. Scattered radiation is collected with F/4 focusing lens and focused at the entrance slit of a monochromator. A 1200 grooves/mm grating dispersed radiation onto a cooled charge-coupled device (CCD, Andor). Typical acquisition time is 30 s.

5.3 Results and Discussion

5.3.1 Hydrogen evolution reaction suppression

Our first experiments were to determine whether choline chloride would inhibit HER. The experiment was to do cyclic voltametry in each of the solutions and see how the hydrogen evolution reaction changed.

Fig. 5.1 presents the cyclic voltammetric measurements of hydrogen evolution reaction on platinum catalyst in 0.5 M solutions containing sulfuric acid, bicarbonate, borax buffer and choline chloride. In each case we plot report the potential versus the measured value of RHE to avoid the issues with the drift in the Ag/AgCl reference electrode. The sulfuric acid data looks similar to those from the previous literature with hydrogen adsorption peaks at 0.11V and 0.27V, and hydrogen desorption peaks at 0.14V, 0.21V and 0.28V. The hydrogen evolution starts at around 0V. In sodium bicarbonate electrolyte, the peaks related to hydrogen reactions are at almost the same potentials as in sulfuric acid. There are hydrogen adsorption peaks at 0.16V and 0.30V, and hydrogen desorption peak at 0.20V and 0.30V. The hydrogen evolution reaction begins at 0V as well. The same situation happened in buffer solution, which shows the hydrogen adsorption peaks at 0.17V and 0.27V, and hydrogen desorption peak at 0.14V and 0.31V. In this case, the hydrogen evolution reaction starts at 0V, but proceeds to bulk reaction slower than in sulfuric acid and sodium bicarbonate.

Everything changes in the choline chloride electrolyte. We do not observe the characteristic hydrogen adsorption and desorption peaks. There is a peak at 0.33V (RHE) that we attribute to the interaction between choline ion and catalyst surface and a hydrogen reduction peak at about -0.4 V vs RHE.

We also tested other catalysts such as Pd and Au. We observed the same suppression phenomenon of hydrogen evolution reaction.

In palladium catalyst, the bulk hydrogen evolution happened at 0.07V in sulfuric acid (see Figure 5.2). Hydrogen adsorption happened at 0.21V and 0.27V, and hydrogen desorption at 0.19V and 0.26V. In sodium bicarbonate, the obvious peaks of hydrogen adsorption and desorption are at 0.20V and 0.30V. The huge peak ranging from 0.30V to 0.66V is related to the reversible reaction of reduction products with catalyst surface, because the peak will increase if we push the potential to more negative value. In buffer solution, we can still observe hydrogen adsorption peak at 0.19V and hydrogen desorption peak at 0.36V. In both sodium bicarbonate and buffer solution, the hydrogen evolution reaction start around the same potential as sulfuric acid, but the bulk hydrogen evolution reaction happened slower than in sulfuric acid.

In choline chloride, there is a smooth line at the point where hydrogen adsorption happens in other electrolytes and we still do not observe the characteristic potential change of hydrogen adsorption. The hydrogen evolution starts smoothly below about -0.5V.

Gold shows less active than the catalysts discussed before according to Figure 5.3. In four kinds of electrolyte, we can hardly see the hydrogen adsorption peaks. In sulfuric acid, hydrogen evolution starts at around 0V in agreement with previous literature[211]. In sodium bicarbonate and buffer solution, the hydrogen evolution happened at the same potential as the sulfuric acid. In choline chloride, however, the hydrogen evolution

reaction starting at -0.3V. Therefore, with gold catalyst, choline chloride still shows the strongest suppression of the hydrogen evolution reaction among all four electrolytes.

5.3.2 Tests to examine the effect of choline chloride on the formic acid electro-oxidation

The results in the previous section indicate that hydrogen formation is strongly suppressed in the presence of choline chloride. The next question we wanted to address is whether we have completely poisoned the catalyst, or whether we have instead had a positive effect of formic acid electrooxiddation.

Figure 5.4 shows a series of CV's of formic acid on a palladium catalyst. There are two formic acid oxidation peaks, one at about zero and a second at about 0.4 V. These are similar positions to those we have observed previously on palladium, although we do see conversion at lower potential than we observe in clean palladium[191, 192, 194, 195, 204, 212]. The only major difference is that the large hydrogen evolution peaks are suppressed. Notice that there is considerable current at voltages between 0.1 and 0.4 V vs RHE. This is the same range where the anodes in formic acid fuel cells operate[191-196, 200-206, 212, 213]. Evidently, choline chloride does not suppress the electro-oxidation of formic acid on palladium.

Figure 5.5 shows the CV of formic acid in choline chloride on platinum. The currents are smaller here, but again we observe some formic acid electroxidation near zero with respect to RHE, and more around 0.6 V. Formic acid electrooxidation can follow two different routes on platinum, a direct pathway and a pathway going through a CO intermediate[193, 195, 213], The oxidation peak around 0 V with respect to RHE, and the reduction peak around -0.1 V with respect to RHE are characteristic of the direct pathway, while the shoulder around 0.6 V is characteristic of the CO pathway. The fact that these positions are at about the same potential as on platinum shows that formic acid electro-oxidation on platinum is not strongly inhibited by the presence of choline chloride.

We have also done the same experiment on a gold surface. Figure 5.6 shows the cyclic voltammetry of formic acid on gold. Formic acid electrooxidation on gold is hard to study because much of the chemistry occurs below RHE, and is swamped by the hydrogen reduction reaction. The hydrogen reduction reaction is suppressed in the presence of the choline chloride, and instead we observe a fairly large formic acid reduction peak at about -0.3 V.

These results demonstrate that formic acid oxidation and reduction are not suppressed in the presence of choline chloride even though hydrogen evolution is suppressed.

5.3.3 Chronoamperometry

The next question is whether formic acid electrooxidation would be enhanced in the presence of choline chloride. Figure 5.7 shows chronoamperometric scans for Pt held at 0.2 V vs RHE in choline chloride electrolyte with 0.01M formic acid compared to pure formic acid. We chose 0.2 V because at this potential is similar to that used in formic acid fuel cells[195, 200-206].

For both chronoamperometric curves, the current density starts out high on the Pt surface. Then as formic acid is depleted near the electrode surface, the current density rapidly drops and later become relatively stable for 5 hours. After around 6 hours, the current density with pure formic acid electrolyte becomes zero and then switches to negative value. The activity of the Pt catalyst with formic acid and choline chloride, however, still stay relatively high even after 6-hour operation. Results also demonstrate above an order of magnitude improvement in the measured current density for this electrolyte over that of pure formic acid solution.

5.3.4 SERS

In other work we have done surface enhanced raman spectroscopy to examine choline chloride adsorption on gold films (Figure 5.8). In all cases we observe strong peaks at 2976 cm^{-1}, 1453 cm^{-1}, 967 cm^{-1}, 717 cm^{-1} as expected for adsorbed choline cations.

Therefore we concluded that choline ions adsorb molecularly on gold as we would have expected.

5.4 Discussion

This work clearly demonstrates that choline chloride can act as a helper catalyst. Previous workers had shown that a different quaternary amine could suppress the HER in batteries[50, 60], but what is special about our work is that we have observed suppression of an undesirable reaction and enhancement of a desirable one.

From the data here we do not know whether it is the choline or the chloride that is enhancing the reaction, but in related work we found that other choline compounds (Choline-BF4, Choline-acetate) give similar effects. Therefore we assert that the choline ion is enhancing the reaction.

Figure 5.9 and Figure 5.10 shows a schematic of our proposed mechanism of the process. Without suppression agent such as choline ion, when the electrode potential is more negative than the potential of zero charge (PZC), the surface will be negatively charged and the protons interact with the surface easily. However, when choline cations are added in the solution, a thin layer of choline ion forms on the catalyst surface as seen in SERS. The thin layer of choline causes the surface to be positive charged, which will block further adsorption of protons on the surface. However, after the potential reaches

so negative that the positive charged choline ion cannot balance the negative charged catalyst surface, protons can finally reach the catalyst surface, and go through reduction process to release hydrogen. This process results in an increased overpotential of proton reduction on the catalyst surface as observed experimentally.

Formic acid electrooxidation shows the opposite effect. This is harder to explain. Formic acid goes by two pathways on platinum: a direct and indirect pathway[191, 192, 194, 195, 204, 212]. While we expected the direct pathway to be enhanced, the results in Figure 5.7 show that the indirect pathway leading to CO poisoning is also suppressed since the reaction was not rapidly poisoned.

We can explain the data if we assume that the mechanism of formic acid electrooxidation follows the a direct pathway such as

$$HCOOH \rightarrow HCOO^{-}_{(ad)} + H^{+}$$

$$HCOO^{-}_{(ad)} + 2\ e^{-} \rightarrow CO_2 + H^{+}$$

And an indirect pathway such as

$$HCOOH + H^{+} \rightarrow HCO_{(ad)}$$

$$HCO_{(ad)} \rightarrow CO_{(ad)} + H^{+}$$

$$CO_{(ad)} + H_2O + 2\ e^{-} \rightarrow CO_2 + 2H^{+}$$

The indirect pathway would be suppressed since adsorbed H^{+} is destabilized, while the direct pathway would be enhanced due to stabilization of the formate. Admittedly, while we have observed the formate and formyl species in ultra high vacuum (UHV)[196, 214-216], we have not observed these species during formic acid electrooxidation on our

most active electrocatalysts. Thus, this mechanism is speculative. Still, it is a reasonable hypothesis given our observations.

5.5 Conclusion

In summary then we find that choline chloride has fascinating effects on the rates of electrocatalytic reactions. On one hand, it suppresses two undesirable reactions: the hydrogen evolution reaction, and CO formation during formic acid electro-oxidation. Yet it enhances another reaction, the direct electrooxidation of formic acid on platinum and palladium. Further it extends the region where electrochemical experiments can be done to lower potentials. These results demonstrate that organic additions can have unexpected influences on electrocatalytic reactions, and therefore need to be explored.

5.6 Acknowledgement

This work was supported by the US Department of Energy under grant DE-SC0004453. The views expressed in this paper are those of the authors and do not necessarily represent the views of the US Department of Energy. The authors thank Nichole Honesty for help with the SERS experiments.

5.7 Figures

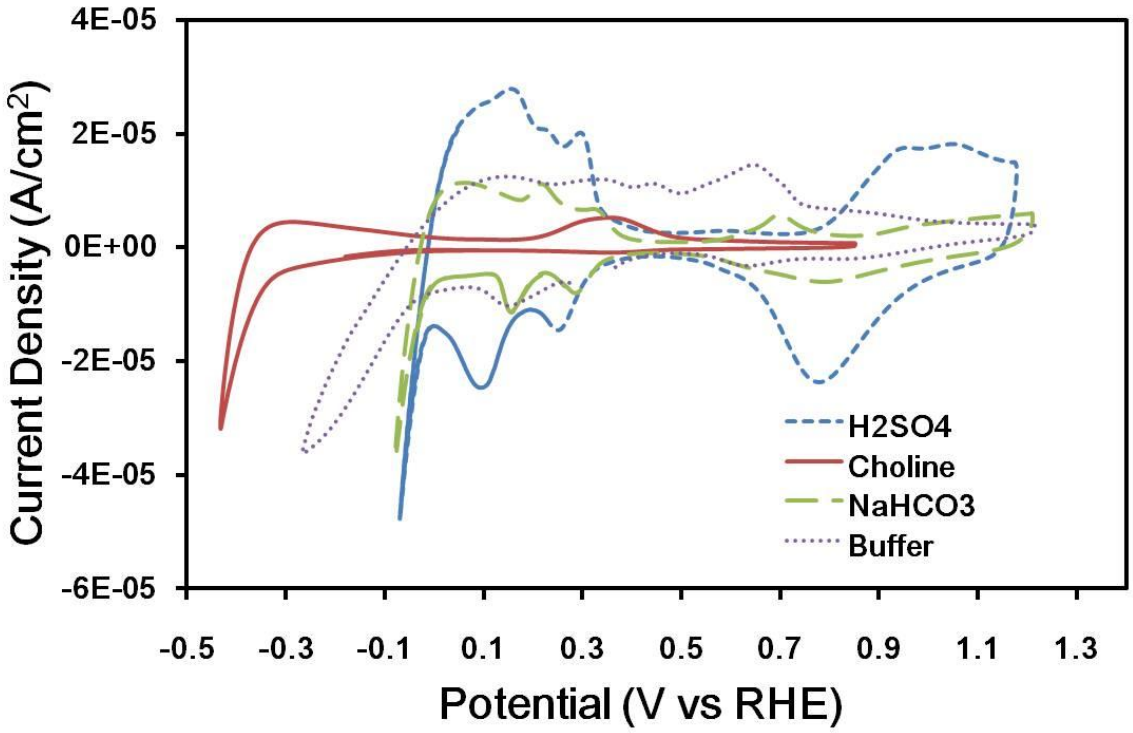

Figure 5.1 Cyclic voltammetry of platinum in different electrolytes: (—) 0.5M choline chloride; (——) 0.5M $NaHCO_3$; (- - -) 0.5M H_2SO_4; (⋯) buffer solution (borax and hydrochloride acid). In each case we report the potential versus the measured value of RHE.

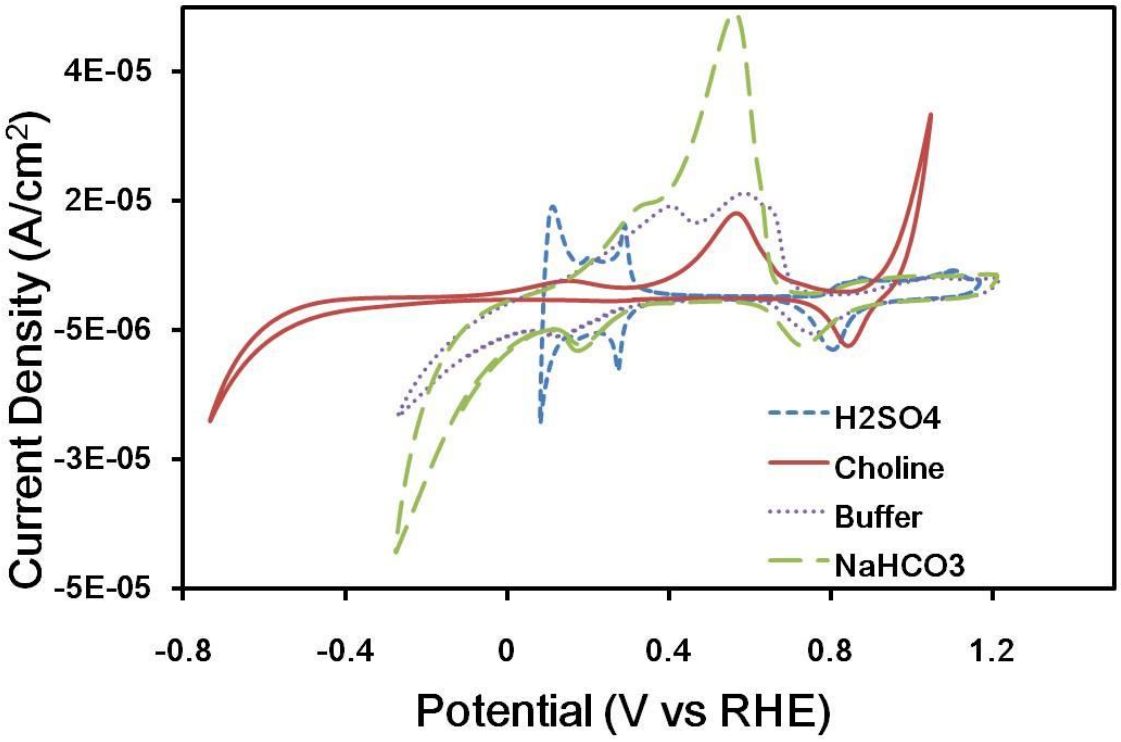

Figure 5.2 Cyclic voltammetry of palladium in different electrolytes: (—) 0.5M choline chloride; (——) 0.5M $NaHCO_3$; (- - -) 0.5M H_2SO_4; (⋯) buffer solution (borax and hydrochloride acid).

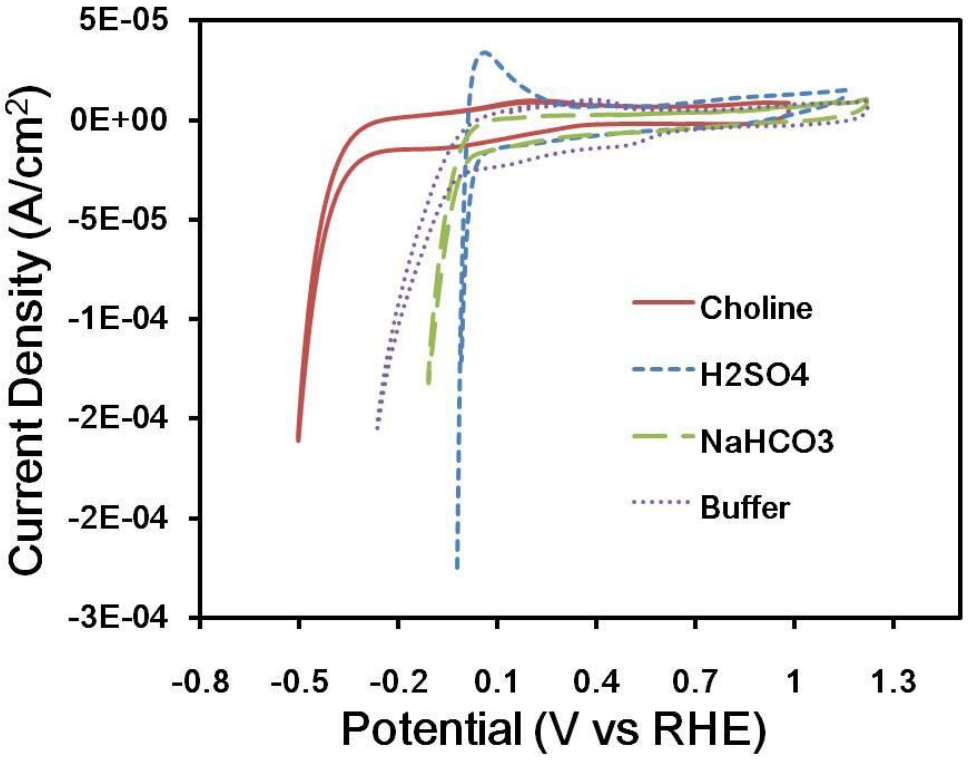

Figure 5.3 Cyclic voltammetry of gold in different electrolytes: (—) 0.5M choline chloride; (— —) 0.5M $NaHCO_3$; (- - -) 0.5M H_2SO_4; (⋯) buffer solution (borax and hydrochloride acid).

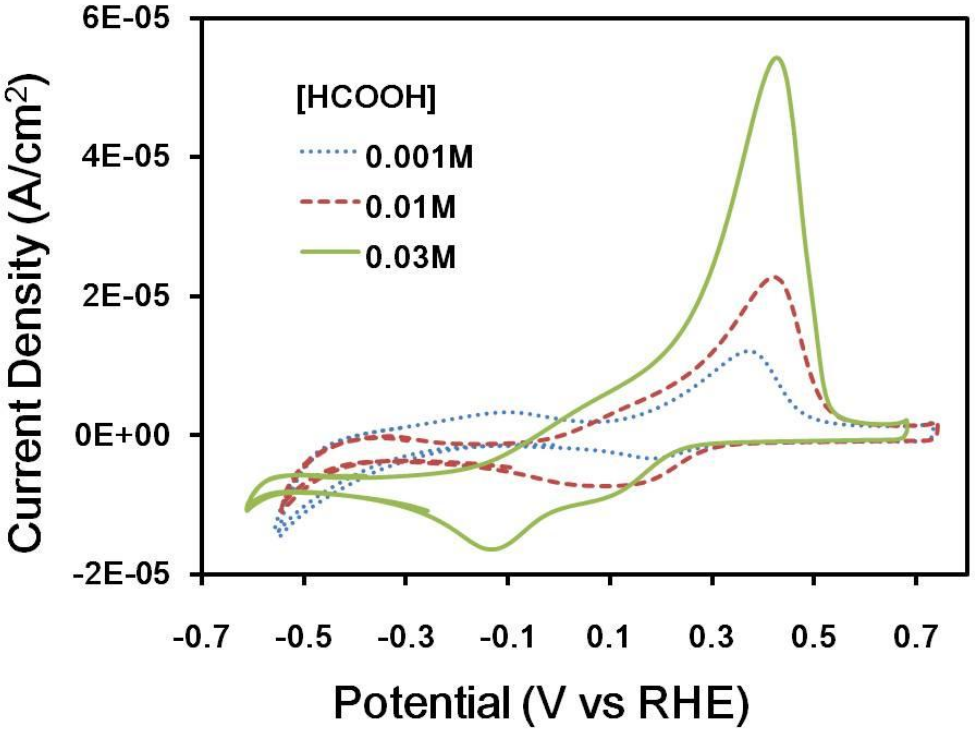

Figure 5.4 Cyclic voltammetry of palladium in choline chloride with different concentration of formic acid: (—) 0.03M formic acid; (- - -) 0.01M formic acid; (⋯) 0.001M formic acid.

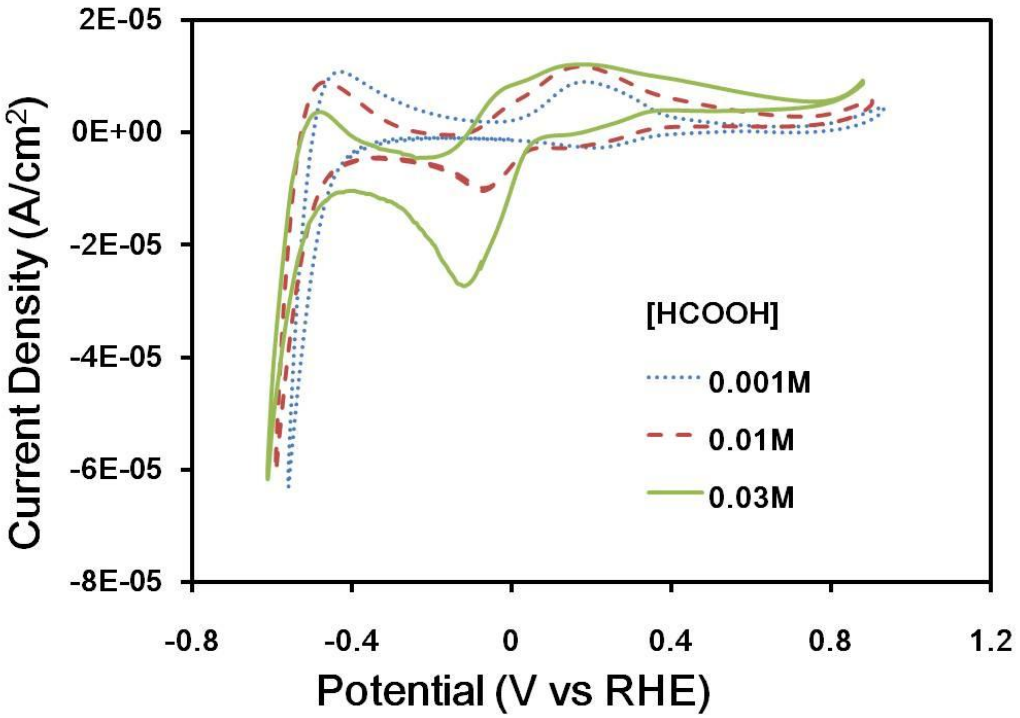

Figure 5.5 Cyclic voltammetry of platinum in choline chloride with different concentration of formic acid: (—) 0.03M formic acid; (- - -) 0.01M formic acid; (⋯) 0.001M formic acid.

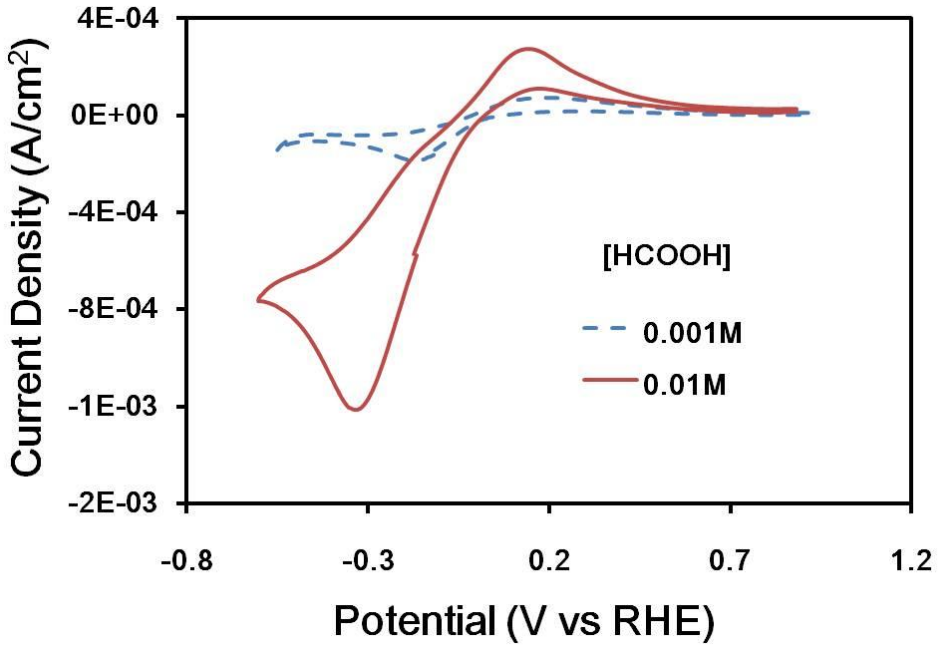

Figure 5.6 Cyclic voltammetry of gold in choline chloride with different concentration of formic acid: (—) 0.01M formic acid; (- - -) 0.001M formic acid.

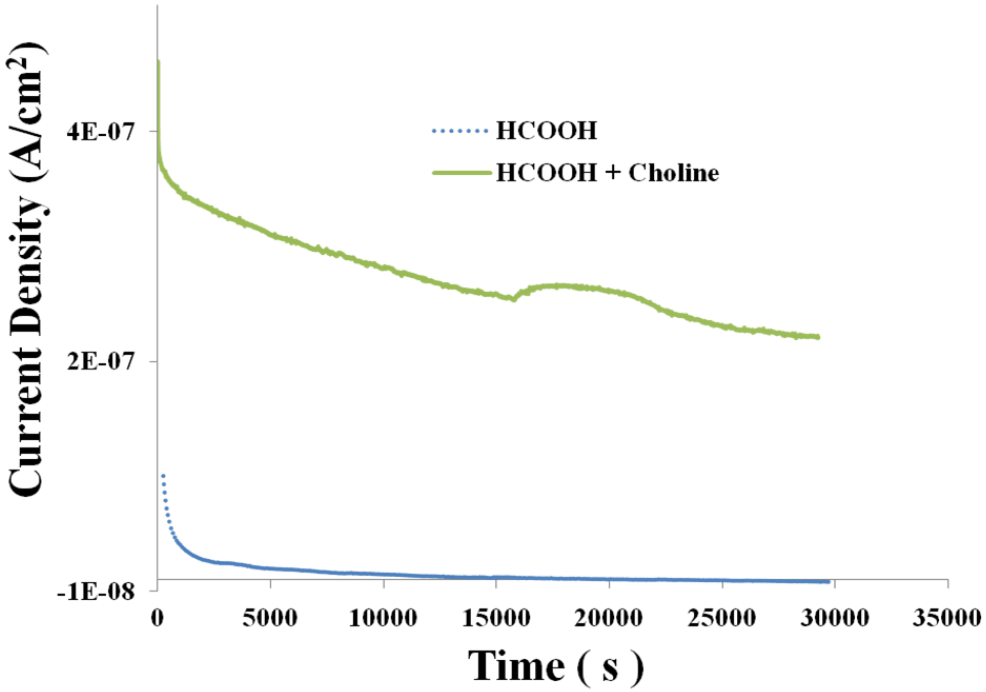

Figure 5.7 Chronoamperometric data for Pt black on gold electrode at 0.2 V vs RHE in pure formic acid solution and formic acid solution with choline chloride

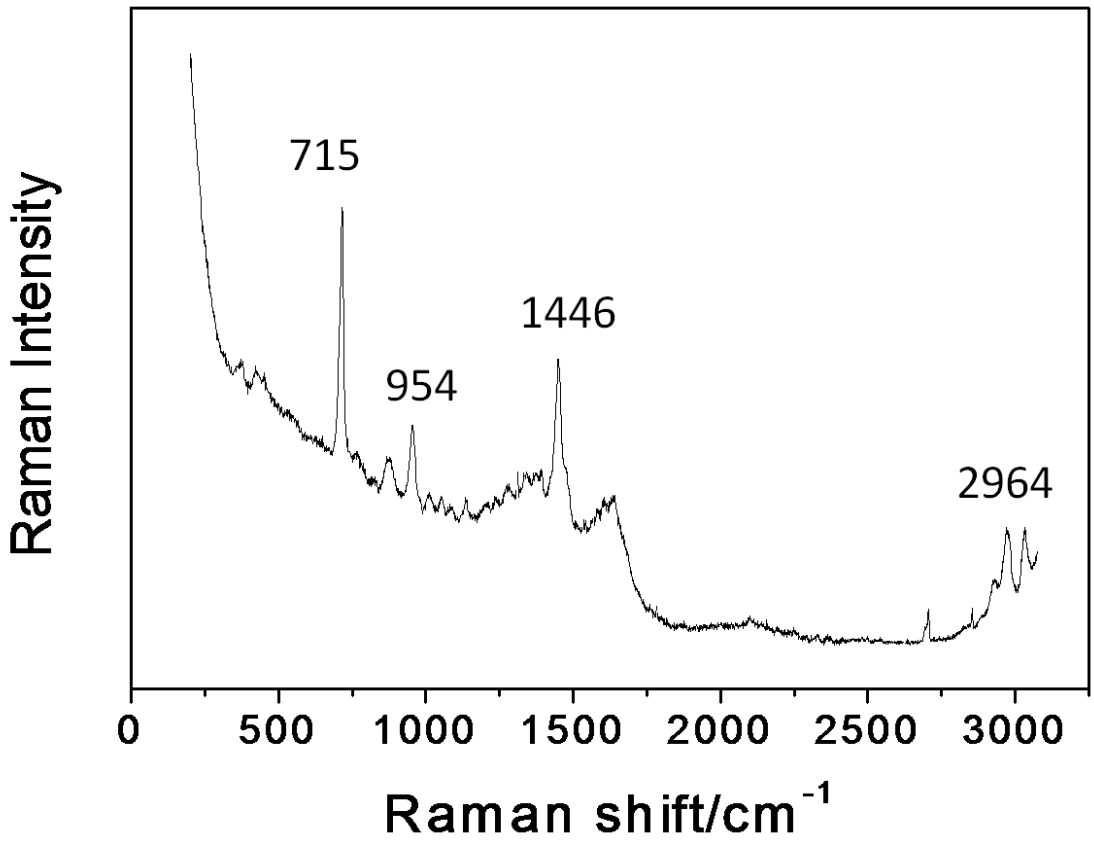

Figure 5.8 SERS spectra of choline chloride with gold catalyst

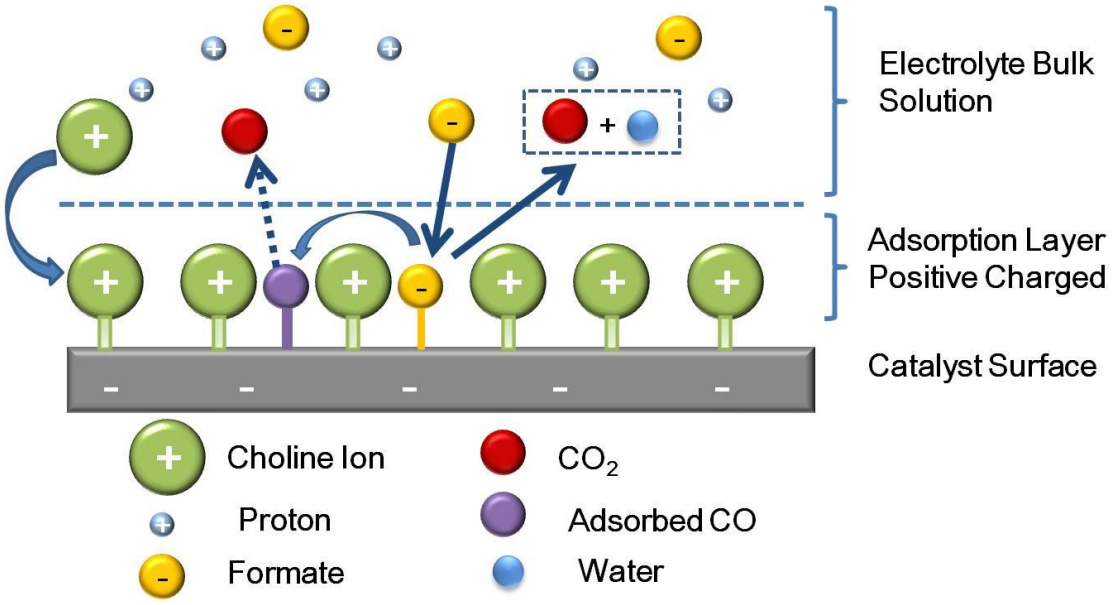

Figure 5.9 Formic acid reaction at so negative potential level on catalyst surface with choline chloride

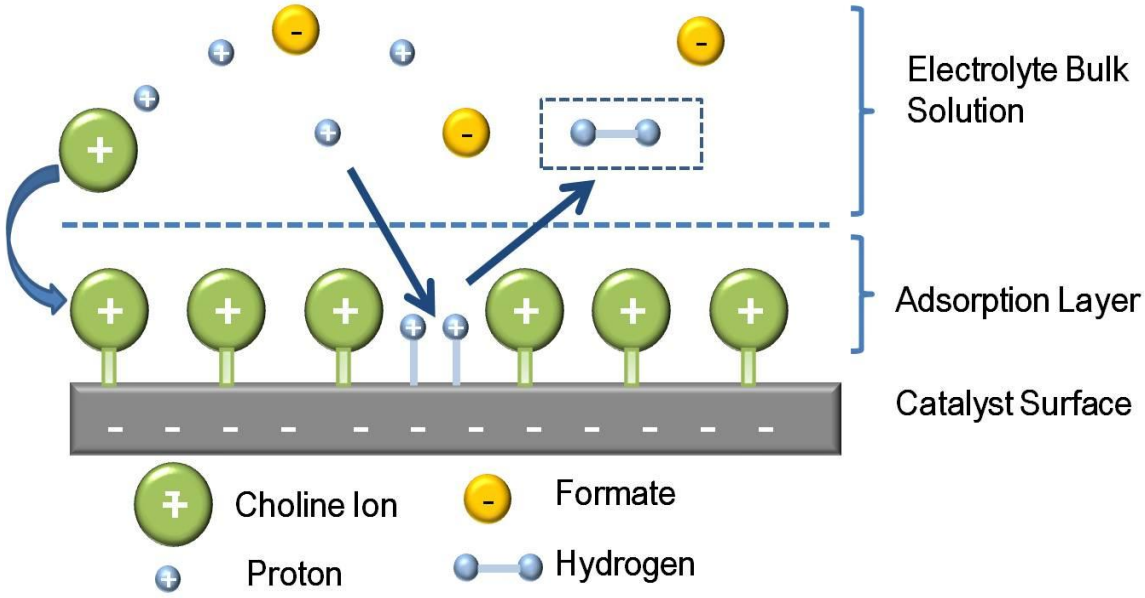

(b)

Figure 5.10 Hydrogen evolution reaction at so negative potential level on catalyst surface with choline chloride

Chapter 6: Carbon Dioxide Conversion in Choline Chloride with Lower Overpotential

6.1 Introduction

Recycling of CO_2 back into fuels or other useful products is critically important to the World's efforts to reduce global warming. CO_2 is a valuable reactant for the synthesis of many chemical products, and electrochemical method is regarded as a promising way. The central problem with this approach, however, is the higher overpotential needed for the conversion of CO_2 into useful fuels. Usually, the overpotential for 50% electron conversion efficiencies is as high as ~1.5V., and no stable catalyst has shown significant conversion at cathode potentials less negative than -1V [217, 218], compared to a thermodynamic potential only about -0.2V in acid solution. Not surprisingly, the overpotential should be reduced to minimum in order to make any electrochemical reaction economically sound.

In this study, we want to see if we can use choline chloride as an electrolyte to lower the overpotential of carbon dioxide reduction. Choline chloride is an important additive in feedstock and one of inexpensive quaternary ammonium salts. Interestingly, our results demonstrate that with choline chloride as the electrolyte, the carbon dioxide reduction happens even above the calculated thermodynamic potential value.

In literature, there have been many studies on the electroreduction of CO_2 in different solvents (protic or aprotic), in which the solubility of the reactant varies [123, 219-221]. In aqueous media, the metal electrode can transform CO_2 into other products with low overpotential. However, the hydrogen evolution prevails after the electrode surface is fully covered with adsorbed intermediate and the reaction does not proceed further.

In a previous work [222], we showed the ability of choline chloride to suppress the hydrogen evolution. Here, we would like to demonstrate its ability to reduce the overpotential in carbon dioxide electroreduction process. We have used three electrode electrochemical cell, 0.5M choline chloride as the electrolyte, and four different working catalysts; Pt, Pd, Au and Pt/Ru. It is shown that carbon monoxide is found mainly accumulated on Pt, Au and Pt/Ru catalysts, and formic acid is found accumulated on Pd catalyst.

6.2 Experimental Section

6.2.1 Catalyst materials

The catalyst metal black ink is prepared by mixing 5.6mg of metal black (Alfa Aesar 99.9% metal basis) with 1ml deoxygenated Millipore water. There are two kinds of counter electrodes used in this experiment. For platinum and palladium catalyst, the counter electrode is made by attaching a 25x25mm platinum mesh (size 52) to a 5 inch platinum wire (99.9%, 0.004 inch diameter). For gold electrode, the counter electrode is made by attaching a 25x25mm gold mesh (size 52) to a 5 inch gold wire (99.9%, 0.002 inch diameter). The reference electrode is a silver-silver chloride electrode with Flexible Connector (Table 1). 0.5M choline chloride is used as electrolyte. The solutions are prepared with triple distilled water. Measurements are taken at 25 ℃ under argon gas (99.999% purity) bubbling at 1 atm.

6.2.2 Instruments

Experiments are carried out in a custom-made 150mL, three-electrode electrochemical glass cell. The working electrode is prepared by applying the metal black ink onto the gold surface of a rotating electrode. The catalyst is applied on the surface of the rotating electrode by adding 12.5 µL of the ink to the surface and allowing the water to evaporate under ambient temperature for 60 minutes. The working electrode, reference electrode and counter electrode are connected to a potentiostat (Solartron SI 1287). (Table 6.1)

6.2.3 Cyclic voltammetry

The electrolytes are first loaded into the glass cell and then purged with dry argon (99.99%) for two hours in order to remove oxygen from the electrolytes. Prior to all experiments, a 20-40 linear sweep cyclic voltammograms at 75mV.s-1 is taken between -1.5V and +1V vs. Ag/AgCl reference electrode in order to conditioning the electrodes, removing oxides from the surfaces. After, several cycles are performed at 10mV.s-1 before the final cycle to insure that the CV had stabilized (i.e., any "dirt" or other material is removed from the surfaces). Finally, cleaning and stabilizing CV cycles are performed at 10mV.s-1 within the range of -1V to 0.3V. Then CO2 was bubbled in the solution at 1atm pressure for 20 minutes. Cyclic voltammetry is conducted again at a sweep rate of 10mV/s in the range from -1V to 0.3V. In order to ensure the quality of the measurements, special attention is paid to the material cleaning and solution purity [207, 208].

6.2.4 Electrochemical identification of the reaction products

Next, the potential is held at the value where carbon dioxide reduction dominated and little hydrogen evolution reaction is seen for 20 minutes. Cyclic voltammetry is once

again conducted at a sweep rate of 10mV/s in the range from 1V to carbon dioxide dominate potential for three cycles.

With the same electrochemical system, CO stripping voltammetry and fomic acid stripping voltammetry are also conducted during the experiment. For CO stripping, the electrolyte is saturated with carbon monoxide by bubbling the CO for 20 minutes. During these 20 minutes, the working electrode is held at -0.5V vs SHE. Then argon is blown into and over the electrolyte solution for 30 minutes to remove the remaining CO in the electrolyte. Then two voltammograms are monitored. The active area of metal catalyst is deduced from the coulometry of the CO-stripping peak in the first cycle.

For fomic acid stripping, electrolytes with different concentration of formic acid (0.001M, 0.01M and 0.03M) are tested. After the blank cyclic voltammetry taken by bubbling argon into the 0.5M choline chloride, different amount of formic acid is added into 0.5M choline chloride. Cyclic voltammetry is taken again and different cyclic voltammetry figures are compared to acquire the formic acid reaction peak in the electrolyte.

6.2.5 SERS Spectroscopy

In-situ SERS spectral measurements are carried out with a laser source(wavelength, power) to excite the samples, a spectrometer (model) to detect the Raman signal, a

computer for the system control and data acquisition, a potentiostat to control the potential of the working electrode and an EC-SERS cell to accommodate the reaction.

In detail, working electrode is a 10 mm diameter Au disk polished to 1 um with a diamond suspension (Buehler) and flamed for 10 minutes with a hydrogen torch. The crystal is then electrochemically roughened as shown previously [210] except in a solution of 0.5 M choline with an anodic limit of 1.5 V vs Ag/AgCl. The counter electrode is a gold wire flamed with hydrogen torch for 2 min and the reference is Ag/AgCl.

Raman experiments are performed using an in-situ electrochemical cell. The He–Ne laser (λ=632.8 nm) is projected onto the sample at ~45° incidence. Scattered radiation is collected with F/4 focusing lens and focused at the entrance slit of a monochromator. A 1200 grooves/mm grating dispersed radiation onto a cooled charge-coupled device (CCD, Andor). Typical acquisition time is 30 s.

Table 6.1 Apparatus and experimental conditions:

Cell	Three-electrode glass cell
Potentiostat	Solartron SI 1287
Potential sweep	Solartron SI 1287
Working electrode	5.6mg/ml Platinum black, Palladium black, Platinum/Ruthenium and Gold surface
\Counter electrode	Platinum mesh, Gold mesh
Reference electrode	RE-5B Ag/AgCl Reference Electrode with Flexible Connector
Electrolyte	Choline Chloride 0.5M
Pressure	1 atm
Potential	-1.0V -0.3V for Choline Chloride
Temperature	298.15K

6.3 Results and discussion

6.3.1 Lowering the Overpotential for Carbon Dioxide Reduction with Different Catalyst

Figure 6.1-6.4 show carbon dioxide reduction in 0.5M choline chloride with different catalysts. In Figure 6.1, carbon dioxide reduction on Pt starts after -0.50V. In the

range from -0.50V to -0.65V, we observe obvious carbon dioxide reduction peaks when hydrogen evolution does not occur.

Figure 6.2 shows that carbon dioxide reduction on Pd happens in the range from -0.36V to -0.66V, mixed with the hydrogen evolution. However, according to the smooth CV curve of control experiment, hydrogen evolution will not outpace the carbon dioxide reduction, as a consequence, but will lower the competition between the two reactions.

In Figure 6.3 carbon dioxide reduction on Pt/Ru begins to at a reduced potential -0.37V. Below -0.67V, carbon dioxide reduction is mixed with hydrogen evolution. Therefore, during the potential window from -0.67V to -0.37V, carbon dioxide reduction is more rapid than hydrogen evolution.

For gold electrode (Figure 6.4), carbon dioxide reduction happens below the potential -0.35V and extends even further below the bulk hydrogen evolution reaction.

We also performed potential static experiments combined with stripping cyclic voltammetry measurements to determine what product resulted from the reaction of CO_2 reduction. During the experiments, we held the potential at the value where CO_2 conversion relatively high and hydrogen evolution is still low (such as -0.6V vs. SHE for Platinum catalyst), then the stripping cyclic voltammetry is conducted in order to record the current change at certain potential levels due to products being removed from surface.

6.3.2 Electrochemical Identification of Carbon Dioxide Reduction Products

Figures 6.5-6.7 depicts the stripping voltammetry characteristics on three catalysts (Pt, Pd and Pt/Ru). Pt (Figure 6.5) initially shows the typical primary stripping peak at 0.71 V, which represents that CO is striped out of catalyst surface. Therefore, in the second cycle, because no or very limited CO will still remain on the catalyst surface, we can hardly see the CO peak anymore.

Pd (Figure 6.6) displays a single stripping peak initially at 0.23 V. At this value, the product of carbon dioxide reduction is formic acid compared to literature value [222]. The peak height decreases in the next cycle because limited amount of formic acid will remain on the surface.

Pt/Ru (Figure 6.7) displays an increasing peak at 0.35V and achieves its maximum at 0.56 V. Compared to literature [223], we can conclude that the peak represents CO interaction with the catalyst surface.

For gold electrode (Figure 6.8), we conducted the stripping experiment after holding the potential at -0.7V for 20 minutes. The stripping figured does not show the distinct faraday peak demonstrating the product formation on the catalyst surface. However, a small increase of the current density in the first cycle compared to the second cycle indicates there are reactions happening on the catalyst surface.

In order to investigate the surface reactions as well as identify the major product of CO_2 reduction on the gold catalyst, we used surface enhanced Raman spectra (SERS) (see Figure 6.9). At -0.7 V vs SHE, almost no adsorption of CO product was observed from SERS signal, which confirms that the increase of the current density in Figure 6.8 is not due to the product of CO. At -0.8 V, a peak appeared at 2100 cm^{-1}. The spectroscopic peak is identified as a linear CO derived from CO_2 on Au [224]. At -0.9 V, the peak intensity increases.

6.3.3 SERS Identification of Carbon Dioxide Reduction Products

It is noticeable that for gold electrode, the carbon dioxide reduction starts at around -0.35V. However, we observed the carbon monoxide product using SERS facility lower than -0.7V. It demonstrates that there is a potential range (-0.7V to -0.35V) where carbon dioxide is reduced but no carbon monoxide forms yet. We assume this result is due to the stable intermediate forming on the catalyst surface during a certain potential range. When the potential become more negative, the stable intermediate finally becomes product.

6.3.3.1 Mechanism Discussion

Previous literature [102, 103, 106, 110, 225-228] demonstrates the kinetics and mechanism of carbon dioxide reduction to formic acid or carbon monoxide in aqueous solutions as follows:

$CO_{2(ads)} + e^- = (CO_2)^-_{(ads)}$

$CO_2\text{-}_{(ads)} + H^+ + e^- \rightarrow HCOO^-$

$CO_2\text{-}_{(ads)} + 2H^+ + 2e^- \rightarrow CO + H_2O$

In these processes, the high overpotential is caused by the large energy barriers due to the transferring between the adsorbed carbon dioxide and $(CO_2)^-_{(ads)}$.

However, when choline cations are added in the solution, a thin layer of choline ions forms on the catalyst surface. There are two possible mechanism routes for carbon dioxide reduction with the thin layer of choline ions The first route (Figure 6.10,Route 1) is that the adsorbed carbon dioxide transfers to $(CO_2)^-_{(ads)}$ at first. Then, the surface with positive charged choline ions will lower energy barriers of the formation of the negatively charged $CO_2)^-_{(ads)}$. Therefore, it causes the lower overpotential for the carbon dioxide reduction. The second possible mechanism route (Figure 6.10, Route 2) is that when carbon dioxide comes close to the catalyst surface, it forms an $(CO_2)^-$ intermediate with the choline ion. This choline-$(CO_2)^-$ intermediate requires lower energy to form, as a result, the energy requirement of the whole process of carbon dioxide reduction will be reduced. This assumption is based on the previous paper written by Brian Rosen et al

[229], which demonstrated that the overpotential for carbon dioxide reduction is lower by the co-catalyst EMIM-BF4 because of the formation of an EMIM-BF4-CO_2^- complex during the reaction. Moreover, the thin layer of choline ion will also block the further adsorption of protons on the surface. Consequently, the hydrogen evolution reaction is suppressed during the carbon dioxide reduction process, which eliminates most of the energy lost due to HER.

In detail, we would like conduct quantitive analysis to show the effect of adding choline chloride to lower the overpotential for carbon dioxide reduction (Table 6.1). In order to calculate the theoretical value of the potential for carbon dioxide reduction in choline chloride, we need to compensate the pH effect on potential value. From the Nernst Equation, for a pH increase of 1, the cyclic voltammetric figure will shift to lower potential by 0.059V. For example, for 0.5M choline chloride, the PH is 8.5. Therefore, their cyclic voltammetric figures will shift to left by 0.089V compare to the cyclic voltammetric figures in neutral solution[230].

In choline chloride electrolyte, products can accumulate on surface at the potential less negative than equilibrium potential in water for platinum, palladium and platinum/ruthenium catalyst. The overpotential for CO_2 conversion with gold catalyst is lowered.

Table 6.2 Potential range of carbon dioxide reduction in different catalyst.

Catalyst	Main Products	Carbon Dioxide reduction potential range (before HER)	Theoretical Potential
Pt	CO	-0.50V ~ -0.65V	-0.609V
Pd	Formic Acid	-0.36V ~ -0.66V	-0.699V
Pt/Ru	CO	-0.37V ~ -0.67V	-0.609V
Au	CO	-0.35V ~ -0.75V	-0.609V

6.4 Conclusion

We have studied using choline chloride, a low-cost type of quandary ammonium slat, as electrolyte in the CO_2 reduction with electrochemical analysis. Different metal catalysts are employed in the reaction. Special procedures are adopted to stabilized catalytic electrodes and purge residue gas from electrolyte solutions. Cyclic voltammograms show that the presence of choline chloride significantly reduced the overpotential, a key challenge causes low efficiency in CO_2 conversion, by suppression of hydrogen evolution and lowering CO_2 conversion potential; therefore reduced the competition between water to hydrogen and carbon dioxide conversion reactions. The stripping voltammetry and SERS experiments help identifying the major products with different catalytic metals. The results have determined that the CO evolution dominates

on platinum, platinum and ruthenium and gold catalysts, and formic acid was the dominating product on palladium catalysts.

6.5 Acknowledgement

This work was supported by the US Department of Energy under grant DE-SC0004453. The views expressed in this paper are those of the authors and do not necessarily represent the views of the US Department of Energy. The authors thank Nichole Honesty for help with the SERS experiments.

6.6 Figures

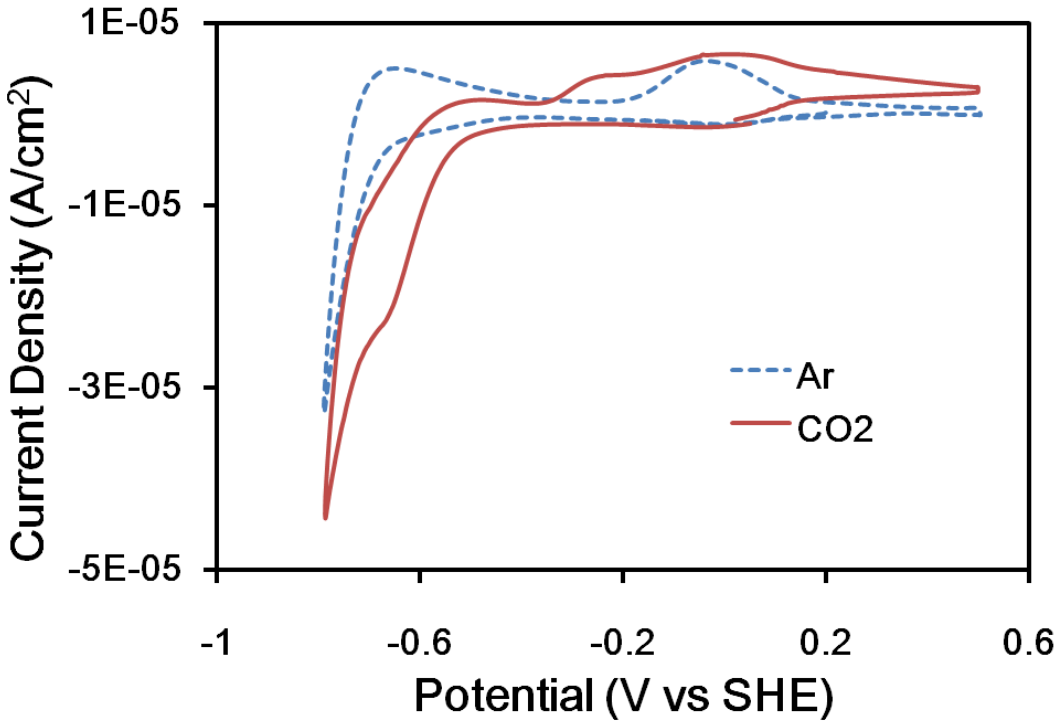

Figure 6.1 Carbon dioxide reduction in 0.5M choline chloride with Pt catalysts. (---)cyclic voltammetry with argon in electrolyte; (—)cyclic voltammertry with CO2 in the electrolyte.

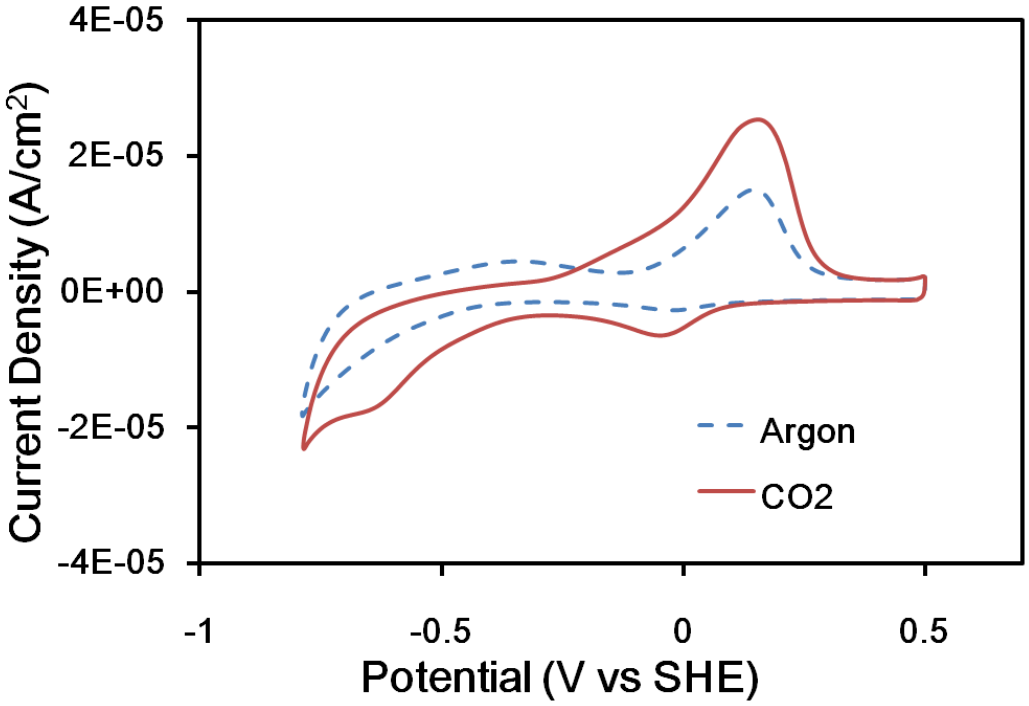

Figure 6.2 Carbon dioxide reduction in 0.5M choline chloride with Pd catalysts. (---)cyclic voltammetry with argon in electrolyte; (—)cyclic voltammertry with CO2 in the electrolyte.

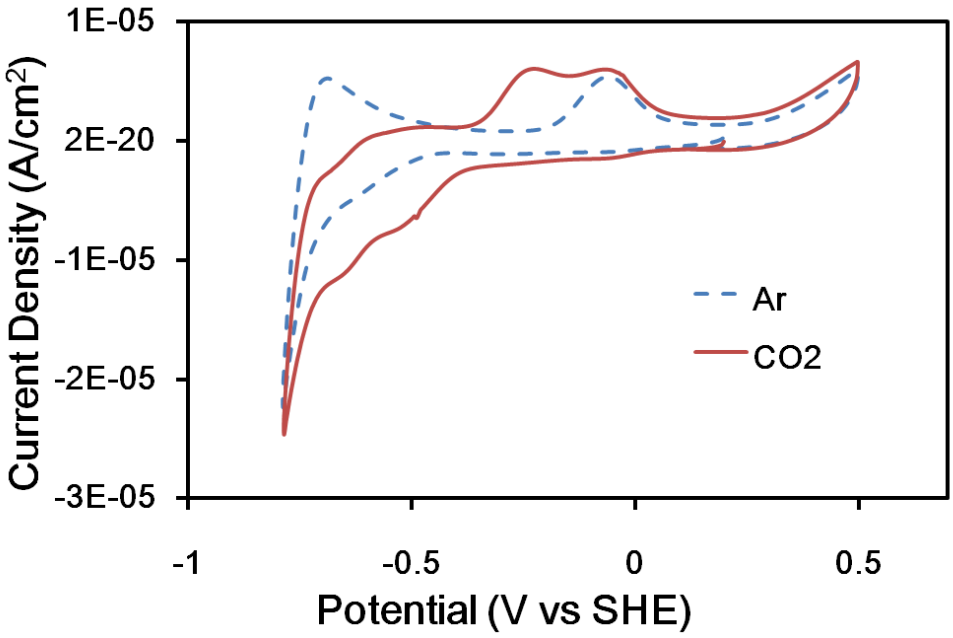

Figure 6.3 Carbon dioxide reduction in 0.5M choline chloride with Pt/Ru catalysts. (---)cyclic voltammetry with argon in electrolyte; (—)cyclic voltammertry with CO2 in the electrolyte.

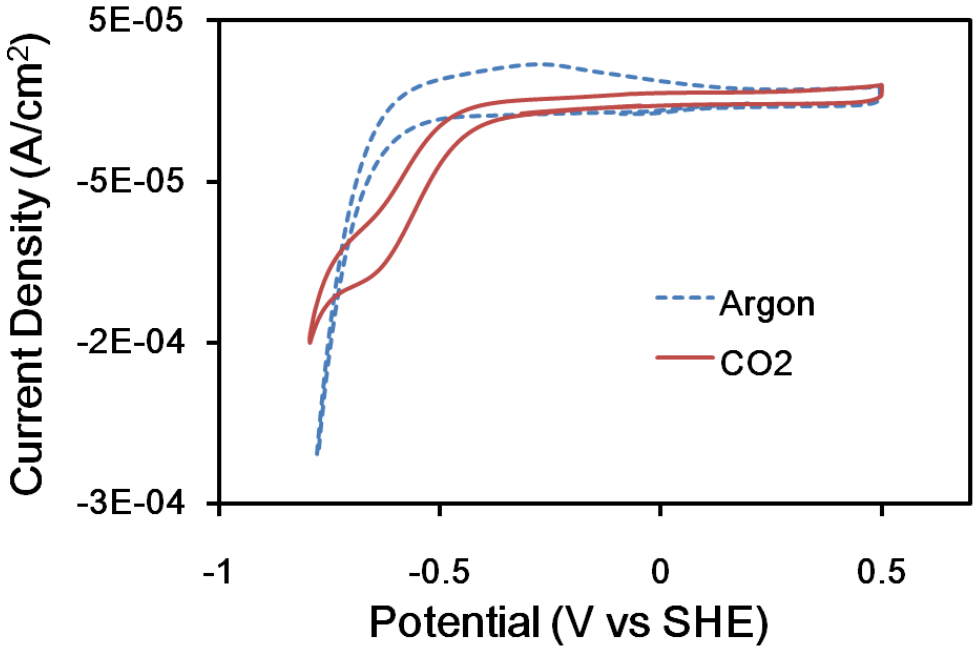

Figure 6.4 Carbon dioxide reduction in 0.5M choline chloride with Au catalysts. (---)cyclic voltammetry with argon in electrolyte; (—)cyclic voltammertry with CO2 in the electrolyte.

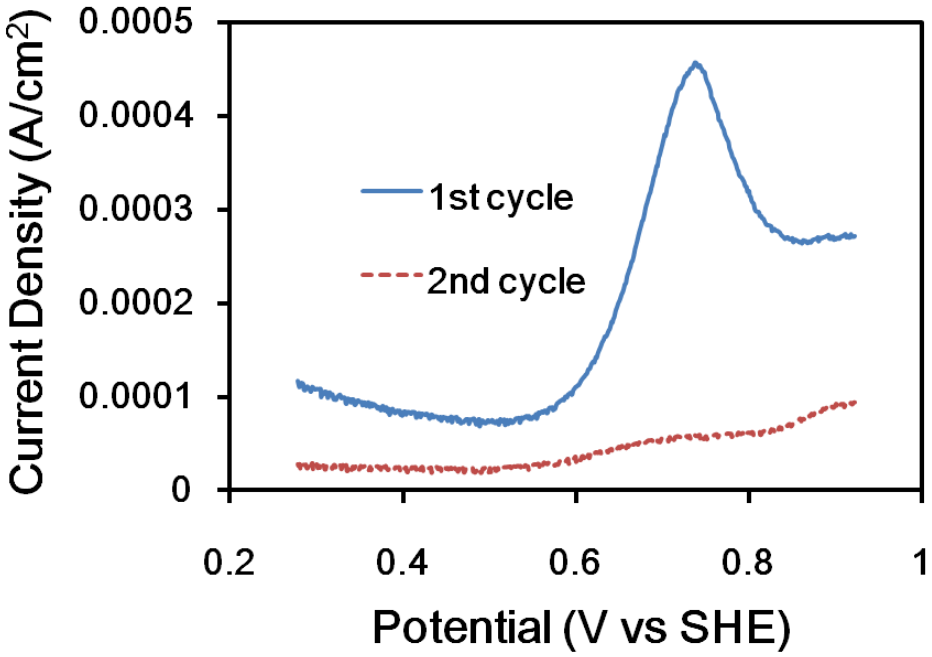

Figure 6.5 Stripping voltammograms with Pt in 0.5M Choline Chloride following 20 min CO2 adsorption and reaction: (---)cyclic voltammetry with argon in electrolyte; (—)cyclic voltammertry with CO2 in the electrolyte.

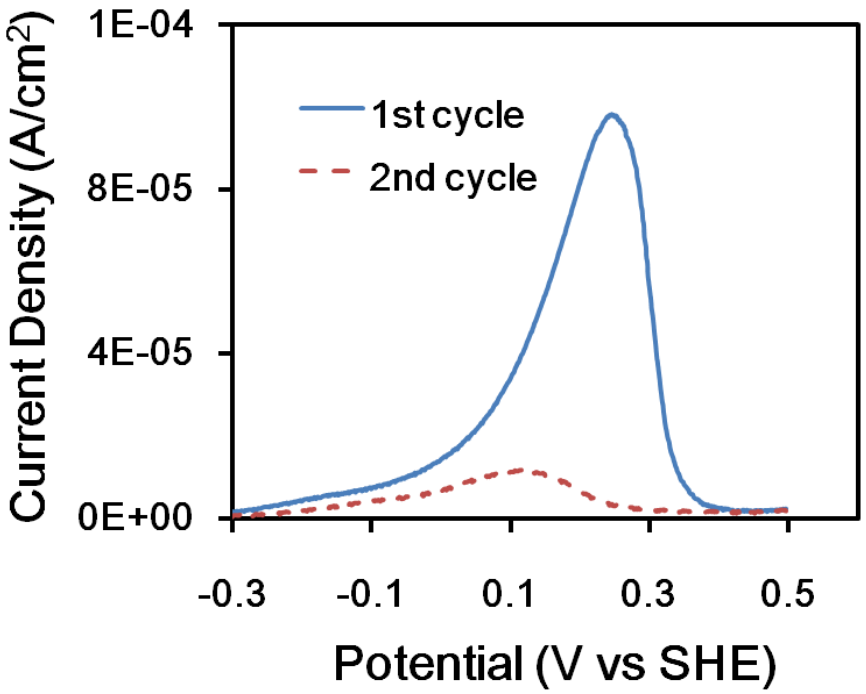

Figure 6.6 Stripping voltammograms with Pd in 0.5M Choline Chloride following 20 min CO2 adsorption and reaction: (---)cyclic voltammetry with argon in electrolyte; (—)cyclic voltammertry with CO2 in the electrolyte.

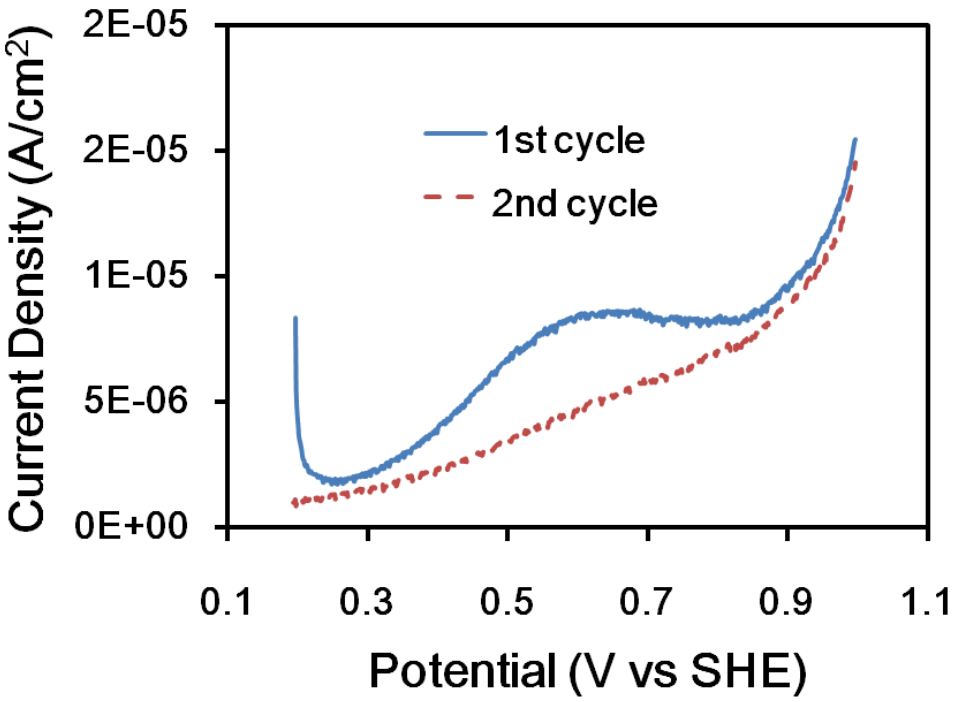

Figure 6.7 Stripping voltammograms with Pt/Ru in 0.5M Choline Chloride following 20 min CO2 adsorption and reaction: (---)cyclic voltammetry with argon in electrolyte; (—)cyclic voltammertry with CO2 in the electrolyte.

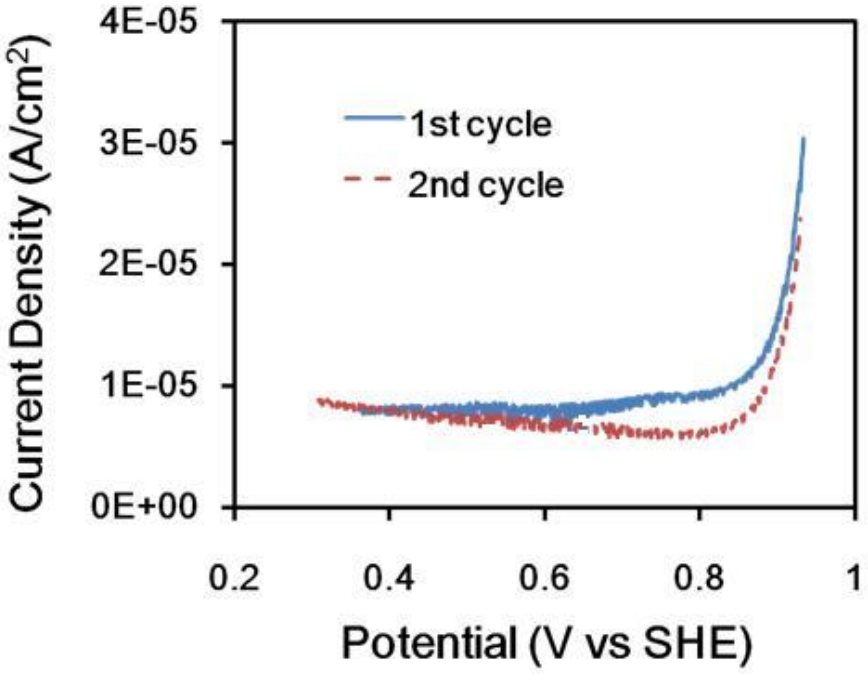

Figure 6.8 Stripping voltammograms with Au in 0.5M Choline Chloride following 20 min CO2 adsorption and reaction: (---)cyclic voltammetry with argon in electrolyte; (—)cyclic voltammertry with CO2 in the electrolyte.

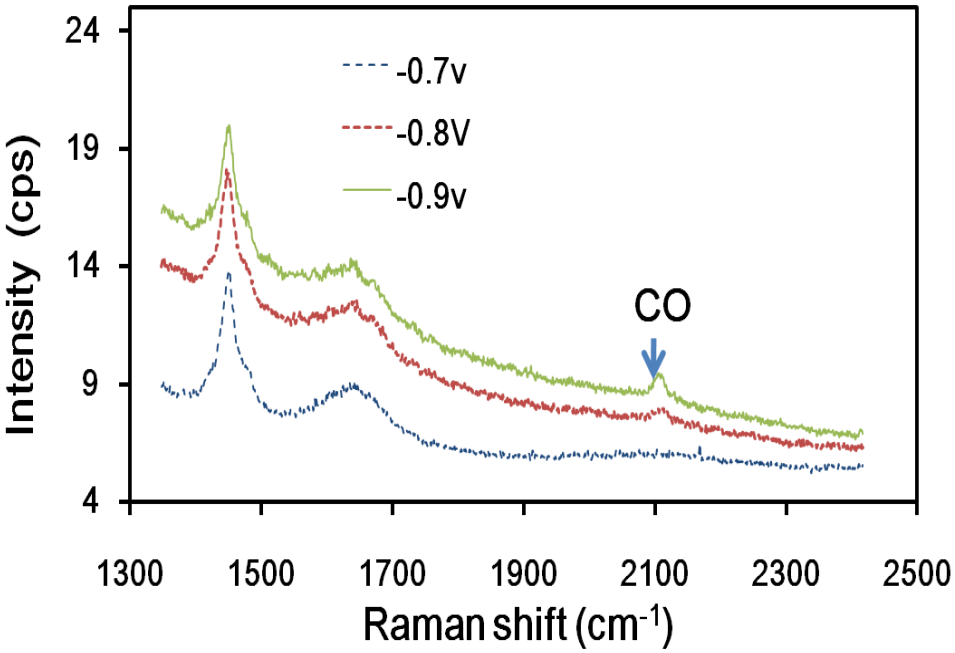

Figure 6.9 SERS spectra of CO_2 reduction on Au surface

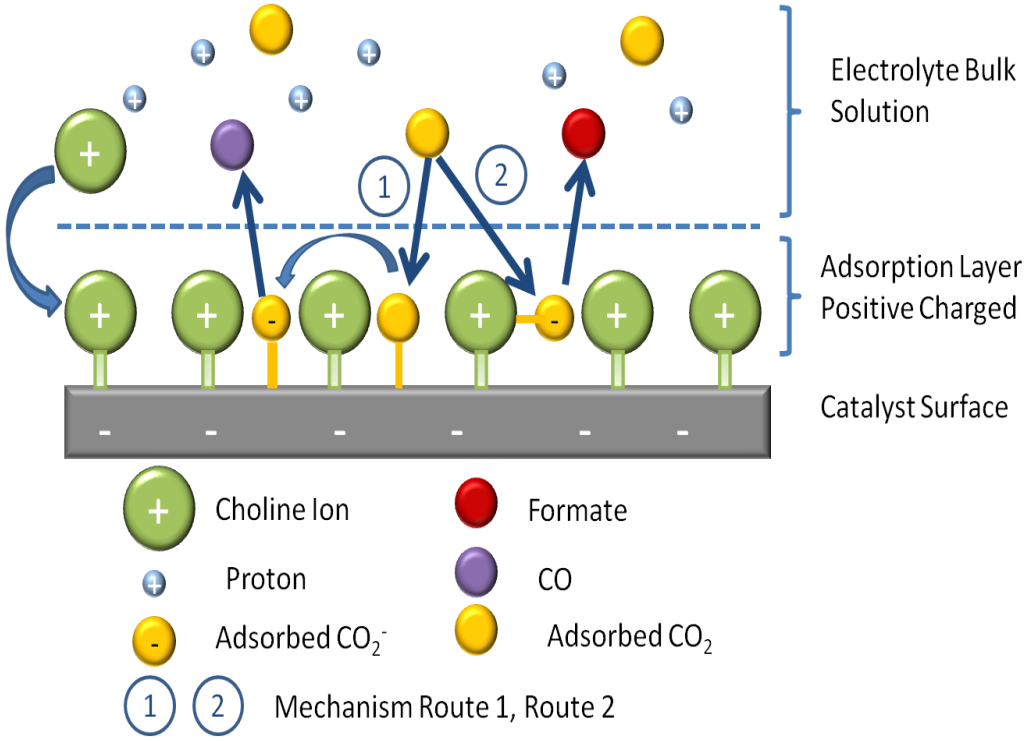

Figure 6.10 Mechanism of CO_2 reduction in choline chloride

Chapter 7 Effect of Different Anions in Choline Based Electrolyte on Hydrogen Evolution Reaction and Carbon Dioxide Reduction

7.1 Introduction

In previous research, hydrogen evolution reaction suppression in aqueous solution has been achieved with choline chloride solution. Moreover, with the same electrolyte, recycling of CO_2 back into fuels or other useful products with lower overpotential is fulfilled. As we know, choline chloride is an important additive in feedstock and one of the inexpensive quaternary ammonium salts, which has its own advantages over other quaternary ammonium salts.

Here, we would like to investigate the effect of different anions on the ability of choline to suppress the hydrogen evolution reaction and convert the CO_2into useful products. Chloride anion is a very interesting ion and deserves our attention. In previous research we assumed the chloride ion has little or no effect on the CO_2 reduction process because of the negative charge on the catalyst surface. However, chloride ion might still have some effects on the reactions happening on catalyst surface. Moreover, in SERS research area, chloride is considered as one of the strongest binding ion on metal surface

[231]. Therefore, it will be important to compare chloride ion with other anions to see the strength of the effect.

There has been extensive research related to the interaction between choline ion and gold surface. Liu et al. [232] studied the adsorption of 3-mercapto-1-propanesulfonic acid (MPS) and bis(3-sulfopropyl)-disulfide (SPS) on Au(111) electrode in a $HClO_4$ aqueous solution. Chloride ions were introduced into the electrolyte solution, and CV results show that chloride ion can induce the adsorption of thiol molecules on the Au(111) surface. Watling et al. [233] used SERS techniques to show that in acidic or neutral solution, chloride ion is adsorbed prior to gold dissolution and the scattering of (AuCl)-(ads) shifts to higher wavenumbers with increasing electrode potential. Vivek and his coworkers [234] analyzed the influence of halide ions on the stability of gold nanoparticles with a monolayer of dimethylaminopyridine (DMAP) or its conjugate acid (DMAPH(+)). Results show that at high pH, chloride ions are able to displace DMAP from the gold surface at low pH. For other kinds of metal electrodes, Ofstad et al. [235] showed that an electrode made from a fuel cell catalyst (50 wt % Pt/C) lost 10% of its platinum content over a 24hour period when exposed to in a sulfuric acid solution containing 10 ppm of chloride. Lubert et al. [236] revealed the existence of a chloropalladate(II) complex at the electrode surface if there were electrode reactions of palladium(II) at non-modified carbon paste electrodes (CPEs) in chloride solution.

Besides the choline chloride, we use other two electrolytes, choline tetrafluoroborate and choline acetate. One reason to use these two quaternary ammonium

salts is that the anion will interact with catalyst surface. Lin et al. [237] revealed that the tetrafluoroborate ion in ionic liquid has effects on a significant long-range surface restructuring of gold surface. Calaza et al. [238] mentioned that acetate is weakly adsorbed on Au/Pd(111) alloy surface. Another reason is that these two kinds of anions have different proton donation and acceptation ability, which will affect the proton transfer process and later the carbon dioxide process. Berna et al. [239] studied acetate adsorption at gold electrodes in perchloric acid solutions by cyclic voltammetry and in-situ infrared spectroscopy. Results showed that bonding of acetate to the surface involves the two oxygen atoms of the carboxylate group, with the OCO plane perpendicular to the metal surface.

In this study, we have used three-electrode electrochemical cell, 0.05M choline chloride, 0.05M choline acetate and 0.05M choline BF_4 individually as the electrolytes, and three different working catalysts, Pt, Pd and Au. Results demonstrated that different anions have little effect on hydrogen evolution reaction and carbon dioxide reduction.

7.2 Experiment

7.2.1 Catalyst materials

The catalyst metal black ink is prepared by mixing 5.6mg of metal black (Alfa Aesar 99.9% metal basis) with 1ml deoxygenated Millipore water. There are two kinds of counter electrodes used in this experiment. For platinum and palladium catalyst, the counter electrode is made by attaching a 25x25mm platinum mesh (size 52) to a 5-inch platinum wire (99.9%, 0.004 inch diameter). For gold electrode, the counter electrode is made by attaching a 25x25mm gold mesh (size 52) to a 5-inch gold wire (99.9%, 0.002 inch diameter). The reference electrode is a silver-silver chloride electrode with Flexible Connector (Table 1). 0.5M choline chloride is used as electrolyte. The solutions are prepared with triple distilled water. Measurements are taken at 25 ℃ under argon gas (99.999% purity) bubbling at 1 atm.

7.2.2 Instruments

Experiments are carried out in a custom-made 150mL, three-electrode electrochemical glass cell. The working electrode is prepared by applying the metal black ink onto the gold surface of a rotating electrode. The catalyst is applied on the surface of the rotating electrode by adding 12.5 μL of the ink to the surface and allowing the water to evaporate under ambient temperature for 60 minutes. The working electrode, reference electrode and counter electrode are connected to a potentiostat (Solartron SI 1287, Table 7.1).

7.2.3 Calibration of the reference electrode

Since the reference electrode is Ag/AgCl and it is desired to report findings in terms of the reversible hydrogen electrode (RHE) to neglect the effect of the PH on hydrogen evolution reaction, the reference electrode has to be calibrated versus RHE. As mentioned in previous chapter, a RHE is set up by bubbling hydrogen over the counter electrode and the potential of this electrode is compared to the reference electrode. To measure RHE potential, we short the working and the counter electrode lead, then, after bubbling the hydrogen under counter electrode for 20 minutes, we measure the open cell potential until it stabilizes. The open cell potential is the RHE vs. Ag/AgCl electrode.

7.2.4 Cyclic voltammetry

The electrolytes are first loaded into the glass cell and then purged with dry argon (99.99%) for two hours in order to remove oxygen from the electrolytes. Prior to all experiments, a 20-40 linear sweep cyclic voltammograms at 75mV.s-1 is taken between -1.5V and +1V vs. Ag/AgCl reference electrode in order to conditioning the electrodes, removing oxides from the surfaces. After, several cycles are performed at 10mV.s-1 before the final cycle to insure that the CV had stabilized (i.e., any “dirt” or other material is removed from the surfaces). Finally, cleaning and stabilizing CV cycles are

performed at 10mV.s-1 within the range of -1V to 0.3V. Then CO_2 is bubbled in the solution at 1atm pressure for 20 minutes. Cyclic voltammetry is conducted again at a sweep rate of 10mV/s in the range from -1V to 0.3V. To ensure the quality of the measurements, special attention is paid to the material cleaning and solution purity [207, 208].

7.2.5 SERS Spectroscopy

In-situ SERS spectral measurements are carried out with a laser source to excite the samples, a spectrometer to detect the Raman signal, a computer for the system control and data acquisition, a potentiostat to control the potential of the working electrode and an EC-SERS cell to accommodate the reaction.

In detail, working electrode is a 10 mm diameter Au disk polished to 1 um with a diamond suspension (Buehler) and flamed for 10 minutes with a hydrogen torch. The electrode is then electrochemically roughened as shown previously [210] except in the electrolyte with an anodic limit of 1.5 V vs Ag/AgCl. The counter electrode is a gold wire flamed with hydrogen torch for 2 min and the reference is Ag/AgCl.

Raman experiments are performed using an in-situ electrochemical cell. A He–Ne laser (λ=632.8 nm) is projected onto the sample at ~45° incidence. Scattered radiation is collected with a F/4 lens and focused at the entrance slit of a monochromator. A 1200

groove/mm grating diffracted radiation onto a cooled CCD detector (Andor model ?). Typical acquisition time is 30 s.

Table 7.1 Apparatus and experimental conditions:

Cell	Three-electrode glass cell
Potentiostat	Solartron SI 1287
Potential sweep	Solartron SI 1287
Working electrode	5.6mg/ml Platinum black, Palladium black, and Gold surface
Counter electrode	Platinum mesh, Gold mesh
Reference electrode	RE-5B Ag/AgCl Reference Electrode with Flexible Connector
Electrolyte	0.05M Choline Chloride, 0.05M Choline Acetate, 0.05M Choline BF_4
Pressure	1 atm
Potential	-1.0V -0.3V
Temperature	298.15K

7.3 Results

7.3.1 Experimental measurement of RHE vs Ag/AgCl electrode

From the Nernst equation, the pH value will affect the cyclic voltammetric curves. Basically, if pH increases by 1, the cyclic voltammetric curve will shift to the left by 0.059V. In order to remove the pH effect, we change the reference electrode to reversible hydrogen electrode (RHE). Theoretically, RHE vs. Ag/AgCl should be calculated with the equation: -0.059*pH-0.197 volt, where 0.197 is the theoretical value of Ag/AgCl vs. standard hydrogen electrode (SHE). In this experiment, we do both experimental and theoretical measurements and compare their values.

Table 7.2: Theoretical and experimental value of RHE vs. Ag/AgCl electrode:

	pH	Theoretical value	Experimental value
Choline Chloride	8.3	-0.69	-0.48
Choline Acetate	8.4	-0.69	-0.63
Choline BF4	3.5	-0.40	-0.39

As shown in Table 2, in choline acetate and choline BF_4, the theoretical values are almost the same as the experimental values (less than 60mV difference). However, in choline chloride, the difference is 200 mV, and thus cannot be neglected. Here, we report the CV curves based on the experimental value of RHE vs. Ag/AgCl electrode.

7.3.2 HER and CO_2 reduction with gold catalyst

For the hydrogen evolution reaction on gold surface (Figure 7.1), the CV curves are very close for choline chloride and choline acetate, and the starting points of the hydrogen evolution reaction are both around -0.3V vs. RHE, which is close to our previous results. However, with choline BF_4, which is more acidic than the other two electrolytes, there are much larger adsorption and desorption peaks and the starting point for the hydrogen evolution reaction is around -0.39V. In addition, the huge Faraday peaks in choline BF_4 might be related to multilayered double layer effect because the appearance of BF_4^- ion [237, 240]. Although the choline BF_4 showed the strongest suppression of the reaction based on the starting point of HER, the huge Faraday peaks revealed the highest ion activity of this electrolyte, which will not be considered as a good electrolyte.

For carbon dioxide reduction in the three electrolytes with gold catalyst surfaces (Figure 7.2- 7.4), all of them showed a lower overpotential for carbon dioxide reduction. In choline BF_4 (Figure 7.2), the carbon dioxide reduction started around -0.38V, and the oxidization and reduction peaks at around -0.25V and -0.26V demonstrated the single electron transfer process of choline cation. In choline acetate, the starting potential of carbon dioxide reduction is around -0.35V; while in choline chloride, the value is around

-0.32V. Although the difference among three kinds of choline based electrolytes is small, chloride still showed a slightly better performance in carbon dioxide reduction.

7.3.3 HER and CO_2 reduction with Platinum catalyst

For the hydrogen evolution reaction on palladium surface (Figure 7.5), unlike on the gold surface, the CV curves are very close for choline chloride and choline BF4. The hydrogen evolution reactions in both electrolytes start at around -0.28V vs. RHE. However, the hydrogen evolution reaction in choline acetate starts a little bit earlier than the other two electrolytes, which is around -0.04V. According to our previous studies, the obvious Faraday peaks in all three electrolytes around 0.4V are related to the interaction between choline ion and catalyst surface. Although the shape of the CV curves are very similar to each other for all three electrolytes, choline chloride and choline BF4 are considered better suppression electrolytes for HER because of their lower starting points of the hydrogen evolution reaction.

For carbon dioxide reduction in three electrolytes with palladium catalyst surface (Figure 7.6- 7.8), all of them demonstrate a lower overpotential for this reaction, the same as with the gold catalyst. In choline acetate (Figure 7.6), the carbon dioxide reduction started around -0.18V, and the oxidization peak demonstrates the interaction of the ion and catalyst surface. The increase of this peak reveals that after adding carbon dioxide in

the solution, the activity of the oxidation becomes larger. In choline BF_4, the starting potential of carbon dioxide reduction is around -0.37V; while in choline chloride, the value is around -0.43V. Here, it seems that choline acetate showed better performance than the other two kinds of electrolytes. However, later SERS data will show that the acetate will be decomposed to CO at very low overpotential, which will mimic the carbon dioxide reduction process.

7.3.4 HER and CO_2 reduction with Palladium catalyst

For the hydrogen evolution reaction on platinum surface (Figure 7.9) , the CV curves are very close for choline chloride and choline BF_4, which is similar to the reactions on the palladium surface. The hydrogen evolution reactions in both electrolytes are around -0.32V. However, the hydrogen evolution reaction in choline acetate still starts a little bit earlier than the other two electrolytes, which are around -0.15V. Therefore, choline chloride and choline BF_4 are considered as better suppression electrolytes for HER.

Carbon dioxide reduction on three electrolytes with platinum catalyst surfaces (Figure 7.10- 7.12) alldemonstrate a lower overpotential for carbon dioxide reduction. In choline acetate, the carbon dioxide reduction started around -0.28V. In choline BF_4, the starting potential of carbon dioxide reduction is around -0.42V; while in choline chloride,

the value is around -0.43V. Here, it seems that choline acetate still showed better performance than the other two electrolytes. However, later SERS data will show that the acetate is decomposed to CO at very low overpotential, which will mimic the carbon dioxide reduction process.

7.3.5 SERS experiment with choline acetate and gold catalyst

Figure 7.13 demonstrates that with a gold electrode, choline acetate will decompose and generate carbon monoxide (peak around 2100 cm^{-1}) even without carbon dioxide. This process is due to the decomposition of acetate anion in the solution. This result explained why the current density in the CV curves changed before the current density change of the choline chloride and choline BF_4. We did not observe the same results in choline chloride and choline BF_4.

7.4 Discussion

We are very interested in why different ions have little effect on electrochemical reactions of hydrogen evolution and carbon dioxide reduction. Scientists discovered the interaction between the chloride ion and different catalyst surface [241, 242] which can

shift the electron transfer to more negative potential. Nevertheless, in our study, comparing with BF_4 ion and acetate ion, the function of anions in choline based electrolyte can be neglected.

We attribute this to the very low negative potential for carbon dioxide reduction comparing to the point of zero charge on different catalyst. The point-of-zero-charge of polycrystalline platinum is 0.2V vs. NHE [243], 0.33V vs. the Ag/AgCl on Au (111) [244] and 0.25V vs. RHE for palladium catalyst [245]. Although the point-of-zero-charge depends largely on several factors such as the type of electrolyte, the structure of the catalyst surface and the temperature, the value will not shift much with certain catalysts. In our experiments, the carbon dioxide reduction and hydrogen evolution reaction always happen at negative potential. At such potential, the catalyst surface is always negatively charged. Therefore, the anion cannot get close to the catalyst surface and only the choline caion can form a layer on the catalyst surface (Figure 7.14).

For acetate anions, previous research does not show that acetate can be converted to carbon monoxide [137, 246]. However, with the monolayer of choline cations, the acetate can be converted to carbon monoxide very easily. We assume it is because the acetate anion mimics the carbon dioxide molecule in the solution, which will form an intermediate with choline. This intermediate will then transfer to carbon monoxide at much lower overpotential.

7.5 Conclusion

In order to investigate the effect of different anions on the hydrogen evolution reaction and carbon dioxide reduction process with choline as cation, we have used three-electrode electrochemical cells, 0.05M choline chloride, 0.05M choline acetate and 0.05M choline BF_4 as the electrolyte, and three different working catalysts; Pt, Pd and Au. Results demonstrate that for the hydrogen evolution reaction, the choline chloride and choline BF_4 showed better performance than choline acetate. Moreover, carbon dioxide reduction in choline acetate seems to have lower overpotential than choline chloride and choline BF_4. However, it is because the acetate ion is decomposed during the electrochemical reduction process. In addition, as ionic liquid, choline acetate and choline BF_4 are not easy to synthesize and very expensive. Overall, choline chloride is still considered as the efficient and economic amine to suppress the hydrogen evolution reaction and promote the carbon dioxide reduction process.

7.6 Acknowledgement

This work was supported by the US Department of Energy under grant DE-SC0004453. The views expressed in this paper are those of the authors and do not

necessarily represent the views of the US Department of Energy. The authors thank Nichole Honesty for help with the SERS experiments.

7.7 Figures

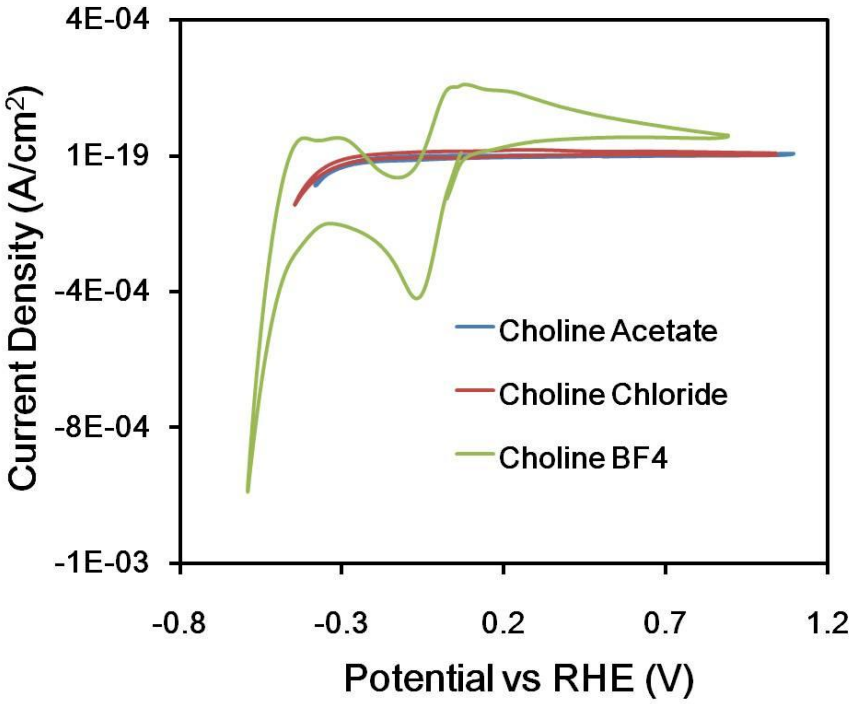

Figure 7.1 Hydrogen evolution reactions with Au electrode

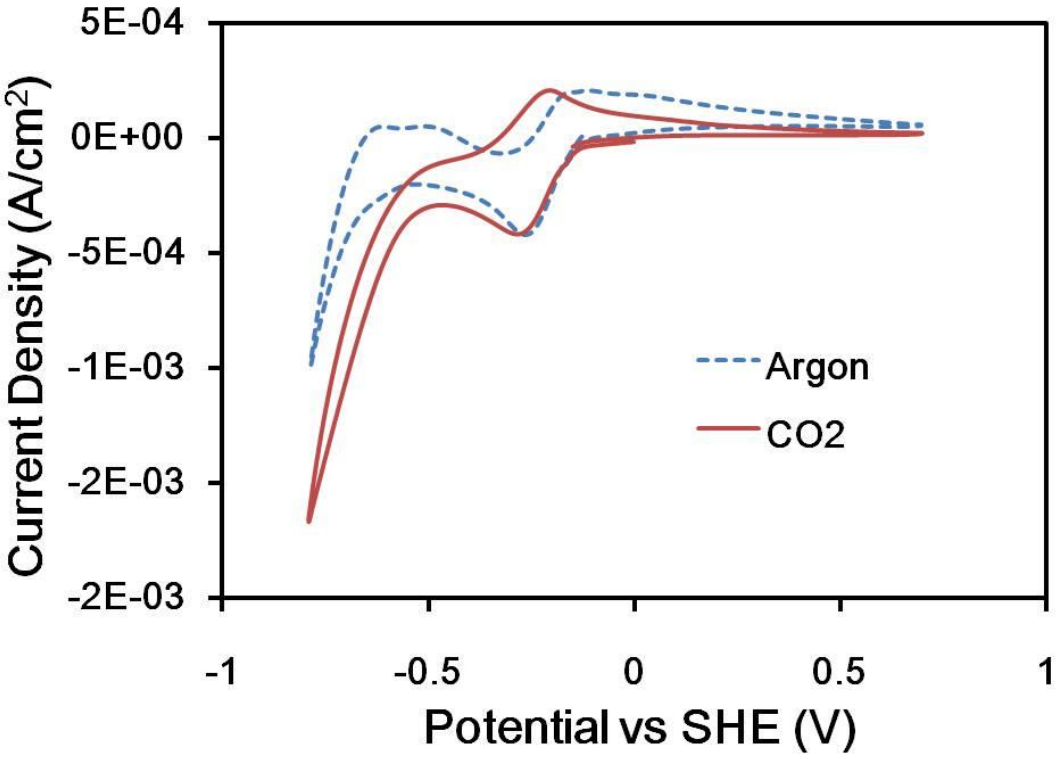

Figure 7.2 CO_2 reduction in choline BF_4 with Au electrode

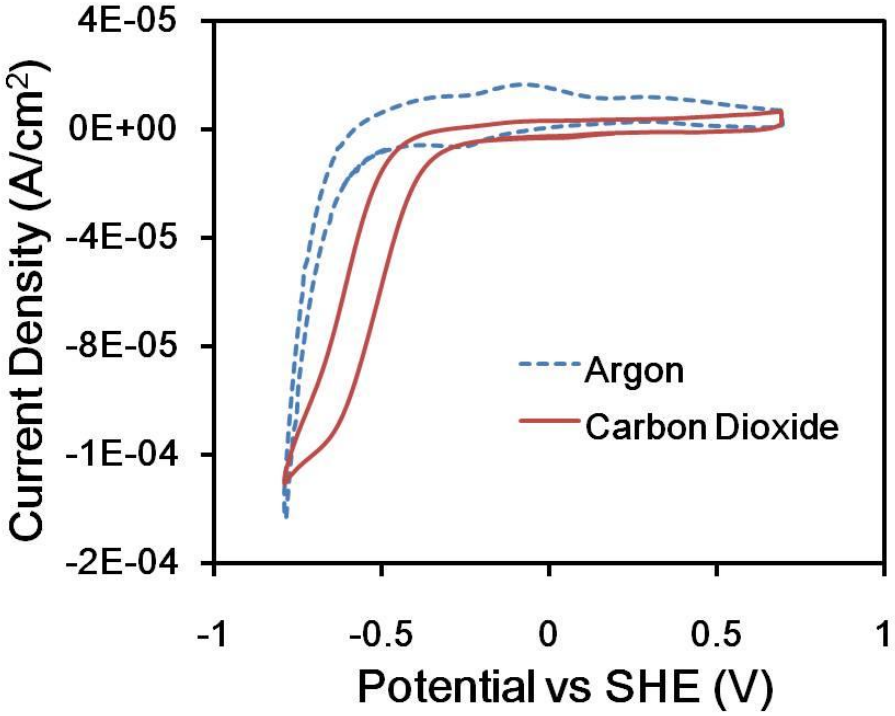

Figure 7.3 CO_2 reduction in choline chloride with Au electrode

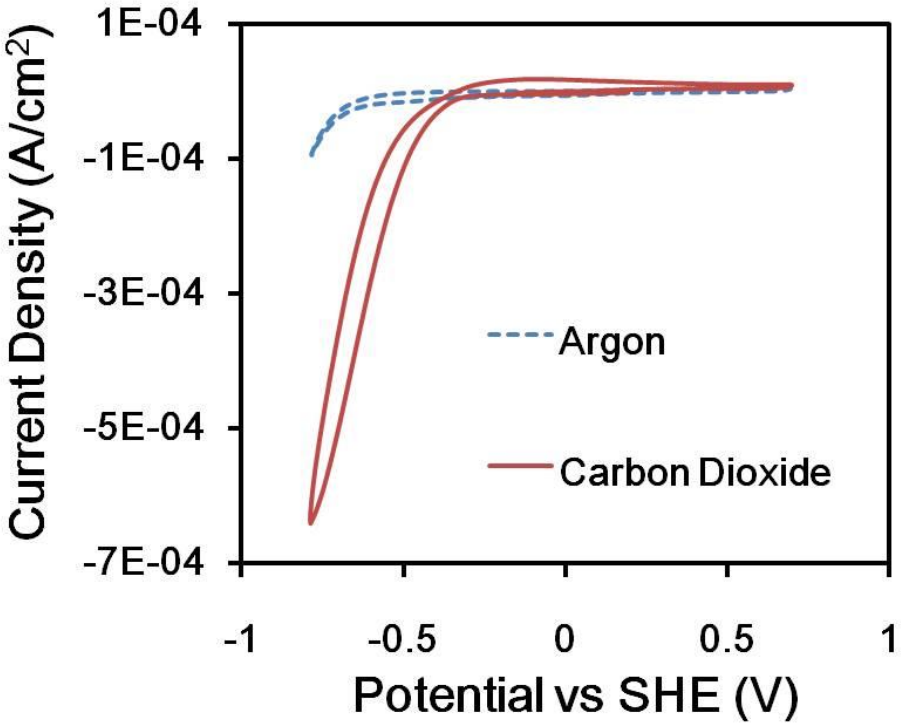

Figure 7.4 CO_2 reduction in choline acetate with Au electrode

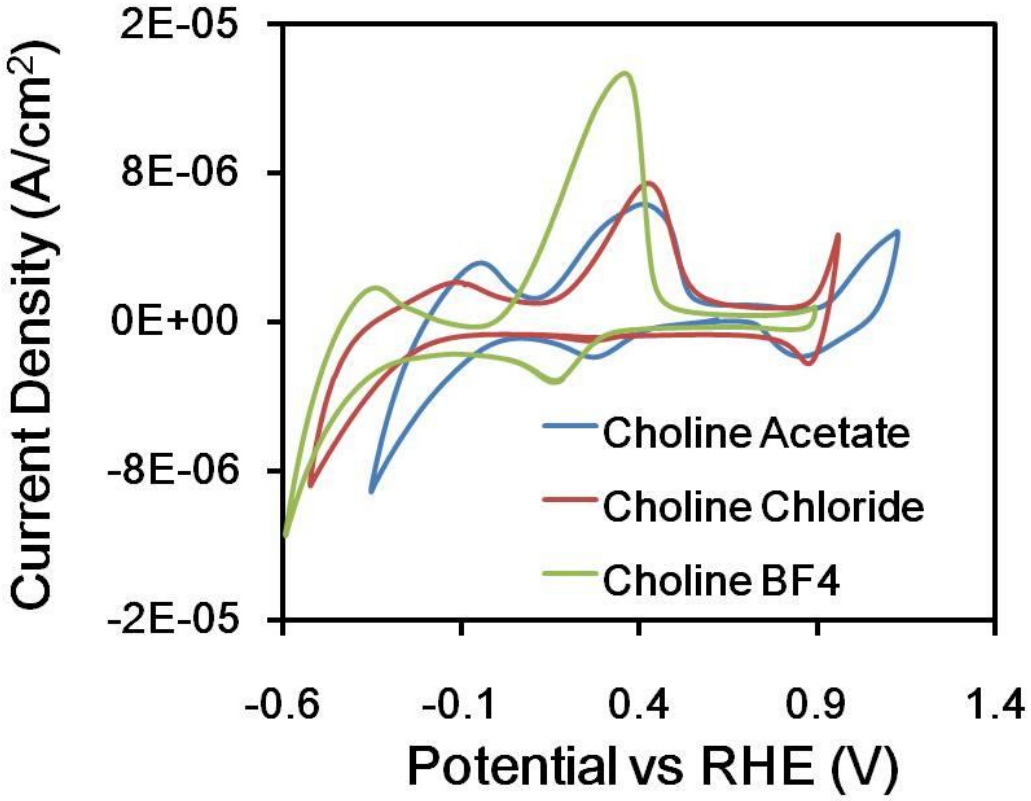

Figure 7.5 Hydrogen evolution reactions with Pd electrode

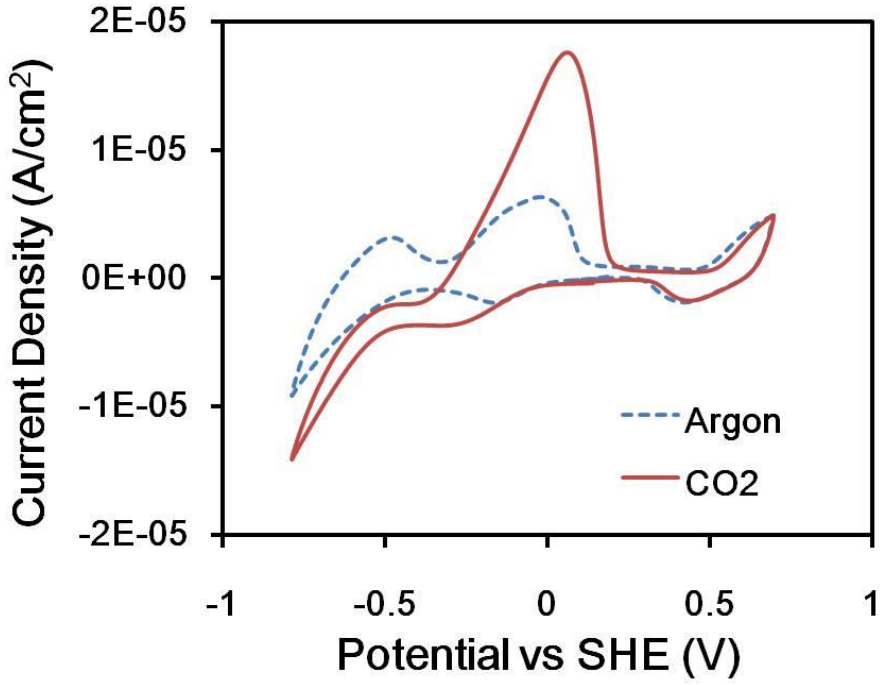

Figure 7.6 CO_2 reduction in choline acetate with Pd electrode

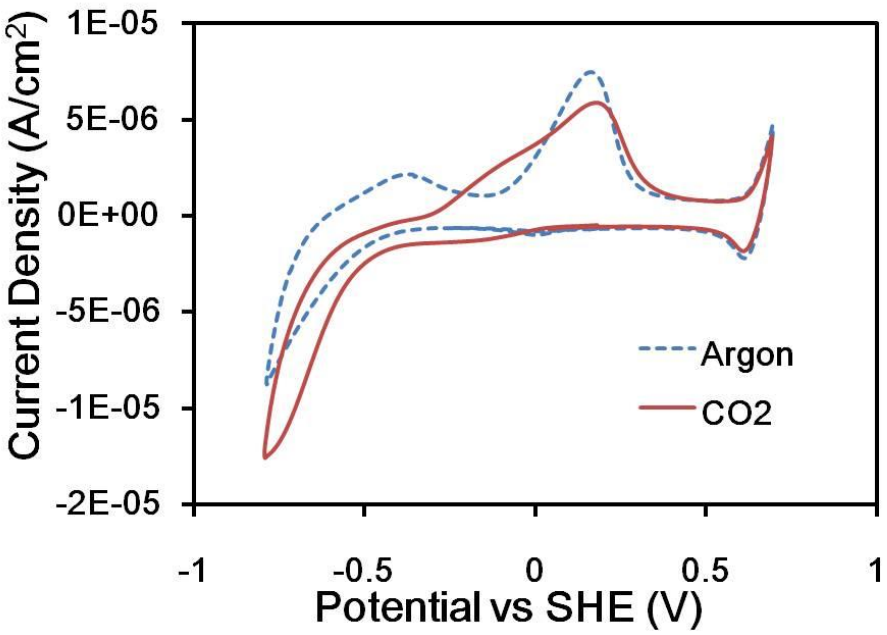

Figure 7.7 CO_2 reduction in choline chloride with Pd electrode

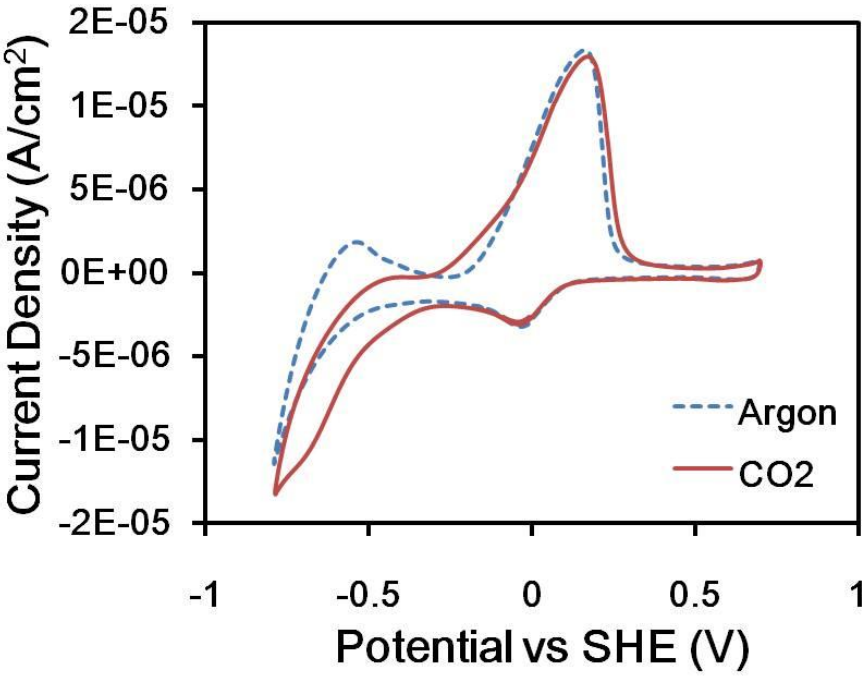

Figure 7.8 CO_2 reduction in choline BF_4 with Pd electrode

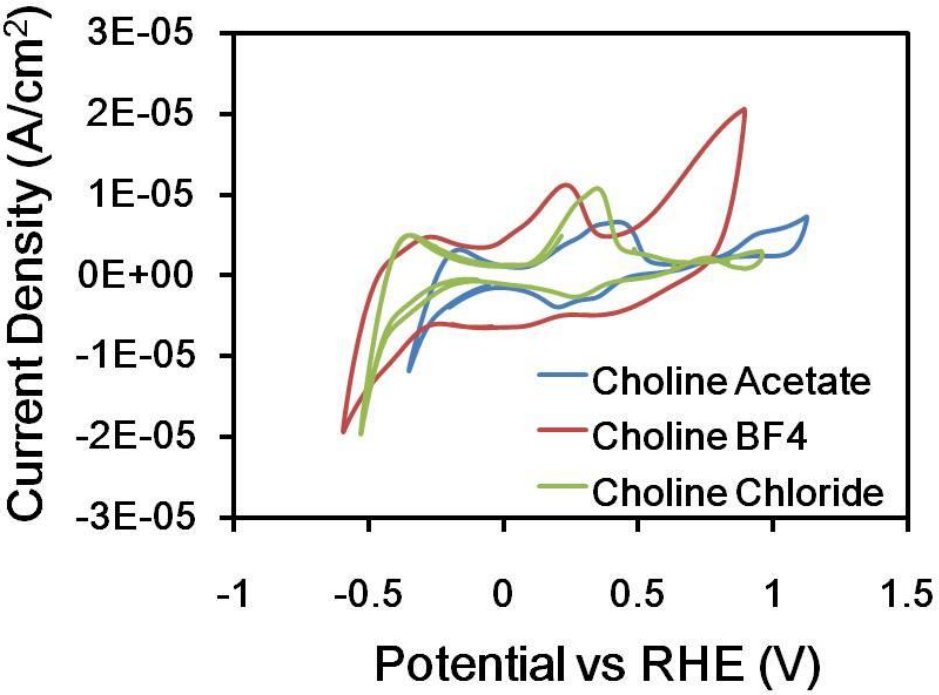

Figure 7.9 Hydrogen evolution reactions with Pt electrode

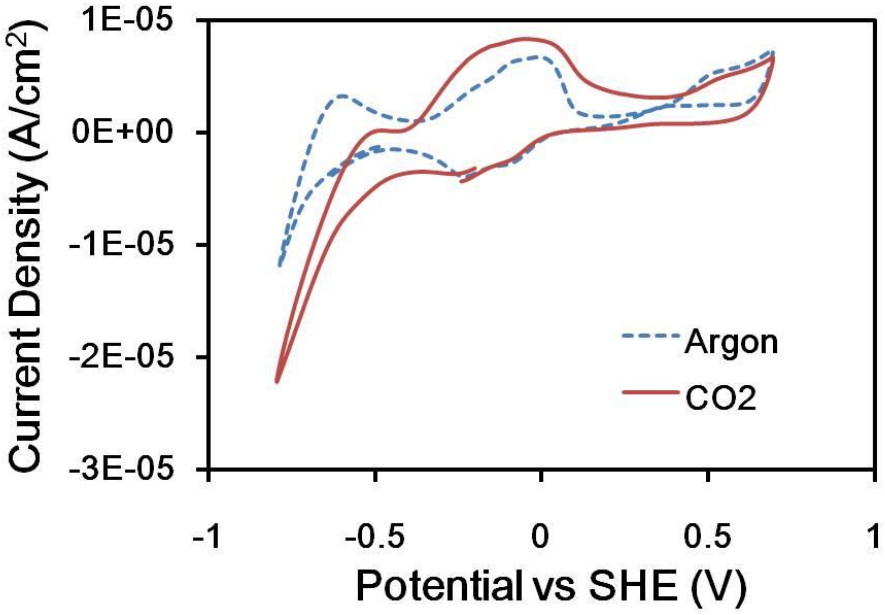

Figure 7.10 CO_2 reduction in choline acetate with Pt electrode

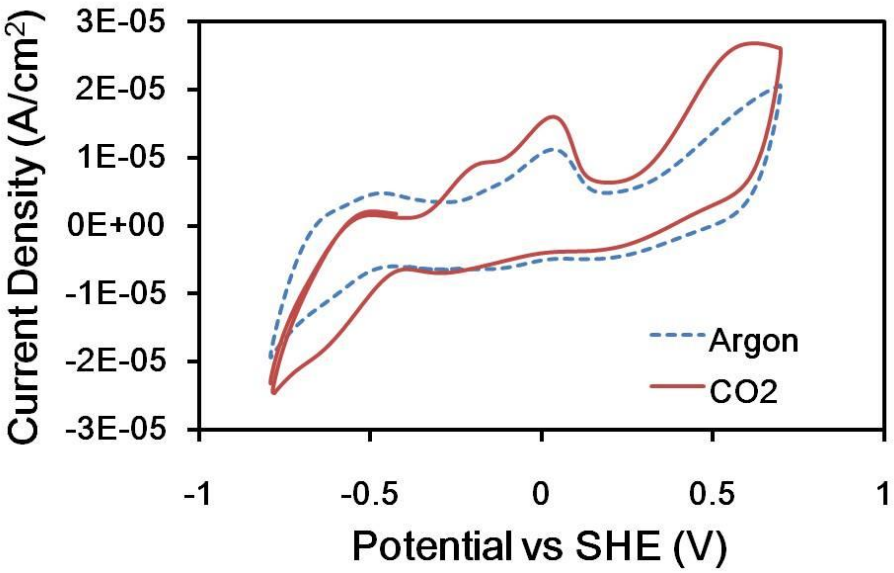

Figure 7.11 CO_2 reduction in choline BF_4 with Pt electrode

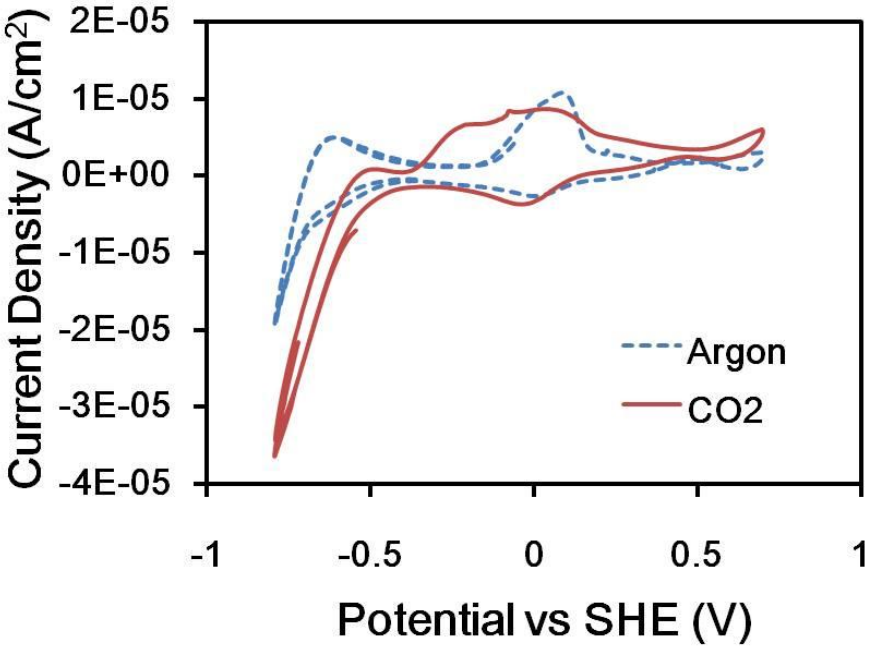

Figure 7.12 CO2 reduction in choline chloride with Pt electrode

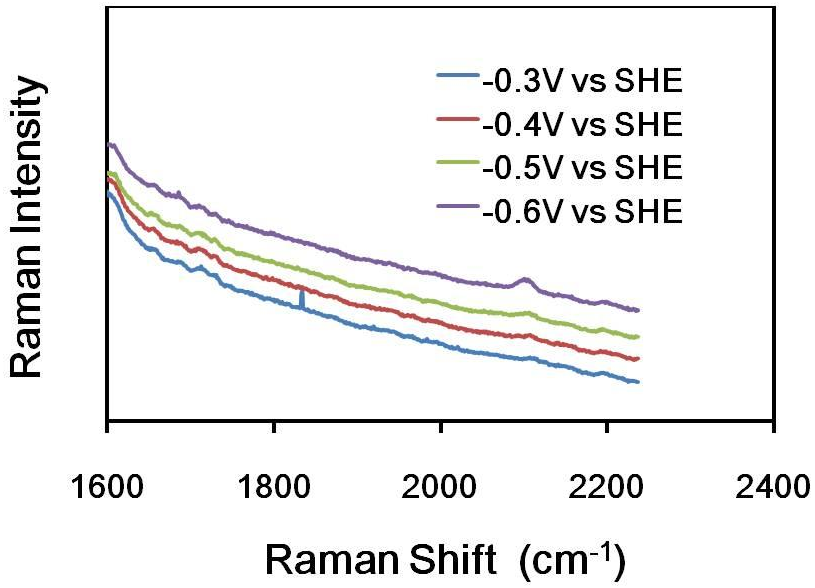

Figure 7.13 SERS of pure choline acetate with gold electrode

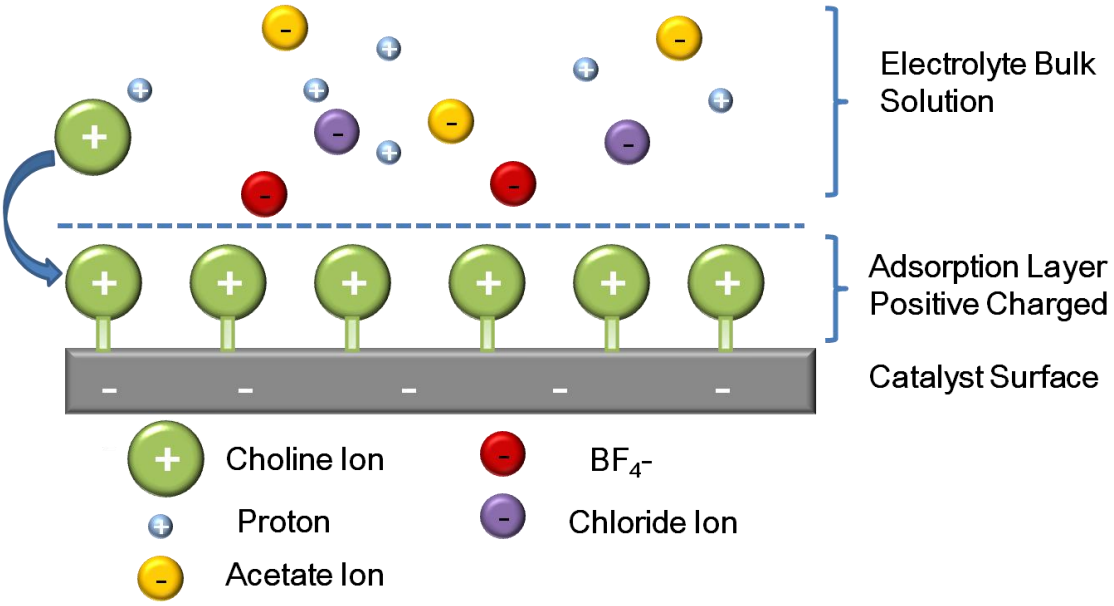

Figure 7.14 Mechanism illustration

Chapter 8 Conclusion and Recommendations

8.1 Conclusion

Artificial photosynthesis of useful carbon products from carbon dioxide remains a critical engineering challenge in the electrochemistry field. In aqueous environment, two key factors limiting the development in this challenge: the low overpotential for water electrolysis and the high overpotential for CO_2 reduction.

In this work, several electrochemistry techniques combined with SERS spectra experiments were utilized to verify that choline based electrolyte, one kind of quaternary ammonium salt, achieved both HER suppression and overpotential decrease for CO_2 reduction.

In particular, several new findings resulted from this study. First, the electrocatalysis of choline chloride electrolyte with different catalytic electrodes was investigated in a specially designed three-electrode cell. When comparing the CV figures among 0.5M choline chloride solution, sodium bicarbonate, buffer solution and sulfuric acid, with 3 catalytic electrodes (Au, Pd and Pt), we showed a correlation between hydrogen adsorption and hydrogen evolution reaction. The choline chloride electrolyte showed the strongest suppression in hydrogen adsorption. Its hydrogen adsorption peaks were nearly invisible while HER potential was pushed far lower than other electrolytes. SERS spectra

indicated that choline chloride's high suppression of the HER could be contributed by the formation of a thin layer of choline cations on catalytic electrodes that blocks the adsorption of H ion and therefore suppresses the hydrogen evolution reaction. Moreover, experiments of formic acid/choline chloride solution indicated that the choline chloride layer targeted the hydrogen adsorption instead of blocking all reactions on the surface. It was shown that catalysts' surface were still active for other molecules, such as negatively charged formate, in the mixed electrolyte.

Second, we have studied CO_2 reduction using choline chloride with different metal catalysts. Cyclic voltammograms show that the presence of choline chloride significantly reduced the overpotential, a key challenge leading to low efficiency in CO_2 conversion, by suppressing the hydrogen evolution and lowering CO_2 conversion potential; therefore, the competition between water electrolysis and carbon dioxide conversion reactions was reduced.

Third, the stripping voltammetry and SERS experiments help identifying the major products with different catalytic metals in choline chloride. The results have determined that the CO evolution dominates on platinum, platinum, ruthenium and gold catalysts, and formic acid is the dominating product on palladium catalyst.

Fourth, after comparing different choline based electrolytes with original choline chloride during the process of the hydrogen evolution reaction and carbon dioxide reduction, we discovered that different anions have little effect on both of these processes.

Choline chloride is still considered overall as the most efficient and economic co-catalyst to promote the desired reactions and suppress the non-desired.

8.2 Recommendations

There is still much work to be done to improve the understanding of electrochemical reduction of CO_2 into useful products. A variety of measurement techniques, such as SFG, could be used to examine the catalyst surface during the reduction process and provide more details about the mechanism of the CO_2 reduction. Moreover, HPLC or GC can be applied to detect small amounts of products in CO_2 reduction process.

Specifically, the details of the mechanism on other catalysts could be studied as well. We have analyzed the HER and CO_2 mechanism on gold catalyst in detail, and it is because gold is one of the limited metal catalysts that can cooperate with SERS technique. However, the mechanism on other catalysts is, at least, as important to be examined in depth. If SFG, for example, can be used, then several other kinds of metals can be studied.

In addition, more products might be formed on the catalyst surface. Although we discovered the main products on different catalysts using electrochemistry methods, other techniques such as HPLC and GC can also be utilized to analyze the formation of other byproducts.

Finally, some kinetic simulation could be also conducted with our experimental data, perhaps through collaboration with other research groups with expertise in kinetic process modeling. The topics related to reaction mechanism, diffusion process, double layer region and active catalyst spots are all intrigue to be explored.

Appendix A Experiment protocol

Gold electrode surface cleaning and polishing

1. Before adding other metal catalysts on gold supporting electrode, the electrode should be cleaned and polished.
2. Wiping the gold surface electrode with a Kimwipe® and rinsing with Millipore® water
3. Use 1000/1500 grit paper with diamond colloid suspension (yellow/red/blue). Note to make figure eight motion when press the gold electrode on the grit paper
4. Clean the gold surface again with Millipore® water. If the surface is still not clean enough, methanol can be used.

Catalyst ink preparation procedure

1. Weight 5.6mg metal black with a small a glass vial using electronic balance
2. Add 1g Millipore water. (Make sure the monitor is calibrated for resistivity around 18.2 MΩ•cm)

3. Place the glass vial into the sonicating bath and sonicate for at least 8 minutes
4. Place 12.5 uL of catalyst ink on the gold electrode surface. Be sure the gold electrode is well covered with the catalyst drop
5. Put the gold electrode under air to dry for one hour or longer. If the drying time is not enough, the catalyst will fall off during experiment For different catalyst ink, the drying time might be vary.

Cleaning the three-electrode glass system

1. After each electrochemistry experiment, the three-electrode glass system should be cleaned very carefully
2. Rinse the glassware with Millipore water.
3. Put the glass system in an acid bath containing 50%/50% sulfuric acid and Millipore water. Note the acid bath should be changed every three to six months.
4. Keep the glassware in the acid bath for at least one day.
5. Before using, carefully clean the three-electrode glass system with Millipore water

Counter electrode preparation

1. Two kinds of counter electrodes were used in this experiment: gold counter electrode and platinum counter electrode
2. Attach a 25x25mm platinum/gold mesh (size 52) to a 5 inch platinum/gold wire (99.9%, 0.004 inch diameter)
3. Let the wire go through a glass joint.
4. Slide a red silicone septum over the wire.
5. Attach a Teflon top to the wire and tighten it with the glass joint.

Electrolytes preparation

1. Weight the desired amount of crystal structure electrolyte materials using beaker. The crystal electrolyte materials used in the experiments include choline chloride, choline acetate, choline BF_4, and sodium bicarbonate.
2. Add 100mL of Millipore water into the beaker and let the crystal to dissolve.
3. Buffer solution is made of borox, hydrochloric acid and Millipore water. The hydrochloric acid is added by a burette to arrange the pH of the buffer solution.
4. Sulfuric acid solution is made by adding the desired amount of concentrated sulfuric acid into 100mL of Millipore water.
5. Choline chloride solution with different concentrated formic acid is prepared by adding formic acid in choline chloride with a burette.

6. The pH of each electrolyte is measured with the electronic pH meter. Note that we should record the pH after it stabilizing.

Reversible hydrogen electrode calibration

1. Prepare the targeted electrolyte solution and fill the cell and reference electrode reservoir with this solution,
2. Place the reference electrode in the reference electrode reservoir and attach the reference electrode lead from the potentiostat to the reference electrode,
3. Attach both the working electrode lead and the counter electrode lead from the potentiostat to the wire attached to the platinum mesh counter electrode of the electrochemical cell,
4. Bubble hydrogen under the counter electrode in the cell,
5. Measure the open cell potential difference between the reference electrode and the counter electrode until it stabilizes. It usually takes 10 minutes.
6. This value can then be used to convert all potentials to the absolute scale of the RHE.

Hydrogen evolution reaction procedure

1. Assemble the three-electrode system based on Figure 4.1. Remove the right glass cap and put the counter electrode there. Leave the reference electrode reservoir open.
2. Pour in the electrolyte through the reference electrode reservoir to avoid the formation of the bubble in the luggin capillary.
3. Place the Ag/AgCl electrode in the reference electrode reservoir.
4. Attach an argon line to the adapter.
5. Attach a control line with a valve to the inlet on the glass cell. Keep the valve close.
6. Attach an outline to the outlet on the glass cell.
7. Turn on the argon cylinder and slowly open the rotameter to let the argon go through the sparging tube into the cell but not the inlet.
8. Begin to bubble argon through the electrolyte at for at least 20 minutes.
9. Turn on the valve on the control line.
10. Screw the working electrode into a RDE controller, which is connected to a potentiostat.
11. Remove the glass cap on the top of the cell and let working electrode go through it and contact the electrolyte in the cell.
12. Scan between -1.5V to 1V at 75mV/s for at least 30 cycles.
13. If the CV is stabilized after 30 cycles, scan again at 10mV for three cycles between desired potential range. The CV obtained here demonstrates the typical HER CV.
14. For testing the reaction activity of formic acid in choline chloride, after gaining the typical HER CV, different amount of formic acid is added into the electrolytes (from

the smallest amount to highest amount).

15. Repeat the procedure 12 and 13 to gain the CVs of formic acid in choline chloride.

Carbon dioxide reduction experiment

1. After HER procedure, turn off argon cylinder and the valve on the control line.
2. Turn on the CO_2 and bubble it into the three electrode cell for at least 20 minutes.
3. Scan between the desired potential range at 10mV/s.
4. Compare the CVs with HER. If current and/or faradaic waves increase, there is the carbon dioxide reduction region.

Chronoamperometry experiment

1. With the setup the same as the HER experiment, chronoamperometry is performed in which the potential was held constant for at least 6 hours.
2. There two kinds of electrolyte used in the experiment: 0.1 M formic acid and 0.1M formic acid with 0.5M choline chloride
3. Potential is held at 0.2 V vs RHE for formic acid oxidation.
4. Sometimes, working electrode is set to rotate at 2000 rpm in order to remove carbon

dioxide bubbles formed at the catalyst surface during formic acid oxidation.

CO stripping experiment

1. After CO_2 reduction experiment, CO stripping is performed.
2. Potential is held at the value where carbon dioxide reduction dominated and little hydrogen evolution reaction is seen (based on CVs obtaining from HER and CO_2 reduction) for 20 minutes.
3. While hold the potential, turn off the CO_2 cylinder and turn on the argon.
4. Blow argon into the cell for at least 20 minutes.
5. Scan between the holding potential to 1V at 5mV/s or 10mV/s for three cycles.
6. The first scan cycle will show the CO peak, while the second and third will not show.

Formic acid oxidation experiment

1. For fomic acid oxidation (stripping), electrolytes with different concentration of formic acid (0.001M, 0.01M and 0.03M) are prepared.
2. After the blank cyclic voltammetry taken by bubbling argon into the 0.5M choline based electrolytes, different amount of formic acid is added into the electrolyte.

3. Cyclic voltammetry is taken again and different cyclic voltammetry figures are compared to acquire the formic acid reaction peak in the electrolyte.

References

1. *Energy - The Changing Climate*. 2007, Royal Commission on Environmental Pollution. p. 2.
2. Boucher, O., J.A. Lowe, and C.D. Jones, *Implications of delayed actions in addressing carbon dioxide emission reduction in the context of geo-engineering.* Climatic Change, 2009. **92**(3-4): p. 261-273.
3. Solomon, S., et al., *Irreversible climate change due to carbon dioxide emissions.* Proceedings of the National Academy of Sciences of the United States of America, 2009. **106**(6): p. 1704-1709.
4. Spataru, N., et al., *Electrochemical reduction of carbon dioxide at ruthenium dioxide deposited on boron-doped diamond.* Journal of Applied Electrochemistry, 2003. **33**(12): p. 1205-1210.
5. Bandi, A. and H.M. Kuhne, *Electrochemical Reduction of Carbon Dioxide in Water: Analysis of Reaction Mechanism on Ruthenium-Titanium-Oxide.* Journal of the Electrochemical Society, 1992. **139**(6): p. 1605-1610.
6. Morris, A.J., G.J. Meyer, and E. Fujita, *Molecular Approaches to the Photocatalytic Reduction of Carbon Dioxide for Solar Fuels.* Accounts of Chemical Research, 2009. **42**(12): p. 1983-1994.
7. Usubharatana, P., et al., *Photocatalytic process for CO2 emission reduction from industrial flue gas streams.* Industrial & Engineering Chemistry Research, 2006. **45**(8): p. 2558-2568.
8. Martin, S.T., C.L. Morrison, and M.R. Hoffmann, *PHOTOCHEMICAL MECHANISM OF SIZE-QUANTIZED VANADIUM-DOPED TIO2 PARTICLES.* Journal of Physical Chemistry, 1994. **98**(51): p. 13695-13704.
9. Flaisher, H., R. Tenne, and M. Halmann, *Photoelectrochemical reduction of carbon dioxide in aqueous solutions on p-GaP electrodes: an a.c. impedance study with phase-sensitive detection.* Journal of Electroanalytical Chemistry, 1996. **402**(1-2): p. 97-105.
10. Halmann, M., *Photoelectrochemical reduction of aqueous carbon dioxide on p-type gallium phosphide in liquid junction solar cells [5].* Nature, 1978. **275**(5676): p. 115-116.
11. Ikeda, S., et al., *Photoelectrochemical reduction products of carbon dioxide at metal coated p-GaP photocathodes in non-aqueous electrolytes.* Journal of Electroanalytical Chemistry and Interfacial Electrochemistry, 1989. **260**(2): p. 335-345.
12. Ikeda, S., K. Ito, and H. Noda, *Electrochemical Reduction Of Carbon Dioxide Using Gas Diffusion Electrodes Loaded With Fine Catalysts.* AIP Conference Proceedings, 2009. **1136**(1): p. 108-113.

13. Subramanian, K., et al., *Electrochemical membrane reactor for the reduction of carbondioxide to formate.* Journal of Applied Electrochemistry, 2007. **37**(2): p. 255-260.
14. Chaplin, R.P.S. and A.A. Wragg, *Effects of process conditions and electrode material on reaction pathways for carbon dioxide electroreduction with particular reference to formate formation*, in *Journal of Applied Electrochemistry*. 2003, Springer Science & Business Media B.V. p. 1107-1123.
15. Stock, J.T., et al. *Electrochemistry, past and present*. Washington, DC: American Chemical Society.
16. Wahl, *A Short History of Electrochemistry.* Galvanotechtnik, 2005. **96**(8): p. 1820-1828.
17. Cai, Y. and A.B. Anderson, *The Reversible Hydrogen Electrode:鈥?Potential-Dependent Activation Energies over Platinum from Quantum Theory.* The Journal of Physical Chemistry B, 2004. **108**(28): p. 9829-9833.
18. Reinmuth, W.H., *Theory of Stationary Electrode Polarography.* Analytical Chemistry, 1961. **33**(12): p. 1793-1794.
19. Hickling, A., *Studies in electrode polarisation. Part IV.-The automatic control of the potential of a working electrode.* Transactions of the Faraday Society, 1942. **38**: p. 27-33.
20. Heinze, J., *Cyclic Voltammetry—"Electrochemical Spectroscopy". New Analytical Methods (25).* Angewandte Chemie International Edition in English, 1984. **23**(11): p. 831-847.
21. Kakiuchi, T., *A theory of voltammetry of ion transfer across a liquid membrane in the absence of supporting electrolytes using the Nernst-Planck equation and electroneutrality assumption.* Electrochimica Acta, 1998. **44**(1): p. 171-179.
22. Bard, A.J.F., L. R., *Electrochemical Methods. Fundamentals and Applications.* 2001.
23. Short, G.D. and E. Bishop, *Concentration Overpotentials on Antimony Electrodes in Differential Electrolytic Potentiometry.* Analytical Chemistry, 1965. **37**(8): p. 962-967.
24. Bard, A.J. and L.R. Faulkner, *Electrochemical Methods: Fundamentals and Applications*. 2nd ed. 2001, New York: John Wiley & Sons, Inc.
25. Eckermann, A.L., et al., *Electrochemistry of redox-active self-assembled monolayers.* Coordination Chemistry Reviews. **254**(15-16): p. 1769-1802.
26. Azizi, O., et al., *The investigation of the kinetics and mechanism of hydrogen evolution reaction on tin.* International Journal of Hydrogen Energy, 2007. **32**(12): p. 1755-1761.
27. de Chialvo, M.R.G. and A.C. Chialvo, *The Tafel-Heyrovsky route in the kinetic mechanism of the hydrogen evolution reaction.* Electrochemistry Communications, 1999. **1**(9): p. 379-382.

28. Ovchinnikov, A.A. and V.A. Benderskii, *Theory of electrochemical hydrogen evolution reactions: Part I. The model and fundamental relationships.* Journal of Electroanalytical Chemistry. **100**(1-2): p. 563-582.
29. Quaino, P.M., M.R. Gennero de Chialvo, and A.C. Chialvo, *Hydrogen electrode reaction: A complete kinetic description.* Electrochimica Acta, 2007. **52**(25): p. 7396-7403.
30. Gennero de Chialvo, M.R. and A.C. Chialvo, *Hydrogen diffusion effects on the kinetics of the hydrogen electrode reaction. Part I. Theoretical aspects.* Physical Chemistry Chemical Physics, 2004. **6**(15): p. 4009-4017.
31. Vilekar, S.A., I. Fishtik, and R. Datta, *Kinetics of the Hydrogen Electrode Reaction.* Journal of The Electrochemical Society. **157**(7): p. B1040-B1050.
32. Langmuir, I., *THE CONSTITUTION AND FUNDAMENTAL PROPERTIES OF SOLIDS AND LIQUIDS. PART I. SOLIDS.* Journal of the American Chemical Society, 1916. **38**(11): p. 2221-2295.
33. Yan, J.H., W.S. Li, and Q.Y. Zhan, *Failure mechanism of valve-regulated lead-acid batteries under high-power cycling.* Journal of Power Sources, 2004. **133**(1): p. 135-140.
34. Wu, Y.M., et al., *Effect of bismuth on hydrogen evolution reaction on lead in sulfuric acid solution.* Journal of Power Sources, 2005. **144**(2): p. 338-345.
35. Lam, L.T., et al., *Oxide for valve-regulated lead-acid batteries.* Journal of Power Sources, 1998. **73**(1): p. 36-46.
36. Mungole, M.N. and R. Balasubramaniam, *Hydrogen desorption kinetics in MmNi4.2Al0.8-H system.* International Journal of Hydrogen Energy, 1998. **23**(5): p. 349-353.
37. Furuya, Y., et al., *Hydrogen desorption from pure titanium with different concentration levels of hydrogen.* Journal of Alloys and Compounds, 2007. **446**: p. 447-450.
38. Momirlan, M. and T.N. Veziroglu, *The properties of hydrogen as fuel tomorrow in sustainable energy system for a cleaner planet.* International Journal of Hydrogen Energy, 2005. **30**(7): p. 795-802.
39. Koca, A., *Hydrogen evolution reaction on glassy carbon electrode modified with titanyl phthalocyanines.* International Journal of Hydrogen Energy, 2009. **34**(5): p. 2107-2112.
40. Winter, C.J., *Hydrogen energy--expected engineering breakthroughs.* International Journal of Hydrogen Energy, 1987. **12**(8): p. 521-546.
41. Serpone, N., D. Lawless, and R. Terzian, *Solar fuels: Status and perspectives.* Solar Energy, 1992. **49**(4): p. 221-234.
42. Karyakin, A.A., et al., *Hydrogenase electrodes for fuel cells.* Biochemical Society Transactions, 2005. **33**(1): p. 73-75.
43. Turner, J.A., *Sustainable hydrogen production.* Science, 2004. **305**(5686): p. 972-974.

44. Krassen, H., et al., *Immobilization of the [FeFe]-hydrogenase CrHydA1 on a gold electrode: Design of a catalytic surface for the production of molecular hydrogen.* Journal of Biotechnology, 2009. **142**(1): p. 3-9.
45. Uchida, T., et al., *Hydrogen Evolution Reaction Catalyzed by Proton-Coupled Redox Cycle of 4,4 鈥?Bipyridine Monolayer Adsorbed on Silver Electrodes.* Journal of the American Chemical Society, 2008. **130**(33): p. 10862-10863.
46. Bukowska, J. and K. Jackowska, *Influence of thiourea on hydrogen evolution at a silver electrode as studied by electrochemical and SERS methods.* Journal of Electroanalytical Chemistry, 1994. **367**(1-2): p. 41-48.
47. Masashi, A., et al., *Electrochemical Reduction of Carbon Dioxide on Various Metal Electrodes in Low-Temperature Aqueous KHCO[sub 3] Media.* Journal of the Electrochemical Society, 1990. **137**(6): p. 1772-1778.
48. Garrison, W.M., et al., *Reduction of Carbon Dioxide in Aqueous Solutions by Ionizing Radiation.* Science, 1951. **114**(2964): p. 416-418.
49. Hammouche, M., et al., *Chemical catalysis of electrochemical reactions. Homogeneous catalysis of the electrochemical reduction of carbon dioxide by iron("0") porphyrins. Role of the addition of magnesium cations.* Journal of the American Chemical Society, 1991. **113**(22): p. 8455-8466.
50. Rezaei, B. and M. Taki, *Effects of tetrabutylammonium hydrogen sulfate as an electrolyte additive on the electrochemical behavior of lead acid battery.* Journal of Solid State Electrochemistry, 2008. **12**(12): p. 1663-1671.
51. Pletnev, M.A., et al., *Effect of tetraalkylammonium salts on the cathodic evolution of hydrogen in concentrated acidic bromide solutions.* Zashchita Metallov, 1995. **31**(4): p. 351-355.
52. Reshetnikov, S.M., V.I. Kichigin, and M.V. Burmistr, *INHIBITION OF CATHODIC EVOLUTION OF HYDROGEN ON IRON IN HYDROCHLORIC-ACID SOLUTIONS BY ADSORPTION OF MONOMERIC AND POLYMERIC QUATERNARY AMMONIUM-SALTS.* Protection of Metals, 1982. **18**(6): p. 741-743.
53. Fowler, D.L., et al., *Some Unusual Hydrates of Quaternary Ammonium Salts.* Journal of the American Chemical Society, 1940. **62**(5): p. 1140-1142.
54. Prokopowicz, A. and M. Opallo, *Electrochemical hydrogen evolution from solid tetraalkylammonium hydroxide hydrates.* Solid State Ionics, 2003. **162-163**: p. 231-236.
55. Opallo, M. and A. Prokopowicz, *Electrochemical hydrogen evolution in hydroxide hydrate down to 110 K.* Electrochemistry Communications, 2000. **2**(1): p. 23-26.
56. Oue, S., *Electrodeposition of Zn-Al2O3 composite from non-suspended solution containing quaternary ammonium salt.* ヒョウメンギジュツ, 2002. **53**(12): p. 920.

57. Magalhaes, A. and Magalhaes, *Influence of some quaternary ammonium salts upon zinc deposition on steel from acidic methanesulfonate electrolyte.* Bulletin of Electrochemistry, 2002. **18**(5): p. 193.
58. Reshetnikov, S. and Reshetnikov, *Mechanism of inhibition of cathodic evolution of hydrogen on nickel with quaternary ammonium salts.* Zaŝita metallov, 1980. **16**(5): p. 623.
59. Reshetnikov, S. and Reshetnikov, *Effect of polymeric and monomeric organic salts of quaternary ammonium on cathodic hydrogen evolution on nickel.* Zhurnal prikladnoĭ khimii, 1981. **54**(4): p. 826.
60. Rezaei, B., S. Mallakpour, and M. Taki, *Application of ionic liquids as an electrolyte additive on the electrochemical behavior of lead acid battery.* Journal of Power Sources, 2009. **187**(2): p. 605-612.
61. Bell, A.T., *Basic Research Needs, Catalysis For Energy*. 2008, Bell, A. T. Ed.
62. Rysselberghe, T.E.T.a.P.V., J. chem. Phys., 1954. **22**: p. 759.
63. Haynes, L.V. and D.T. Sawyer, *Electrochemistry of carbon dioxide in dimethyl sulfoxide at gold and mercury electrodes.* Analytical Chemistry, 1967. **39**(3): p. 332-338.
64. Hori, Y., et al., *Electrochemical reduction of carbon dioxide to carbon monoxide at a gold electrode in aqueous potassium hydrogen carbonate.* Journal of the Chemical Society, Chemical Communications, 1987(10): p. 728-9.
65. C. J. Stalder, S.C., and M. S. Wrighton, *J. Am. Chem. Soc*., 1984. **106**.
66. Ogura, K. and M. Takagi, *Electrocatalytic reduction of carbon dioxide to methanol Part IV. Assessment of the current--potential curves leading to reduction.* Journal of Electroanalytical Chemistry and Interfacial Electrochemistry, 1986. **206**(1-2): p. 209-216.
67. Eggins, B.R., E.M. Bennett, and E.A. McMullan, *Voltammetry of carbon dioxide. Part 2. Voltammetry in aqueous solutions on glassy carbon.* Journal of Electroanalytical Chemistry, 1996. **408**(1-2): p. 165-171.
68. Eggins, B.R., et al., *Photoreduction of carbon dioxide on zinc sulfide to give four-carbon and two-carbon acids.* Journal of the Chemical Society, Chemical Communications, 1993(4): p. 349-350.
69. Jordan, J. and P.T. Smith, *Free-radical intermediate in the electroreduction of carbon dioxide.* Proceedings of the Chemical Society, 1960(JULY): p. 246-247.
70. Augustynski, J., et al., *Electrochemical reduction of CO2 at metallic electrodes*, in *Studies in Surface Science and Catalysis*. 1998, Elsevier. p. 107-116.
71. Hori, Y. and S. Suzuki, *ELECTROLYTIC REDUCTION OF CARBON DIOXIDE AT MERCURY ELECTRODE IN AQUEOUS SOLUTION.* Bulletin of the Chemical Society of Japan, 1982. **55**(3): p. 660-665.
72. Pacansky, J., U. Wahlgren, and P.S. Bagus, *SCF AB-INITIO GROUND-STATE ENERGY SURFACES FOR CO2 AND CO2.* Journal of Chemical Physics, 1975. **62**(7): p. 2740-2744.

73. Stampfl, C. and M. Scheffler, *Anomalous Behavior of Ru for Catalytic Oxidation: A Theoretical Study of the Catalytic Reaction CO + 1/2 O_{2}-->CO_{2}.* Physical Review Letters, 1997. **78**(8): p. 1500.
74. Schiffrin, D.J., *Application of the photo-electrochemical effect to the study of the electrochemical properties of radicals: CO2 and CH.* Faraday Discussions of the Chemical Society, 1973. **56**: p. 75-95.
75. Aurian-Blajeni, B., et al., *The study of adsorbed species during the photoassisted reduction of carbon dioxide at p-CdTe electrode.* Journal of Electroanalytical Chemistry, 1983. **157**(2): p. 399-404.
76. Vayenas, C.G., et al., *Electrochemical CO₂ Reduction on Metal Electrodes*, in *Modern Aspects of Electrochemistry*. 2008, Springer New York. p. 89-189.
77. Aylmer-Kelly, A.W.B., et al., *Studies of electrochemically generated reaction intermediates using modulated specular reflectance spectroscopy.* Faraday Discussions of the Chemical Society, 1973. **56**: p. 96-107.
78. Hori, Y., et al., *Electrocatalytic process of CO selectivity in electrochemical reduction of CO2 at metal electrodes in aqueous media.* Electrochimica Acta, 1994. **39**(11-12): p. 1833-1839.
79. Hori, Y., et al., *Electrochemical reduction of carbon dioxides to carbon monoxide at a gold electrode in aqueous potassium hydrogen carbonate.* Journal of the Chemical Society, Chemical Communications, 1987(10): p. 728-729.
80. Noda, H., et al., *Kinetics of Electrochemical Reduction of Carbon Dioxide on a Gold Electrode in Phosphate Buffer Solutions.* Bulletin of the Chemical Society of Japan, 1995. **68**(7): p. 1889-1895.
81. Beden, B., et al., *On the nature of reduced CO2. An IR spectroscopic investigation.* Journal of Electroanalytical Chemistry, 1982. **139**(1): p. 203-206.
82. Aramata, A., et al., *FT-IR Spectrometry of the Reduced CO2 at Pt Electrode and Anomalous Effect of Ca2+ Ions.* Chemistry Letters, 1991. **20**(5): p. 749-752.
83. Iwasita, T., et al., *On the study of adsorbed species at platinum from methanol, formic acid and reduced carbon dioxide via in situ FT-ir spectroscopy.* Electrochimica Acta, 1992. **37**(12): p. 2361-2367.
84. Rodes, A., E. Pastor, and T. Iwasita, *Structural effects on CO2 reduction at Pt single-crystal electrodes. Part 3. Pt(100) and related surfaces.* Journal of Electroanalytical Chemistry, 1994. **377**(1-2): p. 215-225.
85. Brisard, G.M., et al., *On-line mass spectrometry investigation of the reduction of carbon dioxide in acidic media on polycrystalline Pt.* Electrochemistry Communications, 2001. **3**(11): p. 603-607.
86. Hara, K. and T. Sakata, *Electrocatalytic Formation of CH[sub 4] from CO[sub 2] on a Pt Gas Diffusion Electrode.* Journal of The Electrochemical Society, 1997. **144**(2): p. 539-545.

87. Ikeda, S., T. Takagi, and K. Ito, *SELECTIVE FORMATION OF FORMIC-ACID, OXALIC-ACID, AND CARBON-MONOXIDE BY ELECTROCHEMICAL REDUCTION OF CARBON-DIOXIDE.* Bulletin of the Chemical Society of Japan, 1987. **60**(7): p. 2517-2522.
88. Ohkawa, K., et al., *Electrochemical reduction of carbon dioxide on hydrogen-storing materials. Part II. Copper-modified palladium electrode.* Journal of Electroanalytical Chemistry, 1993. **348**(1-2): p. 459-464.
89. Taguchi, S. and A. Aramata, *Surface-structure sensitive reduced CO2 formation on Pt single crystal electrodes in sulfuric acid solution.* Electrochimica Acta, 1994. **39**(17): p. 2533-2537.
90. Cocke, D.L., T.R. Hess, and D.G. Naugle, *Influence of intrinsic electric fields on passive film chemistry and structure.* Vacuum, 1995. **46**(12): p. 1397-1399.
91. Hori, Y., et al., *Adsorption of CO accompanied with simultaneous charge transfer on copper single crystal electrodes related with electrochemical reduction of CO2 to hydrocarbons.* Surface Science, 1995. **335**: p. 258-263.
92. Köleli, F., et al., *Electrochemical reduction of CO₂ at Pb- and Sn-electrodes in a fixed-bed reactor in aqueous K₂CO₃ and KHCO₃ media.* Journal of Applied Electrochemistry, 2003. **33**(5): p. 447-450.
93. Azuma, M., et al., *Carbon dioxide reduction at low temperature on various metal electrodes.* Journal of Electroanalytical Chemistry, 1989. **260**(2): p. 441-445.
94. Bewick, A. and G.P. Greener, *The electroreduction of CO2 to glycollate on a lead cathode.* Tetrahedron Letters, 1970. **11**(5): p. 391-394.
95. Vassiliev, Y.B., et al., *Electroreduction of carbon dioxide: Part I. The mechanism and kinetics of electroreduction of CO2 in aqueous solutions on metals with high and moderate hydrogen overvoltages.* Journal of Electroanalytical Chemistry and Interfacial Electrochemistry, 1985. **189**(2): p. 271-294.
96. Fischer, J., T. Lehmann, and E. Heitz, *The production of oxalic acid from CO₂ and H₂O.* Journal of Applied Electrochemistry, 1981. **11**(6): p. 743-750.
97. Ikeda, S., et al., *Electrochemical reduction behavior of carbon dioxide on sintered zinc oxide electrode in aqueous solution.* Electrochemistry, 2000. **68**(4): p. 257-261.
98. Vassiliev, Y.B., et al., *ELECTROREDUCTION OF CARBON-DIOXIDE .1. THE MECHANISM AND KINETICS OF ELECTROREDUCTION OF CO2 IN AQUEOUS-SOLUTIONS ON METALS WITH HIGH AND MODERATE HYDROGEN OVERVOLTAGES.* Journal of Electroanalytical Chemistry, 1985. **189**(2): p. 271-294.

99. Koppenol, W.H. and J.D. Rush, *REDUCTION POTENTIAL OF THE CO2/CO2.-COUPLE - A COMPARISON WITH OTHER C1 RADICALS.* Journal of Physical Chemistry, 1987. **91**(16): p. 4429-4430.
100. Udupa, K.S., G.S. Subramanian, and H.V.K. Udupa, *The electrolytic reduction of carbon dioxide to formic acid.* Electrochimica Acta, 1971. **16**(9): p. 1593-1598.
101. Babenko, S.D., et al., *PHOTOCURRENT KINETICS AT THE ELECTRON-EMISSION FROM A METAL INTO ELECTROLYTE SOLUTION .7. ABSOLUTE RATE CONSTANTS OF CO2 ELECTROCHEMICAL REDUCTION ON MERCURY.* Journal of Electroanalytical Chemistry, 1983. **159**(1): p. 163-181.
102. Watanabe, M., et al., *DESIGN OF ALLOY ELECTROCATALYSTS FOR CO2 REDUCTION .3. THE SELECTIVE AND REVERSIBLE REDUCTION OF CO2 ON CU ALLOY ELECTRODES.* Journal of the Electrochemical Society, 1991. **138**(11): p. 3382-3389.
103. Watanabe, M., et al., *DESIGN OF ALLOY ELECTROCATALYSTS FOR CO2 REDUCTION .1. THE SELECTIVE AND REVERSIBLE REDUCTION OF CO2 AT CU-NI ALLOY ELECTRODES.* Denki Kagaku, 1991. **59**(6): p. 508-516.
104. Shiratsuchi, R., et al., *REDUCTION OF CO2 ON FLUORINE-DOPED SNO2 THIN-FILM ELECTRODES.* Journal of the Electrochemical Society, 1992. **139**(9): p. 2544-2549.
105. Nogami, G., Y. Aikoh, and R. Shiratsuchi, *INVESTIGATION OF FIXATION MECHANISM OF CARBON-DIOXIDE ON OXIDE SEMICONDUCTORS BY CURRENT TRANSIENTS.* Journal of the Electrochemical Society, 1993. **140**(4): p. 1037-1041.
106. Nikolic, B.Z., et al., *ELECTROREDUCTION OF CARBON-DIOXIDE ON PLATINUM SINGLE-CRYSTAL ELECTRODES - ELECTROCHEMICAL AND INSITU FTIR STUDIES.* Journal of Electroanalytical Chemistry, 1990. **295**(1-2): p. 415-423.
107. Hoshi, N., et al., *CO2 REDUCTION ON RH SINGLE-CRYSTAL ELECTRODES AND THE STRUCTURAL EFFECT.* Journal of Electroanalytical Chemistry, 1995. **395**(1-2): p. 309-312.
108. Hoshi, N., T. Suzuki, and Y. Hori, *Step density dependence of CO2 reduction rate on Pt(S)-[n(111)x(111)] single crystal electrodes.* Electrochimica Acta, 1996. **41**(10): p. 1647-1653.
109. Hoshi, N., T. Suzuki, and Y. Hori, *Catalytic activity of CO2 reduction on Pt single-crystal electrodes: Pt(S)-[n(111)x(111)], Pt(S)-[n(111)x(100)], and Pt(S)-[n(100)x(111)].* Journal of Physical Chemistry B, 1997. **101**(42): p. 8520-8524.
110. Noda, H., et al., *KINETICS OF ELECTROCHEMICAL REDUCTION OF CARBON-DIOXIDE ON A GOLD ELECTRODE IN PHOSPHATE BUFFER SOLUTIONS.* Bulletin of the Chemical Society of Japan, 1995. **68**(7): p. 1889-1895.

111. Dewulf, D.W., T. Jin, and A.J. Bard, *ELECTROCHEMICAL AND SURFACE STUDIES OF CARBON-DIOXIDE REDUCTION TO METHANE AND ETHYLENE AT COPPER ELECTRODES IN AQUEOUS-SOLUTIONS.* Journal of the Electrochemical Society, 1989. **136**(6): p. 1686-1691.
112. Nakato, Y., et al., *REACTIONS AND MECHANISM OF THE ELECTROCHEMICAL REDUCTION OF CARBON-DIOXIDE ON ALLOYED COPPER-SILVER ELECTRODES.* Denki Kagaku, 1991. **59**(6): p. 491-498.
113. Trovarelli, A., C. Deleitenburg, and G. Dolcetti, *CO AND CO2 HYDROGENATION UNDER TRANSIENT CONDITIONS OVER RH-CEO2 - NOVEL POSITIVE EFFECTS OF METAL SUPPORT INTERACTION ON CATALYTIC ACTIVITY AND SELECTIVITY.* Journal of the Chemical Society-Chemical Communications, 1991(7): p. 472-473.
114. Trovarelli, A., et al., *CO2 METHANATION UNDER TRANSIENT AND STEADY-STATE CONDITIONS OVER RH/CEO2 AND CEO2-PROMOTED RH/SIO2 - THE ROLE OF SURFACE AND BULK CERIA.* Journal of Catalysis, 1995. **151**(1): p. 111-124.
115. deLeitenburg, C., A. Trovarelli, and J. Kaspar, *A temperature-programmed and transient kinetic study of CO2 activation and methanation over CeO2 supported noble metals.* Journal of Catalysis, 1997. **166**(1): p. 98-107.
116. Ogura, K. and I. Yoshida, *ELECTROCATALYTIC REDUCTION OF CARBON-DIOXIDE TO METHANOL IN THE PRESENCE OF 1,2-DIHYDROXYBENZENE-3,5-DISULPHONATOFERRATE(III) AND ETHANOL.* Journal of Molecular Catalysis, 1986. **34**(1): p. 67-72.
117. Lee, J.F., et al., *HYDROGENATION OF CARBON-DIOXIDE ON IRON CATALYSTS DOUBLY PROMOTED WITH MANGANESE AND POTASSIUM.* Canadian Journal of Chemical Engineering, 1992. **70**(3): p. 511-515.
118. Ogura, K., et al., *ELECTROCHEMICAL REDUCTION OF CARBON-DIOXIDE ON DUAL-FILM ELECTRODES MODIFIED WITH AND WITHOUT COBALT(II) AND IRON(II) COMPLEXES.* Journal of the Electrochemical Society, 1994. **141**(2): p. 419-424.
119. Ohta, K., et al., *Electrochemical reduction of carbon dioxide in methanol at ambient temperature and pressure.* Journal of Applied Electrochemistry, 1998. **28**(7): p. 717-724.
120. Tyssee, D.A., et al., *Some cathodic organic syntheses involving carbon dioxide.* Tetrahedron Letters, 1972. **13**(47): p. 4809-4812.
121. Amatore, C. and J.M. Sav 閌 nt, *Product distribution in preparative scale electrolysis: Part VII. Competition at the level of the first-electron intermediate between self-coupling, coupling with the substrate and first-order deactivation followed by further electron transfer.* Journal of Electroanalytical Chemistry and Interfacial Electrochemistry, 1981. **126**(1-3): p. 1-19.

122. Amatore, C. and J.M. Saveant, *Mechanism and kinetic characteristics of the electrochemical reduction of carbon dioxide in media of low proton availability.* Journal of the American Chemical Society, 1981. **103**(17): p. 5021-3.
123. Tomita, Y., et al., *Electrochemical Reduction of Carbon Dioxide at a Platinum Electrode in Acetonitrile-Water Mixtures.* Journal of The Electrochemical Society, 2000. **147**(11): p. 4164-4167.
124. Naitoh, A., et al., *Electrochemical reduction of carbon dioxide in methanol at low temperature.* Electrochimica Acta, 1993. **38**(15): p. 2177-9.
125. Saeki, T., et al., *Electrochemical reduction of CO2 with high current density in a CO2 + methanol medium at various metal electrodes.* Journal of Electroanalytical Chemistry, 1996. **404**(2): p. 299-302.
126. Saeki, T., et al., *Electrochemical Reduction of CO2 with High Current Density in a CO2-Methanol Medium.* Journal of Physical Chemistry, 1995. **99**(20): p. 8440-6.
127. Gressin, J.C., et al., *Electrochemical reduction of carbon dioxide in weakly protic medium.* Nouveau Journal de Chimie, 1979. **3**(8-9): p. 545-54.
128. Ikeda, S., T. Takagi, and K. Ito, *Selective formation of formic acid, oxalic acid, and carbon monoxide by electrochemical reduction of carbon dioxide.* Bulletin of the Chemical Society of Japan, 1987. **60**(7): p. 2517-22.
129. Eggins, B.R., et al., *Improved yields of oxalate, glyoxylate and glycolate from the electrochemical reduction of carbon dioxide in methanol.* Journal of Applied Electrochemistry, 1997. **27**(6): p. 706-712.
130. Kaneco, S., et al., *Electrochemical conversion of carbon dioxide to formic acid on Pb in KOH/methanol electrolyte at ambient temperature and pressure.* Energy, 1998. **23**(12): p. 1107-1112.
131. Haynes, L.V. and D.T. Sawyer, *Electrochemistry of carbon dioxide in dimethyl sulfoxide at gold and mercury electrodes.* Analytical Chemistry, 1967. **39**(3): p. 332-8.
132. Bockris, J.O.M. and J.C. Wass, *The photoelectrocatalytic reduction of carbon dioxide.* Journal of the Electrochemical Society, 1989. **136**(9): p. 2521-8.
133. Tyssee, D.A., et al., *Cathodic organic syntheses involving carbon dioxide.* Tetrahedron Letters, 1972(47): p. 4809-12.
134. Gennaro, A., et al., *Mechanism of the electrochemical reduction of carbon dioxide at inert electrodes in media of low proton availability.* Journal of the Chemical Society, Faraday Transactions, 1996. **92**(20): p. 3963-3968.
135. Saeki, T., et al., *Electrochemical reduction of CO2 to hydrocarbons with high current density in a CO2-methanol medium.* Chemistry Letters, 1995(5): p. 361-2.
136. Saeki, T., et al., *Electrochemical reduction of liquid CO2. Drastic enhancement of current density.* Journal of the Electrochemical Society, 1994. **141**(9): p. L130-L132.

137. Kaneco, S., et al., *High efficiency electrochemical CO2-to-methane conversion method using methanol with lithium supporting electrolytes.* Industrial & Engineering Chemistry Research, 2002. **41**(21): p. 5165-5170.
138. Mazin, V.M., E.I. Mysov, and V.A. Grinberg, *Electrochemical reduction of carbon dioxide on copper electrode in a carbon dioxide-methanol mixture under near-critical conditions.* Russian Journal of Electrochemistry (Translation of Elektrokhimiya), 1997. **33**(7): p. 779-780.
139. Li, J. and G. Prentice, *Electrochemical synthesis of methanol from CO2 in high-pressure electrolyte.* Journal of the Electrochemical Society, 1997. **144**(12): p. 4284-4288.
140. Kaneco, S., et al., *Electrochemical reduction of CO2 at an Ag electrode in KOH-methanol at low temperature.* Electrochimica Acta, 1998. **44**(4): p. 573-578.
141. Kaneco, S., et al., *Electrochemical reduction of carbon dioxide using aqueous LiClO4 solution at less than 273 K.* ITE Letters on Batteries, New Technologies & Medicine, 2001. **2**(1): p. 83-87.
142. Kaneco, S., et al., *Electrochemical reduction of carbon dioxide on an indium wire in a KOH/methanol-based electrolyte at ambient temperature and pressure.* Environmental Engineering Science, 1999. **16**(2): p. 131-137.
143. Kaneco, S., et al., *Electrochemical reduction of CO2 on Au in KOH+methanol at low temperature.* Journal of Electroanalytical Chemistry, 1998. **441**(1-2): p. 215-220.
144. Mizuno, T., et al., *Electrochemical reduction of carbon dioxide at Ti and hydrogen-storing Ti electrodes in KOH-methanol.* Electrochimica Acta, 1998. **43**(8): p. 899-907.
145. Schrebler, R., et al., *Study of the electrochemical reduction of CO2 on electrodeposited rhenium electrodes in methanol media.* Journal of Electroanalytical Chemistry, 2001. **516**(1-2): p. 23-30.
146. Schrebler, R., et al., *Study of the electrochemical reduction of CO2 on a polypyrrole electrode modified by rhenium and copper-rhenium microalloy in methanol media.* Journal of Electroanalytical Chemistry, 2002. **533**(1-2): p. 167-175.
147. Aydin, R. and F. Koleli, *Electrocatalytic conversion of CO2 on a polypyrrole electrode under high pressure in methanol.* Synthetic Metals, 2004. **144**(1): p. 75-80.
148. Aydin, R. and F. Koleli, *Electrochemical reduction of CO2 on a polyaniline electrode under ambient conditions and at high pressure in methanol.* Journal of Electroanalytical Chemistry, 2002. **535**(1-2): p. 107-112.
149. Koleli, F., T. Ropke, and C.H. Hamann, *The reduction of CO2 on polyaniline electrode in a membrane cell.* Synthetic Metals, 2004. **140**(1): p. 65-68.
150. Fleischmann, M., P.J. Hendra, and A.J. McQuillan, *Raman spectra of pyridine adsorbed at a silver electrode.* Chemical Physics Letters, 1974. **26**(2): p. 163-166.

151. Jeanmaire, D.L. and R.P. Van Duyne, *Surface raman spectroelectrochemistry: Part I. Heterocyclic, aromatic, and aliphatic amines adsorbed on the anodized silver electrode.* Journal of Electroanalytical Chemistry and Interfacial Electrochemistry, 1977. **84**(1): p. 1-20.
152. Albrecht, M.G. and J.A. Creighton, *Anomalously intense Raman spectra of pyridine at a silver electrode.* Journal of the American Chemical Society, 1977. **99**(15): p. 5215-5217.
153. Moskovits, M., *Surface-enhanced spectroscopy.* Reviews of Modern Physics, 1985. **57**(3): p. 783.
154. Creighton, J.A. and D.G. Eadon, *Ultraviolet-visible absorption spectra of the colloidal metallic elements.* Journal of the Chemical Society, Faraday Transactions, 1991. **87**(24): p. 3881-3891.
155. Langhammer, C., et al., *Plasmonic Properties of Supported Pt and Pd Nanostructures.* Nano Letters, 2006. **6**(4): p. 833-838.
156. Lombardi, J.R. and R.L. Birke, *A Unified Approach to Surface-Enhanced Raman Spectroscopy.* The Journal of Physical Chemistry C, 2008. **112**(14): p. 5605-5617.
157. Fan, M., G.F.S. Andrade, and A.G. Brolo, *A review on the fabrication of substrates for surface enhanced Raman spectroscopy and their applications in analytical chemistry.* Analytica Chimica Acta. **In Press, Corrected Proof**.
158. Ortiz, C., et al., *Identification of insulin variants using Raman spectroscopy.* Analytical Biochemistry, 2004. **332**(2): p. 245-252.
159. Chalmers, J.M., et al., *Raman spectra of polymorphs of isotactic polypropylene.* Journal of Raman Spectroscopy, 1991. **22**(11): p. 613-618.
160. Vo-Dinh, T., *SERS chemical sensors and biosensors: new tools for environmental and biological analysis.* Sensors and Actuators B: Chemical, 1995. **29**(1-3): p. 183-189.
161. Kneipp, K., et al., *Single molecule detection using surface-enhanced Raman scattering (SERS).* Physical Review Letters, 1997. **78**(9): p. 1667-1670.
162. Kovacs, G.J., Langmuir, 1986. **2**(6): p. 689.
163. Dilella, D.P. and P. Zhou, *Surface-enhanced Raman scattering from molecules adsorbed on gallium surfaces.* Chemical Physics Letters, 1990. **166**(3): p. 240-245.
164. Gao, Y. and T. Lopez-Rios, *Raman scattering of pyridine coadsorbed with Al on quenched Ag films: Evidence of Raman enhancement in the pores.* Surface Science, 1988. **198**(3): p. 509-523.
165. Nie, S.M. and S.R. Emery, *Probing single molecules and single nanoparticles by surface-enhanced Raman scattering.* Science, 1997. **275**(5303): p. 1102-1106.
166. Constantino, C.J.L., et al., *Single molecular detection of a perylene dye dispersed in a Langmuir-Blodgett fatty acid monolayer using surface-enhanced resonance Raman scattering.* Spectrochimica Acta Part a-Molecular and Biomolecular Spectroscopy, 2002. **58**(3): p. 403-409.

167. Klar, T., et al., *Surface-Plasmon Resonances in Single Metallic Nanoparticles.* Physical Review Letters, 1998. **80**(19): p. 4249.
168. Lee, S., et al., *SERS decoding of micro gold shells moving in microfluidic systems.* ELECTROPHORESIS. **31**(10): p. 1623-1629.
169. Eliasson, C., et al., *Surface-enhanced Raman scattering imaging of single living lymphocytes with multivariate evaluation.* Spectrochimica Acta Part a-Molecular and Biomolecular Spectroscopy, 2005. **61**(4): p. 755-760.
170. Chant, H.Y.H. and M.J. Weaver, *A vibrational structural analysis of benzotriazole adsorption and phase film formation on copper using surface-enhanced Raman spectroscopy.* Langmuir, 1999. **15**(9): p. 3348-3355.
171. Sugimasa, M., et al., *Adlayers of benzotriazole on Cu(110), (100), and (111) in HClO4 solution - In situ scanning tunneling microscopy study.* Journal of The Electrochemical Society, 2002. **149**(10): p. E367-E373.
172. Yamada, H. and Y. Yamamoto, *Surface enhanced raman spectra of pyridine adsorbed on silver, gold, nickel and platinum metals.* Chemical Physics Letters, 1981. **77**(3): p. 520-522.
173. Tian, Z.Q., B. Ren, and B.W. Mao, *Extending Surface Raman Spectroscopy to Transition Metal Surfaces for Practical Applications. 1. Vibrational Properties of Thiocyanate and Carbon Monoxide Adsorbed on Electrochemically Activated Platinum Surfaces.* The Journal of Physical Chemistry B, 1997. **101**(8): p. 1338-1346.
174. Ren, B., et al., *Surface raman spectra of pyridine and hydrogen on bare platinum and nickel electrodes.* Journal of Electroanalytical Chemistry, 1996. **415**(1-2): p. 175-178.
175. Guo, L., et al., *Iron nanoparticles: Synthesis and applications in surface enhanced Raman scattering and electrocatalysis.* Physical Chemistry Chemical Physics, 2001. **3**(9): p. 1661-1665.
176. Rubim, J.C., et al., *Raman spectra of silver coated graphite and glassy carbon electrodes.* Applied Surface Science, 1989. **37**(2): p. 233-243.
177. Batista, E.A. and M.L.A. Temperini, *Spectroscopic evidences of the presence of hydrogenated species on the surface of copper during CO2 electroreduction at low cathodic potentials.* Journal of Electroanalytical Chemistry, 2009. **629**(1-2): p. 158-163.
178. Zheng, J.W., et al., *Photoelectrochemical reduction of CO2 mediated with methylviologen at roughened silver electrodes.* Journal of Electroanalytical Chemistry, 2002. **518**(1): p. 6-12.
179. Ichinohe, Y., T. Wadayama, and A. Hatta, *ELECTROCHEMICAL REDUCTION OF CO2 ON SILVER AS PROBED BY SURFACE-ENHANCED RAMAN-SCATTERING.* Journal of Raman Spectroscopy, 1995. **26**(5): p. 335-340.

180. Smith, B.D., et al., *A surface enhanced raman scattering study of the intermediate and poisoning species formed during the electrochemical reduction of CO2 on copper.* Journal of The Electrochemical Society, 1997. **144**(12): p. 4288-4296.
181. Hori, Y., *Electrochemical Carbon dioxide reduction on metal electrodes.* Modern Aspects of Electrochemistry, 2008. **42**: p. 89-189.
182. Bard, A.J., ed. *Encyclopedia of Electrochemistry of the Elements*. Vol. 6. 1973, Marcel Dekker.
183. Feltham, A.M. and M. Spiro, *The variation of area of platinized platinum electrodes with deposition potential at constant mass degree of platinization.* Journal of Electroanalytical Chemistry, 1972. **35**: p. 181-192.
184. Larsen, R.T., *Dissertation.* 2004.
185. Waszczuk, P., et al., *A nanoparticle catalyst with superior activity for electrooxidation of formic acid [Electrochem. Commun. 4 (2002) 599-603]*. Electrochemistry Communications, 2002. **4**(9): p. 732-732.
186. Biegler, T., D.A.J. Rand, and R. Woods, *Limiting oxygen coverage on platinized platinum; Relevance to determination of real platinum area by hydrogen adsorption.* Journal of Electroanalytical Chemistry and Interfacial Electrochemistry, 1971. **29**(2): p. 269-277.
187. Li, X. and A.A. Gewirth, *Peroxide Electroreduction on Bi-Modified Au Surfaces:â€‰ Vibrational Spectroscopy and Density Functional Calculations.* Journal of the American Chemical Society, 2003. **125**(23): p. 7086-7099.
188. Biggin, M.E. and A.A. Gewirth, *Infrared Studies of Benzotriazole on Copper Electrode Surfaces: Role of Chloride in Promoting Reversibility.* Journal of The Electrochemical Society, 2001. **148**(5): p. C339-C347.
189. Masel, R.I., *Novel Catalyst Mixtures*. 2010.
190. Rosen, B.A., et al., *An Electrocatalyst That Converts CO2 to CO At Low Overpotentials.* In Review, 2011.
191. Haan, J.L., K.M. Stafford, and R.I. Masel, *Effects of the Addition of Antimony, Tin, and Lead to Palladium Catalyst Formulations for the Direct Formic Acid Fuel Cell.* J. Phys. Chem. C, 2010. **114**(26): p. 11665-11672.
192. Larsen, R., et al., *Unusually active palladium-based catalysts for the electrooxidation of formic acid.* J. Power Sources, 2006. **157**(1): p. 78-84.
193. Larsen, R. and R.I. Masel, *Kinetic study of CO tolerance during electro-oxidation of formic acid on spontaneously deposited Pt/Pd and Pt/Ru nanoparticles.* Electrochemical & Solid-State Letters, 2004. **7**(6): p. A148-A150.
194. Larsen, R., J. Zakzeski, and R.I. Masel, *Unexpected activity of palladium on vanadia catalysts for formic acid electro-oxidation.* Electrochemical and Solid-State Letters, 2005. **8**(6): p. 291-3.
195. Rice, C., et al., *Catalysts for direct formic acid fuel cells.* Journal of Power Sources, 2003. **115**(2): p. 229-235.

196. Thomas, F.S. and R.I. Masel, *Formic acid decomposition on palladium-coated Pt(110).* Surface Science, 2004. **573**(2): p. 169-175.
197. Lukaszewski, M., H. Siwek, and A. Czerwinski, *Electrosorption of carbon dioxide on platinum group metals and alloys-a review.* Journal of Solid State Electrochemistry, 2009. **13**(6): p. 813-827.
198. Gattrell, M., N. Gupta, and A. Co, *A review of the aqueous electrochemical reduction of Carbon Dioxide to hydrocarbons at copper.* Journal of Electroanalytical Chemistry, 2006. **594**(1): p. 1-19.
199. DuBois, D.L., *Carbon. Electrochemical reactions of carbon dioxide.* Encyclopedia of Electrochemistry, 2006. **7a**: p. 202-225.
200. Ha, S., B. Adams, and R.I. Masel, *A miniature air breathing direct formic acid fuel cell.* Journal of Power Sources, 2004. **128**(2): p. 119-124.
201. Ha, S., Z. Dunbar, and R.I. Masel, *Characterization of a high performing passive direct formic acid fuel cell.* J. Power Sources, 2006. **158**(1): p. 129-136.
202. Ha, S., R. Larsen, and R.I. Masel, *Performance characterization of Pd/C nanocatalyst for direct formic acid fuel cells.* Journal of Power Sources, 2005. **144**(1): p. 28-34.
203. Ha, S., et al., *Direct formic acid fuel cells with 600 mA.cm-2 at 0.4 V and 22 DegC.* Fuel Cells (Weinheim, Ger.), 2004. **4**(4): p. 337-343.
204. Haan, J.L., et al., *Performance of the direct formic acid fuel cell with electrochemically modified palladium-antimony anode catalyst.* Electrochimica Acta, 2010. **55**(7): p. 2477-2481.
205. Kim, H.S., et al., *A miniature direct formic acid fuel cell battery.* Journal of Power Sources, 2009. **188**(1): p. 118-121.
206. Rice, C., et al., *Direct formic acid fuel cells.* J. Power Sources, 2002. **111**(1): p. 83-89.
207. Quaino, P.M., M.R. Gennero de Chialvo, and A.C. Chialvo, *Hydrogen diffusion effects on the kinetics of the hydrogen electrode reaction Part II. Evaluation of kinetic parameters.* Physical Chemistry Chemical Physics, 2004. **6**(18): p. 4450-4455.
208. Montero, M.A., et al., *The evaluation of the polarization resistance in a tubular electrode and its application to the hydrogen electrode reaction.* Electrochimica Acta, 2007. **52**(5): p. 2083-2090.
209. Batista, B.C. and H. Varela, *Open Circuit Interaction of Formic Acid with Oxidized Pt Surfaces: Experiments, Modeling, and Simulations.* The Journal of Physical Chemistry C. **114**(43): p. 18494-18500.
210. Liu, Y.-C., B.-J. Hwang, and W.-J. Jian, *Effect of preparation conditions for roughening gold substrate by oxidation-reduction cycle on the surface-enhanced Raman spectroscopy of polypyrrole.* Materials Chemistry and Physics, 2002. **73**(2-3): p. 129-134.

211. Daniel, R.M., et al., *Electrochemistry of Gold in Aqueous Sulfuric Acid Solutions under Neural Stimulation Conditions.* Journal of the Electrochemical Society, 2005. **152**(7): p. E212-E221.
212. Haan, J.L. and R.I. Masel, *The influence of solution pH on rates of an electrocatalytic reaction: Formic acid electrooxidation on platinum and palladium.* Electrochimica Acta, 2009. **54**(16): p. 4073-4078.
213. Waszczuk, P., et al., *A nanoparticle catalyst with superior activity for electrooxidation of formic acid (vol 4, pg 599, 2002).* Electrochemistry Communications, 2002. **4**(9): p. 732.
214. Thomas, F., et al., *Evidence for a cation intermediate during methanol dehydration on Pt(110).* Catalysis Letters, 2001. **72**(3-4): p. 167-175.
215. Chen, N., P. Blowers, and R.I. Masel, *Evidence for carbocation formation during the coadsorption of methanol and hydrogen on Pt(110).* Surface Science, 1998. **418**(1): p. 329-341.
216. Wang, J. and R.I. Masel, *Methanol adsorption and decomposition on (2*1) platinum(110): enhanced stability of the methoxy intermediate on a stepped surface.* Surf. Sci., 1991. **243**(1-3): p. 199-209.
217. Gattrell, M., N. Gupta, and A. Co, *A review of the aqueous electrochemical reduction of CO2 to hydrocarbons at copper.* Journal of Electroanalytical Chemistry, 2006. **594**(1): p. 1-19.
218. Hori, Y., *Electrochemical CO2 reduction on metal electrodes.* Modern Aspects of Electrochemistry, 2008. **42**: p. 89-189.
219. Louhichi, B., et al., *Electrochemical degradation of an anionic surfactant on boron-doped diamond anodes.* Journal of Hazardous Materials, 2008. **158**(2-3): p. 430-437.
220. Kaneco, S., et al., *Electrochemical reduction of CO2 in copper particle-suspended methanol.* Chemical Engineering Journal, 2006. **119**(2-3): p. 107-112.
221. Isaacs, M., et al., *Electrochemical reduction of CO2 mediated by poly-M-aminophthalocyanines (M = Co, Ni, Fe): poly-Co-tetraaminophthalocyanine, a selective catalyst.* Journal of Molecular Catalysis A: Chemical, 2005. **229**(1-2): p. 249-257.
222. Zhu, W., et al., *Effect of Choline Chloride on Hydrogen Evolution Reaction.* In preparation, 2010.
223. Larsen, R.T., *Fuel cell catalysts with superior activity for formic acid electrooxidation* in *Chemical Engineering*. 2004, University of Illinois: Urbana IL.
224. Tadayyoni, M.A. and M.J. Weaver, *Adsorption and electrooxidation of carbon monoxide at the gold-aqueous interface studied by surface-enhanced Raman spectroscopy.* Langmuir, 1986. **2**(2): p. 179-183.
225. Aurian-Blajeni, B., et al., *The study of adsorbed species during the photoassisted reduction of carbon dioxide at a p-cadmium telluride electrode.* Journal of

Electroanalytical Chemistry and Interfacial Electrochemistry, 1983. **157**(2): p. 399-404.
226. Bockris, J.O. and K. Chandrasekaran, *Fourier transform infrared spectroscopic investigation of adsorbed intermediates in electrochemical reactions.* ACS Symposium Series, 1988. **378**(Electrochem. Surf. Sci.: Mol. Phenom. Electrode Surf.): p. 351-68.
227. Bockris, J.O.M. and J.C. Wass, *On the photoelectrocatalytic reduction of carbon dioxide.* Materials Chemistry and Physics, 1989. **22**(3-4): p. 249-80.
228. Chandrasekaran, K. and J.O.M. Bockris, *In-situ spectroscopic investigation of adsorbed intermediate radicals in electrochemical reactions: carbon dioxide(1-) (CO2-) on platinum.* Surface Science, 1987. **185**(3): p. 495-514.
229. Brian A Rosen, et al., *An Electrocatalyst That Converts CO_2 to CO At Low Overpotentials.* Submitted, 2010.
230. Halmann, M.M., *Chemical fixation of carbon dioxide :methods for recycling CO2 into useful products* 1993, Boca Raton CRC Press.
231. Gao, P. and M.J. Weaver, *Metal-adsorbate vibrational frequencies as a probe of surface bonding: halides and pseudohalides at gold electrodes.* The Journal of Physical Chemistry, 1986. **90**(17): p. 4057-4063.
232. Liu, Y.F., et al., *Effect of Chloride Ions on the Adsorption of 3-Mercapto-1-propanesulfonic acid and Bis(3-sulfopropyl)-disulfide on a Au(111) Surface.* Langmuir. **26**(16): p. 13263-13271.
233. Watling, K., G.A. Hope, and R. Woods, *SERS investigation of gold dissolution in chloride and cyanide media.* Journal of The Electrochemical Society, 2005. **152**(6): p. D103-D108.
234. Vivek, J.P. and I.J. Burgess, *Insight into chloride induced aggregation of DMAP-monolayer protected gold nanoparticles using the thermodynamics of ideally polarized electrodes.* Journal of Physical Chemistry C, 2008. **112**(8): p. 2872-2880.
235. Ofstad, A.B., et al., *Assessment of Platinum Dissolution from a Pt/C Fuel Cell Catalyst: An Electrochemical Quartz Crystal Microbalance Study.* Journal of The Electrochemical Society. **157**(5): p. B621-B627.
236. Lubert, K.H., M. Guttmann, and L. Beyer, *Electrode reactions of palladium(II) in chloride solution at carbon paste electrodes modified with derivatives of N-benzoylthiourea.* Journal of Solid State Electrochemistry, 2002. **6**(8): p. 545-552.
237. Lin, L.G., et al., *An in situ STM study on the long-range surface restructuring of Au(111) in a non-chloroaluminumated ionic liquid.* Electrochemistry Communications, 2003. **5**(12): p. 995-999.
238. Calaza, F., et al., *The adsorption and reaction of vinyl acetate on Au/Pd(111) alloy surfaces.* Surface Science, 2008. **602**(22): p. 3523-3530.

239. Berna, A., et al., *Spectroelectrochemical study of the adsorption of acetate anions at gold single crystal and thin-film electrodes.* Electrochimica Acta, 2008. **53**(5): p. 2309-2321.
240. Graves, A.D. and D. Inman, *The electrical double layer in molten salts. Part 2. The double-layer capacitance.* Journal of Electroanalytical Chemistry, 1970. **25**(3): p. 357-372.
241. Mai, Z.B., et al., *Investigation of the chloride effect on hemoglobin by adsorptive transfer voltammetry.* Analytical Biochemistry. **399**(1): p. 23-29.
242. Sun, Y.T., et al., *Electrochemical investigation of the chloride effect on hemoglobin.* Bioelectrochemistry, 2004. **64**(1): p. 23-27.
243. Willsau, J. and J. Heitbaum, *Analysis of adsorbed intermediates and determination of surface potential shifts by dems.* Electrochimica Acta, 1986. **31**(8): p. 943-948.
244. Hamm, U.W., et al., *The pzc of Au(111) and Pt(111) in a perchloric acid solution: an ex situ approach to the immersion technique.* Journal of Electroanalytical Chemistry, 1996. **414**(1): p. 85-89.
245. B, A., B., et al., *Determination of different local potentials of zero charge of a Pd-Au(111) heterogeneous surface.* Electrochemistry Communications, 2000. **2**(6): p. 427-430.
246. Kaneco, S., et al., *Electrochemical reduction of CO2 to methane at the Cu electrode in methanol with sodium supporting salts and its comparison with other alkaline salts.* Energy & Fuels, 2006. **20**(1): p. 409-414.

Author's Biography

Wei Zhu was born in Changsha City, Hunan Province, P.R. China on October 15th, 1985. She entered the Tianjin University in Tianjin, P.R. China, and graduated with a degree in Bioengineering in 2007.

Wei immediately began her graduate studies at the University of Illinois in fall 2007, majoring in chemical engineering. She completed a Doctor of Philosophy in Chemical Engineering from the University of Illinois in 2011. Following the completion of her Ph. D., Wei will begin work as a Research Scientist at Dioxide Materials located in Champaign, Illinois.